UCGE Reports

Number 20392

Department of Geomatics Engineering

GNSS Multipath Mitigation Using Channel Parameter Estimation Techniques

by

Negin Sokhandan Asl

November 2013

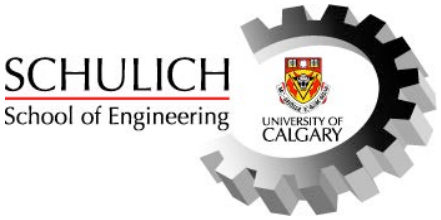

UNIVERSITY OF CALGARY

GNSS Multipath Mitigation Using Channel Parameter Estimation Techniques

by

NEGIN SOKHANDAN ASL

A THESIS

SUBMITTED TO THE FACULTY OF GRADUATE STUDIES

IN PARTIAL FULFILMENT OF THE REQUIREMENTS FOR THE

DEGREE OF DOCTOR OF PHILOSOPHY

DEPARTMENT OF GEOMATICS ENGINEERING

CALGARY, ALBERTA

November 2013

Abstract

Multipath propagation can pose significant challenges to satellite based navigation systems. It remains a dominant source of accuracy degradation and is a major issue for high precision GNSS applications. Multipath can result in biased GNSS measurements, which can lead to inaccurate position estimates or, through fading and self-interference, can cause loss of lock of the signals. Without accurate LOS delay estimation in multipath environments GNSS receivers cannot provide reliable positions, velocity and time (PVT) estimates. Although there are many algorithms proposed in the literature which endeavor to mitigate the effects of multipath, this research topic is still active as no final solution has yet been found.

Given the above, the problem of GNSS multipath mitigation is pursued in this work through the estimation of the parameters of multipath components. For this purpose, three different approaches are proposed and tested. First, a sequential ML-based approach is proposed that sequentially estimates the channel parameters with a smaller computational load compared to the conventional ML-based approaches. This approach uses a detection procedure to avoid over-estimating or underestimating the number of multipath components. For this reason, the proposed approach is more robust in dealing with severe multipath situations such as urban areas. Afterwards, this ML-Based approach is combined with a low-complexity Bayesian tracking algorithm to further decrease the computational load. In this way, the receiver switches between two modes of operation depending on the severity of the variations of the multipath channel. A set of simulation

and data processing results is then used to assess the performance of this technique. The results show that the proposed system outperforms both the classical DLLs and the conventional ML-based algorithms. This algorithm is also used to characterize the distribution of the number of multipath components for some of the visible satellites in the collected data set.

Second, some of the most well-known adaptive filters (LMS, NLMS, RLS and APA) are modified and developed to be used for the purpose of equalization of the multipath channel. The very low computational load associated with these techniques make them more suitable for implementation in hand-held receivers. The innovative hard decision block used in the structure of their feedback procedure increases their efficiency. The presented simulation and data processing results show that the estimation performances of some of these techniques (RLS and APA) are comparable to near-optimal ML-based techniques at higher SNR values.

Third, the possibility of employing the Doppler shifted copies of the received signal in a fast fading channel for the purpose of improving the estimation performance of subspace-based methods is analyzed and tested through simulation and experimental results. The results demonstrate a considerable improvement in the estimation accuracy of the proposed system compared to the cases where diversity approaches are used.

Preface

This thesis includes some materials (e.g. figures, tables and texts) previously published, accepted or submitted in three conference papers and two journal paper as follows:

1. **Sokhandan N.**, J. T. Curran and G. Lachapelle (2013) "A Novel Multipath Estimation Algorithm for CDMA-Based Ranging and Navigation Applications", *submitted to IEEE Transactions on Aerospace and Electronic Systems*, April.

2. **Sokhandan N.**, A. Broumandan, J. T. Curran, and G. Lachapelle (2013) "High Resolution GNSS Delay Estimation for Vehicular Navigation Utilizing a Doppler Combining Technique" *Provisionally accepted by The Journal of Navigation, Cambridge University Press,* June.

3. **Sokhandan N.** (2013), "A Novel Multipath Estimation and Tracking Algorithm for Urban GNSS Navigation Applications," *ION GNSS 2013 conference*, 17-21 September 2013, Nashville, Tennessee, 15 pages

4. **Sokhandan N.**, A. Broumandan, J. T. Curran and G. Lachapelle (2012) "High Resolution Multipath Delay Estimation in Urban GNSS Vehicular Navigation" *ION GNSS 2012 conference*, 17-21 September, Nashville, Tennessee, 11 pages

5. **Sokhandan N.** , A. Broumandan, G. Lachapelle (2011), "Multipath Error Reduction in Harsh Environments", *ION GNSS 2011 conference*, Portland, Oregon, 9 pages

The above papers were produced by the author during the research phase of this thesis.

The co-authors' valuable feedback on the above materials is acknowledged. Use of the above material in this thesis is allowed by the co-authors and the journal/proceedings publishers.

Acknowledgements

I would like to gratefully and sincerely thank my supervisor, Prof. Gérard Lachapelle for his expertise and his constant guidance, understanding and caring. His support and encouragement over the duration of this research have been of immeasurable value to me.

My sincerest thanks are due to my advisor Dr. James Curran for his excellent guidance and patient support. I would never be able to finish my thesis without his valuable advice and caring assistance.

My particular thanks to my second advisor Dr. Ali Broumandan for his precious advice, insightful guidance and constant support that made this research possible.

Additional gratitude is offered to my friends Mohammad, Elmira, Ali, Anup, Peng and other colleagues for providing me with a warm and friendly office environment during the past three years.

I am deeply thankful to my parents. They are always supporting me and encouraging me with their best wishes.

Finally and most importantly, my deepest thanks to my husband, Saeed. His support, encouragement, quiet patience and unwavering love were undeniably the bedrock upon which the past three years of my life have been built.

Dedication

To my husband Saeed,

My parents, My sister & My brother

Table of Contents

List of Tables

List of Figures and Illustrations

List of Acronyms

ACF	Autocorrelation Matrix
APA	Affine Projection Algorithm
AWGN	Additive White Gaussian Noise
C/A	Coarse/Acquisition
CAF	Correlation Ambiguity Function
CDF	Cumulative Distribution Function
CDMA	Code Division Multiple Access
CIR	Channel Impulse Response
CRLB	Cramer-Rao Lower Band
C/N_0	Carrier to Noise Ratio
DFE	Decision Feedback Equalizer
DLL	Delay Locked Loop
DS	Direct Sequence
ELS	Early-Late Slope
EML	Early Minus Late
ES-LMS	Error Sign Least Mean Squares
FIM	Fisher Information Matrix
GLRT	General Likelihood Ratio Test
GOF	Goodness Of Fit
GPS	Global Positioning System
GNSS	Global Navigation Satellite System
HRC	High Resolution Correlator
IC	Interference Cancellation
IMU	Inertial Measurement Unit
INS	Inertial Navigation System
LMF	Least Mean Fourth
LMMN	Least Mean Mixed Norm
LMS	Least Mean Squares
LMS	Land Mobile Satellite
LMSE	Least Mean Squared Error
LOS	Line-Of-Sight
LS	Least Squares
MEDLL	Multipath Elimination Delay Lock Loop
ML	Maximum Likelihood
MSE	Mean Squared Error
MSML	Modified Sequential Maximum Likelihood
MUSIC	Multiple Signal Classification
NC	Narrow Correlator
NLMS	Normalized Least Mean Squares
PDF	Probability Distribution Function
PN	Pseudo-Noise
PRN	Pseudo-Random Noise

SC	Strobe Correlator
SD	Steepest Descent
SG	Stochastic Gradient
SML	Sequential Maximum Likelihood
SNR	Signal to Noise Ratio
RLS	Recursive Least Squares
RMS	Root Mean Squared
RMSE	Root Mean Squared Error
TOA	Time Of Arrival
SML	Sequential Maximum Likelihood

List of Symbols

$r(t)$	Received continuous signal
$n(t)$	Noise term in the received signal before despreading
A_k	The instantaneous absolute amplitude of the k^{th} multipath component
ϕ_k	The instantaneous phase of the k^{th} multipath component
τ_k	The value of delay corresponding to the kth multipath component
a_k	Complex coefficient of the kth multipath component
$s(t)$	Transmitted signal
$y(\tau)$	Correlation function of the received signal before sampling
$g(\tau)$	Ideal correlation function
T_s	Sampling period
T_p	Code period
T_c	Coherent integration time
M	Number of multipath components including LOS
σ_w^2	Noise variance
$w(\tau)$	Noise term after despreading
$\mathbf{y}$	Vector of the samples of the correlation function of the received signal
$\mathbf{G}$	Matrix with the shifted versions of the ideal correlation function by true multipath delays on its columns
$\mathbf{a}$	Vector of the complex coefficients of the multipath components
$\boldsymbol{w}$	Vector of noise samples at the output of correlators
$\mathbf{g}_{\tau_m}$	Shifted version of ideal correlation function
$\boldsymbol{Q}$	Noise covariance matrix at the output of correlators
N	Length of $\mathbf{y}$
T	Duration of search region
L	Number of delay search points
$\bar{\mathbf{G}}$	Matrix with the shifted versions of the ideal correlation function for all of delay values within the search region on its columns
$\bar{\mathbf{a}}$	Vector of CIR for all of the delay values within the search region
T_δ	Delay step used in the search region
$\hat{\mathbf{a}}$	Vector of estimated CIR
$\mathbf{I}(\bar{\mathbf{a}})$	Fisher information matrix in estimating $\bar{\mathbf{a}}$
$\mathbf{C}_{\bar{\mathbf{a}}}$	Covariance matrix of estimation in estimating $\bar{\mathbf{a}}$

$y^{(i)}(\tau)$	Correlation matrix at ith iteration
m	Number of multipath components that is going be estimated
$\bar{\mathbf{G}}_m$	Matrix that only includes those columns of $\bar{\mathbf{G}}$ that correspond to the m estimated components
$\hat{\mathbf{a}}_m$	Vector of the m estimated complex coefficients at the refinement stage
γ''	Threshold of detection
$T(z)$	Sufficient statistic
P_{FA}	Probability of false alarm
λ_p	Mean of the Poisson distribution
b	Mean of the exponential distribution
μ	Mean of the Rician distribution
σ	Standard deviation of the Rician distribution
$\mathbf{M}_{\hat{\mathbf{a}}}$	Error covariance matrix
$\mathbf{M}_0$	Initial value of $\mathbf{M}_{\hat{\mathbf{a}}}$
N_{ML}	Number of time epochs that MSML is applied to initiate the LMMSE tracking
$\mathbf{K}_k$	Matrix of Kalman gain
q_k	Moving averaged MSE
γ	Transition threshold
$\mathbf{C}_k$	Matrix of equalizer coefficients at the kth epoch
$\mathbf{C}_0$	Optimal point of $\mathbf{C}_k$ in MSE cost function space
$J(\mathbf{C})$	MSE cost function
μ	Step-size parameter
$\mathbf{d}$	Vector of correlation function samples of LOS
$\mathbf{R}$	Autocorrelation matrix of the received signal
$\mathbf{\Gamma}$	Cross-correlation matrix of the received signal and $\mathbf{d}$
$\mathbf{P}$	Matrix of update direction
$J_{\min}$	Minimum value of MSE cost function
$\mathbf{R}_\mathbf{d}$	Autocorrelation matrix of $\mathbf{d}$
$\mathbf{U}$	Matrix of eigen-vectors of $\mathbf{R}$
$\mathbf{\Lambda}$	Diagonal matrix with eigenvalues of $\mathbf{R}$ on its main diagonal
λ_n	nth eigenvalue of $\mathbf{R}$ (in decreasing order)
$\mathbf{I}$	Identity matrix
ρ	Eigen-spread coefficient
ε	Regularization parameter
λ	A design parameter used in RLS method
K	Number of epochs used in averaging to compute $\mathbf{R}$ in APA approach

μ_o	Optimal value of the step-size
$\lambda_{\max}$	Largest eigenvalue of **R**
$\hat{\mathbf{R}}$	Estimate of **R**
$\mathbf{e}_k$	*A priori* estimation error vector
$\mathbf{r}_k$	*A posteriori* estimation error vector
$\mathbf{Y}_k$	Matrix with *K* successive vectors of $\mathbf{y}_k$ on its rows
$\mathbf{D}_k$	Matrix with *K* successive vectors of $\mathbf{d}_k$ on its rows
$p(t)$	Spreading waveform
b_q	Navigation data bits
E_b	Bit energy
B	Signal bandwidth
N_c	Spreading factor
$h(t,\tau)$	Time varying channel impulse response
N_B	Number of Doppler branches
N_{ST}	Number of spatial-temporal diversity branches
$\psi(\theta,\tau)$	Spreading function
$\delta(\tau)$	Dirac delta function
B_d	Doppler spread parameter
v	Speed of the receiver
$\mathbf{\Psi}$	Matrix of spreading function samples
$\mathbf{Y}$	Matrix including Doppler shifted versions of **y** on its columns
$\mathbf{H}$	Matrix including channel frequency response vectors on its columns
$\mathbf{F}$	Digital Fourier transform matrix
$\mathbf{U}_s$	Signal sub-space
$\mathbf{U}_N$	Noise sub-space
$\mathbf{P}_{\mathbf{U}_N}$	Noise projection matrix
$SDP(\tau)$	MUSIC delay profile
$\mathbf{R}_D^k$	Estimated correlation matrix using the Doppler combining method
$\mathbf{R}_{ST}$	Estimated correlation matrix using spatial-temporal diversity

Chapter One: INTRODUCTION

1.1 Motivation

As the interest in positioning and localization applications is growing, higher performance Global Navigation Satellite Systems (GNSSs) are required for emerging and future applications. GNSSs provide services to a wide range of military and civilian applications. Moreover, outstanding performance of GNSS in outdoor scenarios is alluring individuals and industry to extend its application in signal degraded environments such as urban canyons. However, the achievable positioning accuracy of a satellite navigation system, such as Global Positioning System (GPS), is seriously hindered by several phenomena that affect the main observable in these systems: the signal's time of arrival (TOA).

Undoubtedly, the problem of accurate Line-of-Sight (LOS) delay estimation is encountered among the most challenging synchronization problems in the context of GNSSs.

Although modern GPS receivers achieve high pseudorange estimation accuracy under line-of-sight conditions, it is well-known that multipath remains as a dominant source of ranging error in high precision GNSS positioning applications. Measurements have shown that in challenging environments such as urban areas, multipath signals may introduce positioning errors of the order of several tens of metres (Parkinson & Spilker 1996). For this reason, extensive research has been recently dedicated to the reduction of multipath errors in these types of environments and numerous multipath mitigation approaches have been developed.

The main scope of this thesis is the analysis of multipath mitigation techniques and the development of enhanced one for stand-alone GNSS applications with a focus on dense multipath environment such as urban and sub-urban areas.

1.2 Limitations of the Previous Work

Among the multipath mitigation techniques, probably the simplest ones are those that apply special antenna designs such as the use of choke rings and dual-polarization (Manandhar & Shibasaki 2004) antennas to prevent secondary reflections from entering the receiver front-end. However, these techniques are not able to completely eliminate multipath reflections in dense multipath environments (Dragunas & Borre 2011) since they can only remove reflections arriving from low elevation angles.

The most common delay measurement techniques implemented in today's commercial GNSS receivers are the classical feedback code delay tracking loops that make use of a few correlators (Lohan et al 2012). The most widely known feedback-delay estimator is the standard wide correlator Delay Lock Loop (DLL) or Early-Minus-Late (EML) loop (Fock et al 2001). In this estimator, two correlators spaced by one chip (early and late) are used to form a discriminator function. The output of this discriminator function determines how much the correlators must be shifted to compensate the effect of multipath. This classical EML is not able to compensate the effect of multipath components with relative (to LOS) delays smaller than one chip (Braasch 1992). A modification of the EML that provides some multipath rejection is the Narrow Correlator (NC) technique which is based on the idea of narrowing the Early-Late spacing of the Delay-Lock Loop (DLL) and increasing the correlation bandwidth (Van Dierendonck et al 1992). With this technique, the jitter is reduced and the range of multipath delays that

affect the DLL tracking point is shorter (Selva 2003). The receiver's front-end filter bandwidth and the sampling rate of its digitizer are the two parameters that must be considered in determining a proper value for correlator spacing (Betz & Kolodziejski 2000). The implementation of narrow correlator spacing reduces the multipath bias on the Coarse/Acquisition (C/A) code pseudorange measurements compared to the standard EML but even with this advantage, the bias due to multipath is still dominant and can be very large in dense multipath environments. Another discriminator-based technique proposed for use in GNSS receivers is the so-called Double-Delta technique, which uses four or five correlators in the tracking loop (Irsigler & Eissfeller 2003). This technique provides enhanced multipath immunity to the receiver under good Carrier-to-Noise-density ratio (C/N_0) conditions (Hurskainen et al 2008), however it degrades the noise performance of the DLL (McGraw & Braasch 1999). A number of well-known examples of the double-delta technique are the High Resolution Correlator (HRC) (McGraw & Braasch 1999), the Pulse Aperture Correlator (PAC) (Jones et al 2004) or Strobe Correlator (SC) (Garin & Rousseau 1997) and the modified correlator reference waveform (Weill 2003). The SC discriminator is a linear combination of NC discriminators with different values of correlator spacing. The HRC uses multiple correlators from a conventional GNSS receiver to form a linear combination of correlator outputs that yields a net correlation function that is much narrower than the usual C/A code autocorrelation function.

Another feedback-tracking structure is the Early-Late-Slope (ELS), which is also known as the Multipath Elimination Technique (MET) (Townsend & Fenton 1994). The ELS technique still takes full advantage of narrow correlator spacing but decreases the

multipath bias on the pseudorange bias compared to the NC technique. Its structure is based on two correlator pairs at both sides of the correlation function's central peak. Once both slopes are known, they can be used to estimate a pseudorange correction that can be applied to pseudorange measurements. Moreover, an improvement of ELS, Slop-Based Multipath Estimation (SBME) (Bhuiyan et al 2010), uses an additional correlator at the late side of the correlation function to estimate and compensate for the multipath bias of a NC tracking loop.

Although all of these techniques achieve much better results than the conventional standard DLL in terms of multipath bias, since their structure is based on the shape of the autocorrelation function, they cannot mitigate the effect of closely spaced multipath. In particular, when the number of paths is larger than two, their performance degrades significantly and the timing synchronization may fail (Closas et al 2006). In general, the important common property between all of these correlation-based techniques is that their stable lock point is at the maximum power of the autocorrelation function (Townsend & Fenton 1994) no matter how much this peak has been shifted with respect to the peak that corresponds to the actual LOS. This effect is the main source of biases in the output of these DLLs in dense multipath environments where the correlation function peak is shifted considerably. This shift in the PRN code autocorrelation function peak usually happens when the number of paths is large or when at least one of the multipath components is stronger than the LOS signal (this is shown in Chapter 2 through simulations).

The other class of multipath mitigation techniques includes the advanced methods such as the Multipath Estimating Delay Locked Loop (MEDLL) (Townsend et al 1995, Nee et al

1992, Nee et al 1994), the Multipath Mitigation Technique (MMT) (Weill 2002), the Vision Correlator (VC) (Fenton & Jones 2005), which is an implementation of MMT, the Fast Iterative Maximum Likelihood Algorithm (FIMLA) (Sahmoudi & Amin 2008), Sequential Maximum Likelihood (Sahmoudi & Amin 2009), the Reduced Search Space Multipath Likelihood (RSSML) algorithm (Bhuiyan et al 2009), the deconvolution approaches (Skournetou et al 2011) and MUSIC based delay estimators (Groh & Sand 2011). This class of techniques is based on Maximum Likelihood (ML) estimation. The ML-based multipath estimation techniques are driven to approach theoretical performance upper limits (*i.e.* Cramer-Rao Lower Band). These algorithms are typically computationally complex and sometimes difficult to implement since they require employing a large number of correlators and applying complex procedures to process the correlator outputs (Lohan et al 2005) which are normally based on exploring a large search-space.

The MEDLL, which is one of the most promising advanced multipath estimation and mitigation techniques (Bhuiyan & Lohan 2010), normally uses numerous correlators in order to accurately determine the shape of the multipath corrupted correlation function. Afterwards, it determines the best combination of the parameters of LOS and multipath components by using a reference correlation function (ideal correlation function of the PRN code). Therefore, a large search space is explored at each time epoch (equal to coherent integration period) in order to find the best combination of amplitudes, delays and phases for all the paths. At the cost of this complex multi-correlator structure, MEDLL introduces multipath mitigation performance superior to that of correlation-based techniques. Moreover, MEDLL has motivated the design of different other ML-

based techniques for the purpose of multipath mitigation such as the non-coherent MEDLL, described in (Bhuiyan & Lohan 2008). A special implementation of MEDLL is the so-called CADLL (Coupled Amplitude-Delay Lock Loop) technique (Chen & Dovis 2011), which assigns two amplitude lock loops (for tracking the real and imaginary parts of the path coefficients) and one delay lock loop to every estimated path.

If the receiver is equipped with an antenna array, then it is possible to employ standard beamforming techniques (Van Trees 2002) in a way that the main beam is directed to the LOS signal and nulls are approximately placed at the multipath angles of arrival. In (Daneshmand et al 2012, Seco-Granados 2007) the motion of the antenna array is employed to decorrelate the multipath components and also synthesize an augmented array to increase the degree of freedom of the array.

There are also several techniques that make use of some external devices or signals to aid GNSS in degraded signal environments such as indoors. Some examples are inertial sensors, optical systems and wireless networks such as WiFi, Bluetooth or RFID. The issue with these techniques is that they require their own infrastructure and are normally used for indoor localization (Dragunas & Borre 2011).

1.3 Objectives

Considering the limitations of the previous work, the objectives of this thesis can be outlined as follows:

a) The main objective is to design, test and analyze optimal or near optimal (in the sense of estimation mean square error) multipath estimation and mitigation techniques, which require a reasonable computational burden for navigation receivers and are based upon realistic signal and noise models.

b) The second objective is to study the statistical distribution of the number of multipath components in an urban channel using real data measurements.

c) The third objective of this thesis is to analyze the effectiveness of employing the Doppler-frequency shifted copies of the received signal in a fast fading channel encountered in vehicular navigation as a means of decorrelating the multipath signals. The decorrelation of the multipath signals improves the performance of the subspace-based multipath delay estimation algorithms.

1.4 Contributions

To attain objective (a), the following approaches are considered:

1) The Maximum Likelihood principle is employed in order to derive an optimal estimator (Cramer-Rao bound). An ML-based multipath estimation-detection technique is proposed that sequentially removes the contribution of multipath components from the correlation function of the received signal. Unlike the other ML-based techniques in the same context, the number of paths is not assumed to be known in advance. Using a novel method, after estimating the parameters of the previously detected multipath components and their removal, the existence of a probable new path is tested via a General Likelihood Ratio test for a certain probability of false-alarm. Furthermore, the estimated parameters are refined after detecting every new multipath component. These steps improve the estimation performance compared to current ML-based algorithms. Moreover, since the detection stage uses the

results of the estimation stage, the additional computation burden that it imposes to the system is insignificant.

2) In order to reduce the computational cost of the receiver that employs the sequential ML-based method discussed above, it is combined with a low-complexity Bayesian tracking technique, namely the Linear Mean Squared Error (LMMSE) technique. The combination of the two techniques is based on a mechanism that automatically switches the system to the low-complexity Bayesian tracking mode whenever the variations of the channel are slow.
3) Another class of algorithms is investigated and extended for GNSS multipath mitigation application. Techniques from this class are sub-optimal approximations of the optimal steepest descent algorithms. The computational complexity of this class of techniques, which are known as stochastic gradient algorithms, is smaller than any of the ML-base techniques. These algorithms adaptively adjust the coefficients of a filter designed to remove the contribution of multipath components from the received correlator function. An optimum hard decision block is designed to evaluate the error vector that is fed back to system to modify the filter coefficients adaptively.

To attain objective (b), using a real data collected in an urban environment, the proposed sequential ML-based channel estimation-detection technique is used to derive the histogram of the number of detected multipath components for all visible satellites to investigate their distributions and their stochastic characteristics.

To attain objective (c), the last chapter of this thesis employs a Doppler-combining technique to take advantage of the Doppler-spectrum broadening of the received signal in a fast fading channel to combat signal coherency and improve the estimation accuracy of the Multiple Signal Classification (MUSIC) technique. The performance results of this technique are then compared to some other techniques for different values of coherent integration time to assess its effectiveness.

1.5 Thesis Outline

The structure of this dissertation can be summarized as follows:

Chapter 2 begins with a brief overview on the theoretical background related to the propagation of the GNSS signal in a typical Land Mobile Satellite (LMS) channel. The main functionalities of a GNSS receiver are then discussed with particular attention to signal acquisition and tracking. Finally, a review of current multipath mitigation algorithms is presented to provide a benchmark against which the proposed methods can be assessed.

Chapter 3 presents a novel ML-based delay estimation algorithm designed to provide robustness against multipath propagation. The proposed algorithm solves a combined detection-estimation problem to sequentially estimate the parameters of each individual multipath component and predict the existence of a further possible component. A comparison between contemporary maximum likelihood based multipath estimation techniques and this new technique is provided. A selection of realistic channel simulation models is used to assess relative performance under different operating scenarios.

In **Chapter 4** the proposed sequential ML-based algorithm presented in Chapter 3 is combined with a Bayesian tracking technique, namely Linear Least Mean Squared Error

(LLMSE) technique, which uses the estimated channel by the ML-based method as *a priori* knowledge to track the slow variations in the channel as time progresses and reduce the total computational complexity of the system. A set of real life data processing results is then presented to compare the performance of the combined technique with the ones of the conventional tracking algorithms introduced in Chapter 2 in terms of pseudorange and positioning errors.

Chapter 5 introduces a sub-optimal class of techniques with relatively small computational complexity. The algorithms of this class, which are generally referred to as adaptive filters, are extended for the application of GNSS multipath mitigation in a way that, instead of direct estimation of multipath channel, they adaptively adjust the coefficients of a filter designed to remove the effect of multipath from the correlation function of the received signal. Simulation and real data processing results are presented to compare the performance of different algorithms of this class. Moreover, a comparison in terms of complexity of the well-known algorithms in this class is provided.

In **Chapter 6** the Doppler spectrum broadening of the fast fading channel resulting from the motion of the receiver or surrounding objects is employed to decorrelate signal reflections for the purpose of high-resolution estimation of multipath delays through a subspace-based technique. Specifically, delay-domain correlator outputs at different Doppler frequencies are combined to enhance the rank of the signal autocorrelation matrix. Simulation and results of real data collected in an urban environment are then presented to compare the performance of the proposed method with the spatial-temporal-diversity-based-MUSIC technique and the double-delta correlator technique.

Chapter 7 provides conclusions and presents recommendations for future work.

Chapter Two: Technical Background

In this chapter, the structure of GNSS signals, channel and receiver will be introduced and the required technical background to support the development in the rest of thesis will be presented.

2.1 GNSS Signal and Channel Structure

Most navigation satellite systems take advantage the Direct Sequence Code Division Multiple Access (DS/CDMA) technology to spread the spectrum of the transmitted navigation signal and benefit from the provided multiple access property. The focus of this thesis is on this class of signals.

The complex baseband GNSS signal at the output of the transmitter can be represented as

$$s(t) = \sum_{q} \sqrt{E_b} b_q m(t - qT_b) d(t - qT_b) \tag{2.1}$$

where b_q's are the navigation data bits, T_b is the bit period, $m(t)$ is the modulating waveform and $d(t)$ is represented by

$$d(t) = \sum_{k=1}^{N_b} p(t - kT_p) \tag{2.2}$$

where T_p is the code period duration, N_b is the integer number of code periods occurring during one bit interval, and $p(t)$ is the spreading waveform with the chip interval of T_c and can be represented as

$$p(t) = \sum_{n=1}^{Nc} c[n] v(t - nT_c) \tag{2.3}$$

where $c[n]$ is the pseudo-noise (PN) spreading code which is pseudo-random sequence of ± 1 values, N_c is the code length and $v(t-nT_c)$ is the chip waveform. The received baseband signal in multipath environment is modeled as an *M*-path signal composed of a direct path and (*M*-1) reflected rays the plus noise term, *n*(*t*), which is assumed to be additive Gaussian in this thesis and can be represented as

$$r(t)=\sum_{k=1}^{M} A_k s(t-\tau_k) e^{j(\phi_k)} + n(t) \tag{2.4}$$

where A_k, ϕ_k and τ_k are the time-variant amplitude, instantaneous phase and delay parameters corresponding to the *k*-th path, respectively. Furthermore, ϕ_k can be represented by

$$\phi_k = 2\pi\delta f_k t + \varphi_k \tag{2.5}$$

where φ_k is the initial phase offset corresponding to the k-th path and δf_k is the corresponding Doppler frequency shift which can be expressed as

$$\delta f_k = \frac{(V_s - V_u).\mathbf{u}}{\lambda} \tag{2.6}$$

where V_s is the velocity of the satellite, V_u is the velocity of the receiver, $\mathbf{u}$ is the spatial unit vector in the direction of LOS between the transmitter and the receiver and λ is the wavelength of the carrier signal. The reflection of a GNSS signal in a multipath environment has been shown in Figure 2-1.

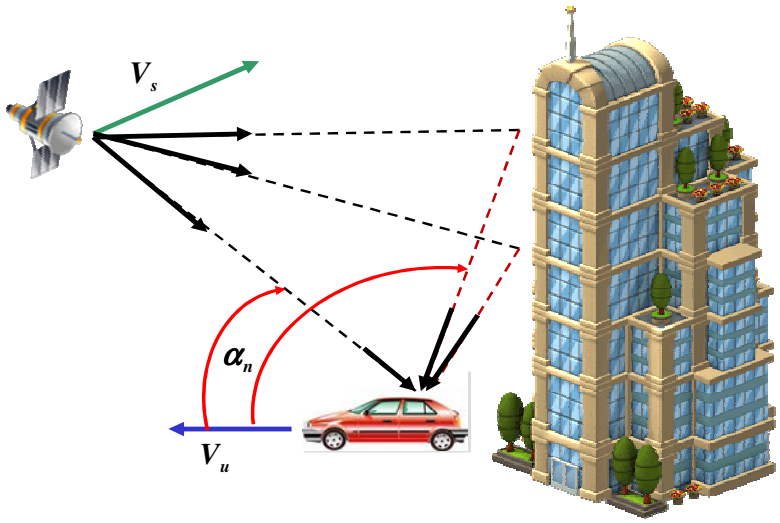

Figure 2-1: Signal reflections in multipath environment

In the receiver, the received signal after being down converted, filtered and sampled is correlated to a replica of the transmitted PN code to become *de-spread*. This process decreases the bandwidth of the signal N_c times. The autocorrelation function of a PN code, $g(\tau)$, with a length of N_c is shown in Figure 2-2. For the GPS C/A signal, the PN codes are Gold codes with a length of $N_c = 1023$. This family of codes has very low cross-correlation values which makes them suitable for multi-access communication.

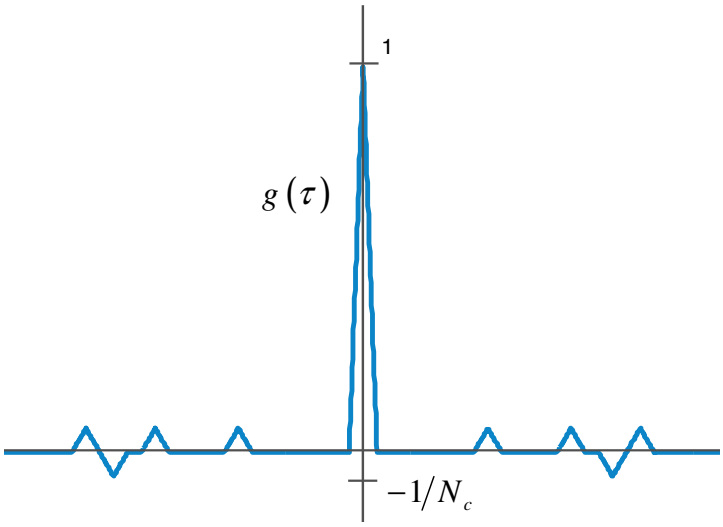

Figure 2-2: Autocorrelation function of a PN code

It is important to remember that if the additive noise process prior to correlation is white, it is no longer white after the correlation, instead its successive time samples are correlated with the correlation function $g(\tau)$. Herein, the distorting effect of the front-end filter on the shape of the autocorrelation function has been ignored.

Considering the above signal model, the output of the correlator can be expressed as:

$$y(t) = \sum_{k=1}^{M} a_k g(t - \tau_k) + w(t)$$
$$t = 0, T_s, \ldots, (N-1)T_s \qquad (2.7)$$

where $a_k = A_k e^{j\phi_k}$ is the complex path coefficient corresponding to the k-th path and g is the ideal autocorrelation function of the PN code and $w(t)$ is the noise term at the output of the correlator.

After the de-spreading process, the output signal enters the acquisition/tracking process wherein the synchronization parameters are estimated and used in the computation of the

navigation solution. In the next section these stages of the GNSS receivers will be introduced.

2.2 Architecture of a GNSS Receiver

In this chapter, different functionalities of a typical GNSS receiver will be explained starting from signal reception by the Radio Frequency (RF) front-end to the computation of the navigation solution which is basically the user's position. The block diagram of a typical GNSS receiver is shown in Figure 2-3 and the highlighted part denotes the area of this thesis.

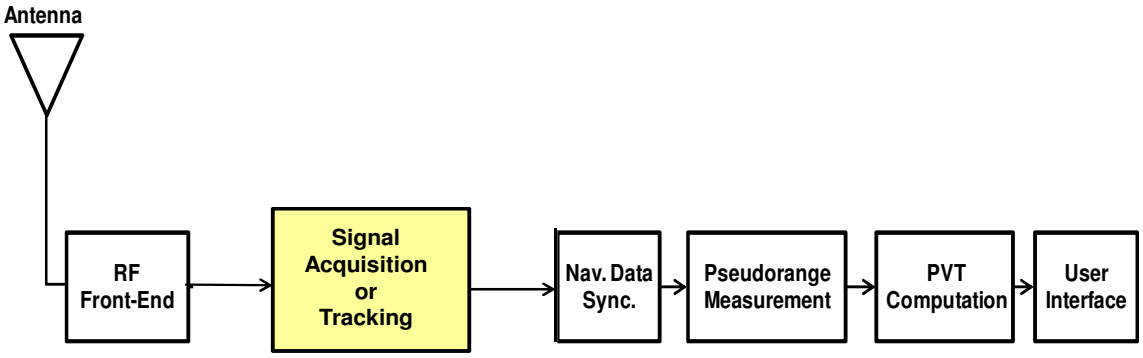

Figure 2-3: Block diagram of typical GNSS receiver

2.2.1 RF Front-End

The receiver's RF front-end starts with a Right-Hand Circularly Polarized (RHCP) antenna since this is the polarization of the transmitted GNSS signals (after each reflection the polarization of the signal changes). Immediately after the antenna, there is a Low Noise Amplifier (LNA). The LNA is a fundamental block in any receiver's front-end since not only it amplifies the received signal but it also acts as a band-pass filter and rejects the out-of-band interferences. Typically after the LNA, there is a Local Oscillator (LO) that down-converts the received RF signal to Intermediate Frequency (IF). The

stability of the receiver's clock is very low compared to the atomic clock of the satellites. Therefore, the time offset produced by the internal LO is considered as an unknown parameter to be estimated by the GNSS receiver.

Afterwards, the IF signal is digitized by a Analog to Digital Converter (ADC) that outputs a stream of signal samples which are then quantized by a certain number of bit levels.

Lastly, the signal must be down-converted from IF to base-band. For this purpose, a conventional I&Q demodulator is used which consists of a second LO followed by another ADC. This procedure produces I&Q samples by splitting the signal into two, multiplying the arms by LO and its 90° shifted version and finally low-pass filtering and quantizing the signal at both of the arms.

The complex signal at the output of the front-end is buried in noise. Therefore, the next step is de-spreading the signal and then estimating the synchronization parameters through acquisition and tracking procedures. These synchronization parameters include the code delay, carrier phase and Doppler frequency of the received signal and provide information about the distance between the satellite and the GNSS receiver used in the computation of navigation solution. The acquisition and tracking stages are explained in the following sections.

2.2.2 Signal Acquisition

The acquisition operation of a GNSS receiver aims to determine and track the satellites visible and achieve a coarse estimate of the synchronization parameters of those satellites. The search stage in the acquisition procedure is a three-dimensional search process that includes searching over satellite numbers, code delays and Doppler

frequency domains. For each satellite, a two-dimensional search space is produced by correlating the received signal and the corresponding locally generated code, which is moved in delay and frequency to cover the range of all the possible time delays and Doppler shifts. The maximum power of the generated correlation values provides a rough estimate of the synchronization parameters of the given satellites. There are several alternatives for performing the two-dimensional search. The most common and simplest technique is the FFT-based procedure (Tsui 2000). Figure 2-4 shows the correlation outputs for two possible cases: when the tested satellite is visible and when it is not visible or the SNR of the received signal from the tested satellite is not high enough to be detected. In order to detect the signal of a visible satellite, the maximum correlation power must exceed an established threshold that is defined based on a desired probability of false alarm. For further improvement of the acquisition performance, a number of correlation outputs can be coherently averaged to increase the SNR of the correlation peak.

Finally, the searching technique used in the acquisition stage can be a serial search (Hurskainen 2009), a parallel search or a hybrid search. In a serial search, the search bins are explored one by one and therefore the search is very slow but computationally simple. In a parallel search, a bank of matched filters is used to explore all of the search bins in parallel and is therefore fast but computationally complex. A hybrid search is a balanced trade-off between the serial and parallel search techniques. In this thesis, the parallel search technique is considered.

In cases where the receiver has some rough information about the position of the receiver, the initialization of the acquisition processed is referred to as *warm start* as opposed to *cold start* initialization wherein no prior information is available.

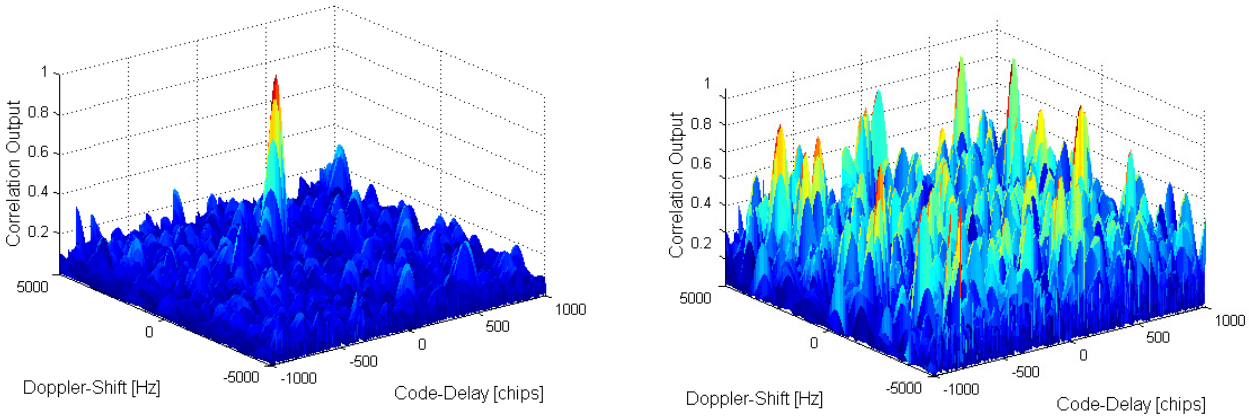

(a) (b)

Figure 2-4: Normalized correlation output for a given satellite when (a) the satellite is visible (b) the satellite is not visible

2.2.3 Signal Tracking

After the acquisition is performed and the visible satellites along with the rough estimates of their synchronization parameters are determined, the receiver initiates the tracking mode of the operation. The purpose of this mode is to provide fine estimates of the synchronization parameters of the detected satellites while keeping track of them as well as extracting the navigation data bit streams. Provided that the estimates of the synchronization parameters outputted by the acquisition mode are roughly correct, the tracking loops are able to lock on the parameters by continuous adjustment of the local code. The tracking loops that are used in a GNSS receiver include the Delay Lock Loop (DLL) that tracks the time delay, the Phase Lock Loop (PLL) that tracks carrier phase

and the Frequency Lock Loop (FLL) that tracks the Doppler frequency. Since in tracking stage the search space has been reduced, the computation complexity of this stage is smaller than that of the acquisition stage. As in the acquisition stage, most of the commonly-used DLLs attempt to find the maximum of the correlation function in the reduced search space. This is based on the assumption that there is no multipath component in the received signal. The structure of some of the most well-known DLLs is explained in the next section.

2.2.4 Navigation Solution

The objective of the navigation solution unit is to demodulate the navigation messages and compute the position of the receiver using the pseudorange measurements obtained during the acquisition and tracking stages.

The navigation message provides the receiver with the orbital parameters required to determine the orbits and clock bias of the satellites. This information is used in the computation of the receiver's location. The time duration required by the receiver to produce the first position solution is referred to as the Time To First Fix (TTFF). This parameter mostly depends on the acquisition and positioning strategies used by the receiver.

The pseudorange parameter for each satellite is computed by multiplying the estimate of LOS time delay by the speed of the light (c). There is a nonlinear relation between the coordinates of the receiver and the measured pseudorange that can be expressed as

$$\rho_k = \sqrt{\left(x_s^k - x_u\right)^2 + \left(y_s^k - y_u\right)^2 + \left(y_s^k - y_u\right)^2} + c\left(\delta t - \delta t_k\right) + \varepsilon_k \qquad (2.8)$$

where ρ_k indicates the pseudorange between the receiver and the k-th satellite, $P_u = [x_u \ y_u \ z_u]$ is the location of user, $P_s^k = [x_s^k \ y_s^k \ z_s^k]$ denotes the location of the k-th satellite, δt and δt_k are the clock offsets associated to the receiver and the satellite respectively, and ε_k includes errors from different sources such as noise, multipath and atmospheric delays. At least four visible satellites are required to solve (2.8) for x_u, y_u, z_u and δt. Moreover, taking derivative of both sides of (2.8) provides a relation between the Doppler frequency and the relative velocity of receiver with respect to the satellite.

2.3 Conventional Multipath mitigation Techniques

In this section the structure of some of the classical DLL algorithms that are used as a benchmark for performance comparison in some of the next chapters is briefly introduced.

2.3.1 Narrow Correlator

One of the primary approaches used to reduce the influences of code multipath is the Narrow Correlator technique, which was first proposed by Van Dierendonck et al (1992). The NC discriminator output is computed by subtracting an early and a late sample of the correlation function with a sub-chip code-phase spacing and can be expressed as

$$\Delta\tau = y_1 - y_2 \tag{2.9}$$

where y_1 and y_2 are the value of ACF at early and late samples. These two samples are initially on the opposite sides of the roughly estimated code phase in the acquisition process. Usually a correlator spacing of 0.1 chips is used to build up the discriminator function (Irsigler & Eissfeller 2003).

2.3.2 Double-Delta Correlator

The term "Double Delta (ΔΔ) Correlator" is a general expression for special code discriminators formed by a linear combination of two correlator pairs instead of only one. In Figure 2-5 the general structure of this class of discriminators is shown. The most well-known techniques of this class are the Early-Late-Slope (ELS), the Pulse Strobe Correlator (SC) and the High Resolution Correlator (HRC) which will be introduced in the following sub-sections.

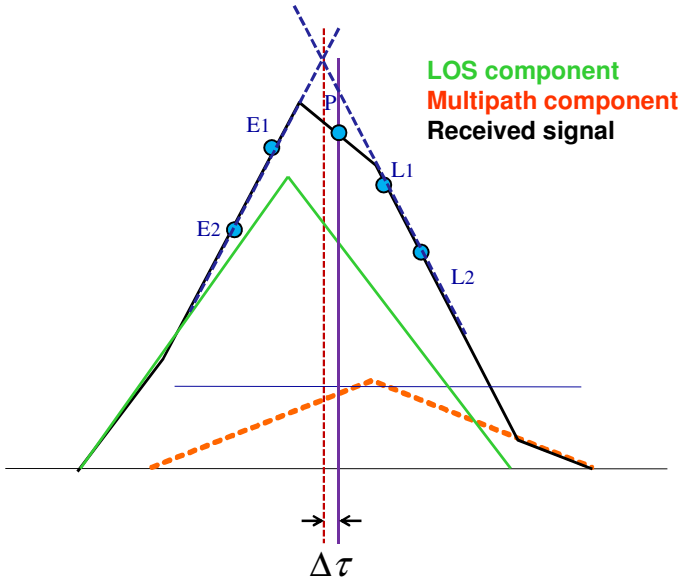

Figure 2-5: Structure of a double delta correlator discriminator

2.3.2.1 Early-Late Slope

The basic idea behind the ELS technique is to compute the slope of the correlation function on both sides of its central peak and then use the values to compute a code-phase correction term that is fed back to the system to shift the pairs of correlators. It can be noticed in Figure 2-5 that the in the presence of multipath, the autocorrelation function of the received signal is distorted so that the slopes at the early and late sides of the central peak are no longer of the same magnitude. In the ELS technique, the correction term is

computed in a way to compensate for the slope difference of the rising and falling edges of the ACF peak and it can be expressed as

$$\Delta\tau = \frac{y_1 - y_2 + (d/2)(a_1 + a_2)}{a_1 - a_2} \tag{2.10}$$

where $a_1 = \frac{2(E_1 - E_2)}{d}$ and $a_2 = \frac{2(L_2 - L_1)}{d}$ are the ACF slopes at the early and late sides respectively, y_1 and y_2 are the values of ACF at E_1 and L_1 (in Figure 2-5), and d is the spacing between E_1 and L_1 (the spacing between E_2 and L_2 is $2d$).

2.3.2.2 Strobe Correlator

The strobe correlator discriminator is implemented through a linear combination of two narrow correlators with different correlator spacing parameters (d_1 and d_2) and can be expressed as

$$\Delta\tau = \left(d_2 / d_1\right)\Delta\tau_1 - \Delta\tau_2 = \left(d_2 / d_1\right)(E_1 - L_1) - (E_2 - L_2) \tag{2.11}$$

where $\Delta\tau_1$ and $\Delta\tau_2$ are the code-phase error terms produced by the narrower and wider NCs respectively. This combination increases the sensitivity of the discriminator to short-range multipath components compared to original NCs.

2.3.2.3 High Resolution Correlator

The High Resolution Correlator (HRC) combines five correlator outputs (E2, E1, P, L1, L2) from a conventional GNSS receiver (similar to Figure 2-5) to form an approximation to the gated correlator (Kanekal & Braasch 1998). E1 and L1 are spaced d chips, E2 and

L2 are spaced 2d chips and P (prompt) is in the middle. The idea behind HRC is to yield a net correlator function that is much narrower than that of the C/A correlation function. Firstly, a synthesized correlator, namely HRC Prompt, is formed as follows:

$$P_{HRC} = 2P - (E_1 + L_1) \tag{2.12}$$

At the next step, early and late HRC correlators are computed to form an EML discriminator function for the purpose of code tracking as follows:

$$\begin{aligned} E_{HRC}(\tau) &= P_{HRC}(\tau + d) = 2E_1 - (E_2 + P) \\ L_{HRC}(\tau) &= P_{HRC}(\tau - d) = 2L_1 - (L_2 + P) \end{aligned}, \tag{2.13}$$

And the corresponding EML discriminator function will be

$$D_{HRC}(\tau) = (E_{HRC} - L_{HRC})/2 = (E_1 - L_1) - (E_2 - L_2)/2 . \tag{2.14}$$

The discriminator function in (2.14) is the same as the Strobe correlator discriminator function in (2.11). Using the above synthesized correlators, the performance of HRC is identical to the gated correlator for short to medium delay multipath reflections (Garin & Rousseau 1997) which are of a greater concern in real scenarios. However, this technique only helps to reduce code multipath and also the reduction in signal power degrades the tracking accuracy at low C/N_0 values (McGraw & Braasch). To deal with these issues, another version of HRC was proposed by McGraw & Braasch (1999) that uses the following discriminator function:

$$\Delta\tau_{HRC} = \frac{ID_{HRC}.IP + QD_{HRC}.QP}{SP} . \tag{2.15}$$

where ID_{HRC} and IP_{HRC} denote the real parts of D_{HRC} and P_{HRC}, QD_{HRC} and QP_{HRC} denote the imaginary parts of D_{HRC} and P_{HRC} and $SP = IP^2 + QP^2$. This implementation of HRC reduces carrier phase multipath as well as providing an improved reduction in code multipath.

2.4 Drawback of classic DLLs

In Chapter One it was explained that in cases where the peak of the correlation function is shifted in the delay-domain due to the effect of severe multipath, the classical DLLs produced biased estimates. In this section, this drawback is shown through a simple simulation. Consider the autocorrelation function for a multipath simulation scenario with four reflected paths in Figure 2-6. The position of the true simulated paths and the estimated channel impulse response by a simple Least Squares (LS) estimator (refer to Section 2.4.3) is also shown for comparison. Table 2-1 shows the simulation path parameters.

The purple points in Figure 2-6 depict the five correlator used in the structure of correlation-based DLLs. The green arrow shows the area within which pseudorange measurements can be corrected. Since the correlation peak has shifted considerably, the correlation based DLLs are not able to correct the bias. Since the correlators are well centered about the correlation peak, the values of the feedback produced by the discriminator functions are close to zero and the corresponding DLLs are not able to correct the measurement errors.

This effect is the main source of biases in the output of these DLLs in dense multipath environments.

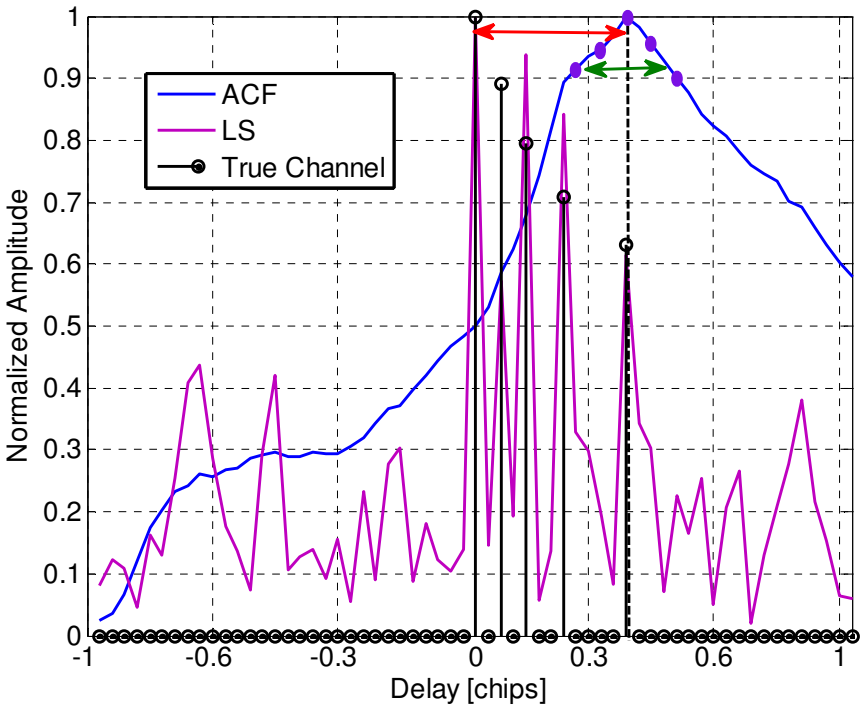

Figure 2-6: Shifted autocorrelation function peak (C/N_0 = 30 dB-Hz)

Table 2-1: Simulation parameters

Path #	Attenuation (dB)	Delay (chips)
1	-2	0.07
2	-3	0.15
3	-4	0.25
4	-6	0.4

Figure 2-7 shows the pseudorange measurement errors produced by NC, ELS and HRC discriminators for this multipath simulation scenario corresponding to Table 2-1. It is observed that, since the number of paths is large and the correlation function peak has considerably shifted, there is large bias in measurement errors produced by all of these three DLLs.

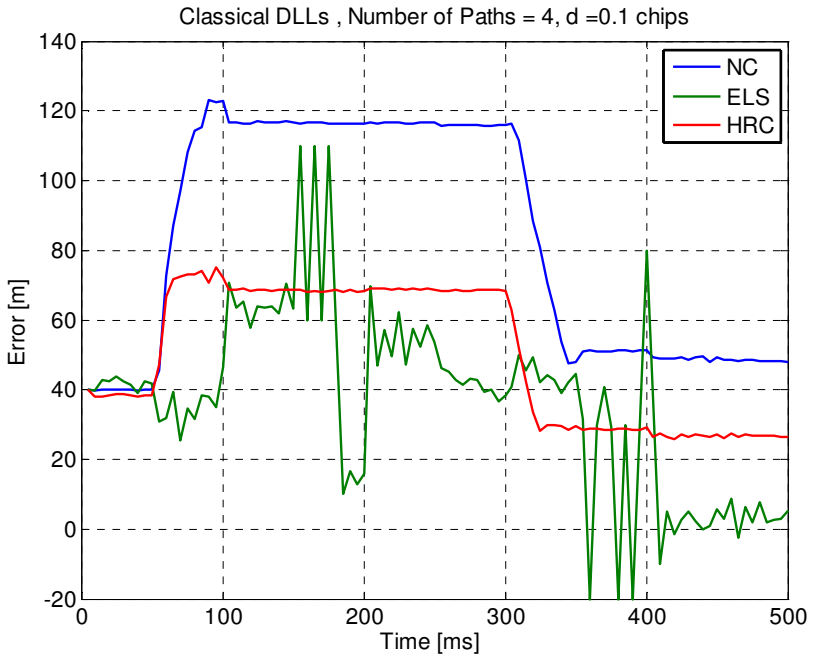

Figure 2-7: Pseudorange measurement errors in a four-path channel (C/N_0 = 30 dB-Hz)

2.5 GNSS Channel Estimation

As it was briefly discussed in Chapter One, as opposed to the classical DLLs, there are some advanced ranging measurement techniques based on the estimation of the channel parameters and which are the main focus of this thesis. In this section, the general theories behind some of the most well-known classes of these techniques are introduced.

2.5.1 Cramer-Rao Lower Bound

Within different channel estimation techniques, we start from those estimators that provide unbiased estimates of unknown deterministic parameters with the minimum estimation error variance. These techniques are referred to as Unbiased Minimum Variance (MVU) estimators and they are optimal with the optimality criterion being to attain the minimum estimation variance. Moreover, there is a lower bound for the estimation variance of unbiased estimators, which is referred to as the Cramer-Rao Lower Bound (CRLB). Therefore, any unbiased estimator that uniformly attains CRLB is an MVU estimator. Since the unknown parameters were assumed to be deterministic, this bound depends on the PDF of the noise process.

In cases where there is a vector of unknown parameters, as it is the case in this thesis, an estimation error matrix is associated to the MVU estimator that includes the CRLB of the unknown parameters on its main diagonal. The inverse of this matrix is referred to as the Fisher Information Matrix (FIM). Assuming that **y** is the vector of the received data and **a** is the vector of deterministic unknown parameters, FIM is defined as

$$\left[\mathbf{I}(\mathbf{a})\right]_{ij} = -E\left[\frac{\partial^2 \ln p(\mathbf{y};\mathbf{a})}{\partial \mathbf{a}_i \partial \mathbf{a}_j}\right], \tag{2.16}$$

where $\left[\mathbf{I}(\mathbf{a})\right]_{ij}$ is the i-j-th element of **I**(**a**) and $p(\mathbf{y};\mathbf{a})$ is the PDF of the received data. Given (2.16), the CRLB for the i-th entry of **a** is found as

$$\mathrm{var}(\hat{\mathbf{a}}_i) \geq \left[\mathbf{I}^{-1}(\mathbf{a})\right]_{ii}. \tag{2.17}$$

It is important to notice that although there is not always an MVU estimator for any estimation problem, CRLB can be always used as a benchmark to assess the performance of other unbiased estimators.

2.5.2 Maximum Likelihood Techniques

The Maximum Likelihood (ML) estimator is the most popular practical estimator that approaches the theoretical performance limit. For most of cases of practical interest the ML estimator is approximately (asymptotically) the MVU estimator for large data records (Kay 1993). In other words if $\hat{\mathbf{a}}_{\text{MLE}}$ is the ML estimate of $\mathbf{a}$ and N is the available length of data over which $\mathbf{a}$ is deterministic, then one has

$$\text{as} \quad N \to \infty : \quad E\left[\hat{\mathbf{a}}_{\text{MLE}}\right] \to \mathbf{a} \qquad \text{and} \qquad \text{cov}\left(\hat{\mathbf{a}}_{\text{MLE}}\right) \to \mathbf{I}^{-1}\left(\mathbf{a}\right). \tag{2.18}$$

However, for specific case of linear system model and Gaussian noise (which is the case in this thesis), the ML estimator is exactly (not approximately) the MVU estimator and it attains the CRLB.

For any unknown deterministic vector of parameters $\mathbf{a}$, the ML estimate is defined as the value that maximizes the likelihood function which is $p\left(\mathbf{y};\mathbf{a}\right)$, the maximization being performed over the possible range of $\mathbf{a}$. Considering a linear system model as

$$\mathbf{y} = \mathbf{G}\mathbf{a} + \mathbf{w}, \tag{2.19}$$

where w is the vector of noise samples which is assumed to be zero-mean and Gaussian with the covariance matrix of $\mathbf{Q}$, $p(\mathbf{y};\mathbf{a})$ can be represented as

$$p(\mathbf{y};\mathbf{a}) = \frac{1}{(2\pi)^{\frac{N}{2}} \det^{\frac{1}{2}}(\mathbf{Q})} \exp\left[-\frac{1}{2}(\mathbf{y}-\mathbf{G}\mathbf{a})^{\mathrm{H}} \mathbf{Q}^{-1}(\mathbf{y}-\mathbf{G}\mathbf{a})\right]. \tag{2.20}$$

Therefore the ML estimate of **a** is found by minimizing the following expression:

$$-2\ln p(\mathbf{y};\mathbf{a}) = (\mathbf{y}-\mathbf{G}\mathbf{a})^{\mathrm{H}} \mathbf{Q}^{-1}(\mathbf{y}-\mathbf{G}\mathbf{a}). \tag{2.21}$$

This minimization is obtained by setting the derivative of (2.21) to zero as

$$\frac{\partial \ln p(\mathbf{y};\mathbf{a})}{\partial \mathbf{a}} = \mathbf{G}^{\mathrm{H}}\mathbf{Q}^{-1}(\mathbf{y}-\mathbf{G}\mathbf{a}) = 0. \tag{2.22}$$

Solving (2.22) for **a** results in

$$\hat{\mathbf{a}}_{\mathrm{MLE}} = \left(\mathbf{G}^{\mathrm{H}}\mathbf{Q}^{-1}\mathbf{G}\right)^{-1} \mathbf{G}^{\mathrm{H}}\mathbf{Q}^{-1}\mathbf{y}, \tag{2.23}$$

which is, as explained before, the MVU estimate of **a**. This estimate of a, is itself a random variable with Gaussian distribution and can be represented by

$$\hat{\mathbf{a}}_{\mathrm{MLE}} \sim \mathcal{N}\left(\mathbf{a}, \mathbf{I}^{-1}(\mathbf{a})\right), \tag{2.24}$$

where in this case $\mathbf{I}(\mathbf{a}) = \mathbf{G}^{\mathrm{H}}\mathbf{Q}^{-1}\mathbf{G}$ (Kay 1993).

2.5.3 Least Squares Techniques

The optimal estimator described in the previous sub-section was based on the assumption of having prior knowledge about the PDF of the received data. However, there may be some cases where no assumption about the distribution of data can be made. In this sub-section another estimator is introduced that estimates deterministic unknown parameters without any assumption about the statistics of data, and only the signal model is assumed

to be linear. This estimator, namely the Least Squares (LS) estimator, has no optimality properties associated with it in general.

The LS approach attempts to minimize the squared difference between the received data and the estimated data. Considering the linear model in (2.19) and assuming that G is a full rank matrix, the LS estimator chooses the estimate of $\mathbf{a}$, $\hat{\mathbf{a}}_{\mathrm{LS}}$, so that it minimizes the following cost function:

$$J(\mathbf{a}) = (\mathbf{y} - \mathbf{G}\mathbf{a})^{\mathrm{H}} (\mathbf{y} - \mathbf{G}\mathbf{a}). \tag{2.25}$$

Setting the derivative of (2.25) results in

$$\frac{\partial J(\mathbf{a})}{\partial \mathbf{a}} = 2\mathbf{G}^{\mathrm{H}} (\mathbf{y} - \mathbf{G}\mathbf{a}) = 0. \tag{2.26}$$

Solving (2.26) for $\mathbf{a}$ results in the following solution:

$$\hat{\mathbf{a}}_{\mathrm{LS}} = (\mathbf{G}^{\mathrm{H}}\mathbf{G})^{-1} \mathbf{G}^{\mathrm{H}}\mathbf{y}. \tag{2.27}$$

The equality $\mathbf{G}^{\mathrm{H}}\mathbf{G}\mathbf{a} = \mathbf{G}^{\mathrm{H}}\mathbf{y}$ that leads to the solution in (2.27) is known as the normal equation.

It is important to notice that under the assumption of white noise process ($\mathbf{Q} = \sigma^2\mathbf{I}$) the ML solution in (2.23) reduces to the LS solution in (2.27).

Different alternatives of the LS estimation such as de-convolution approaches have been suggested in the literature for the problem of multipath delay estimation.

2.5.4 Bayesian Estimators

All estimators introduced by this sub-section were based on the assumption that unknown parameters to be estimated are deterministic constants. In this sub-section a class of

estimators will be introduced that assumes the unknown parameters are random variables whose particular realizations are to be estimated. This consideration provides the opportunity to take any available prior knowledge about the statistics of the parameters to be estimated into account, which leads to a more accurate estimation. This class of estimators is known as the Bayesian Approach since it is derived based on the Bayes' theorem. The objective of a Bayesian estimator is to minimize the Bayesian Mean Square Error (BMSE) of estimation. The resultant estimate can then be said to be optimal in the minimum BMSE sense with respect to the assumed prior PDF for the unknown random variables.

This Bayesian MSE which is fundamentally different from MSE in classical estimators, is defined as

$$BMSE\left(\hat{\mathbf{a}}_{\mathrm{B}}[i]\right)=\iint\left(\mathbf{a}[i]-\hat{\mathbf{a}}_{\mathrm{B}}[i]\right)^{2}p(\mathbf{y},\mathbf{a})\,d\mathbf{y}\,d\mathbf{a}\,. \tag{2.28}$$

where $p(\mathbf{y},\mathbf{a})$ is the joint PDF of $\mathbf{y}$, $\hat{\mathbf{a}}_{\mathrm{B}}$ is the Bayesian estimate of $\mathbf{a}$ and $\mathbf{a}[i]$ and $\hat{\mathbf{a}}_{\mathrm{B}}[i]$ are the i-th entry of $\mathbf{a}$ and $\hat{\mathbf{a}}_{\mathrm{B}}$, respectively. In fact, the BMSE in (2.28) is independent from the unknown random variable since it is obtained by averaging over the PDF of **a**. Taking advantage of the following Bayes' theorem

$$p(\mathbf{y},\mathbf{a})=p(\mathbf{a}|\mathbf{y})\,p(\mathbf{y}), \tag{2.29}$$

the equality in (2.28) can be simplified to

$$BMSE\left(\hat{\mathbf{a}}_{\mathrm{B}}\right)=\int\left(\mathbf{a}-\hat{\mathbf{a}}_{\mathrm{B}}\right)^{2}p(\mathbf{a}|\mathbf{y})\,d\mathbf{a}\,. \tag{2.30}$$

Minimizing (2.30) with respect to $\hat{\mathbf{a}}_{\mathrm{B}}$ results in the following Bayesian estimate:

$$\hat{\mathbf{a}}_{\mathrm{B}} = \int \mathbf{a} p\left(\mathbf{a}|\mathbf{y}\right) d\mathbf{a} = E\left[\mathbf{a}|\mathbf{y}\right]. \tag{2.31}$$

The right side of (2.31) is the mean of the *posteriori* PDF which is the PDF of **a** after data have been observed. For this reason, the estimator in (2.31) is referred to as the Minimum Mean Square Error (MMSE) estimator.

In cases where the system model is the linear model in (2.19) and the unknown random variables and noise samples are jointly Gaussian so that $\mathbf{a} \sim \mathcal{N}\left(\mu_{\mathbf{a}}, \mathbf{Q}_{\mathbf{a}}\right)$, the estimate in (2.31) can be simplified in a closed form as (Kay 1993):

$$\hat{\mathbf{a}}_{\mathrm{B}} = \boldsymbol{\mu}_{\mathbf{a}} + \mathbf{Q}_{\mathbf{a}}\mathbf{G}^{\mathrm{H}}\left(\mathbf{G}\mathbf{Q}_{\mathbf{a}}\mathbf{G}^{\mathrm{H}} + \mathbf{Q}\right)^{-1}\left(\mathbf{y} - \mathbf{G}\boldsymbol{\mu}_{\mathbf{a}}\right). \tag{2.32}$$

In this case **G** does not need to be full rank. An alternative form of (2.32) can be represented as

$$\hat{\mathbf{a}}_{\mathrm{B}} = \boldsymbol{\mu}_{\mathbf{a}} + \left(\mathbf{Q}_{\mathbf{a}}^{-1} + \mathbf{G}^{\mathrm{H}}\mathbf{Q}^{-1}\mathbf{G}\right)^{-1}\mathbf{G}^{\mathrm{H}}\mathbf{Q}^{-1}\left(\mathbf{y} - \mathbf{G}\boldsymbol{\mu}_{\mathbf{a}}\right). \tag{2.33}$$

It is important to consider that in the case where there is no prior information, $\mathbf{Q}_{\mathbf{a}}^{-1} \to \mathbf{0}$, the equality in (2.33) reduces to the ML estimate in (2.23), i.e. $\hat{\mathbf{a}}_{\mathrm{B}} \to \left(\mathbf{G}^{\mathrm{H}}\mathbf{Q}^{-1}\mathbf{G}\right)^{-1}\mathbf{G}^{\mathrm{H}}\mathbf{Q}^{-1}\mathbf{y}$. The linear MMSE estimator can be also solved sequentially as explained in Chapter 4.

Chapter Three: Sequential Maximum Likelihood Multipath Estimation

Given the limitations of the traditional code phase estimation techniques, this chapter considers another class of code tracking algorithms where the GNSS receiver endeavors to characterize the propagation channel by estimating the relative delay and amplitude of the first signal component to arrive and each individual reflection. Within this class, the most well-known approaches are those that are based on maximum likelihood (ML) estimation of the channel. In this chapter, some of the most promising ML-based multipath estimation algorithms are theoretically and empirically compared and a novel technique is then proposed. The studied algorithms include basic vector ML estimation of the channel that provides a delay profile for the entire search region, multipath delay estimation lock loop (MEDLL) (Van Nee 1992, Van Nee et al 1994, Townsend et al 1995, Van Nee 1997, Lohan et al 2005) that provides delay and amplitude estimates for a few of the strongest multipath components iteratively, and sequential maximum likelihood (SML) (Sahmoudi & Amin 2009) that sequentially estimates the path parameters using scalar ML estimation and iteratively modifies the estimates. In this chapter the disadvantages of each approach are addressed and a novel technique is proposed that targets these disadvantages. In the proposed approach, which is referred to as the modified sequential maximum likelihood (MSML), a sequential maximum-likelihood channel estimation technique is developed in which the multipath components are estimated recursively and the effect of each path is removed before estimation of the next. Instead of considering a fixed number of paths, this algorithm predicts the existence

of each probable new path at every recursion through a General Likelihood Ratio Test (GLRT) for a certain probability of false-alarm after each refinement stage.

The performances of these four techniques are compared through a selection of simulation scenarios including urban, suburban, rural and open sky conditions. The main focus in the performance comparison of the algorithms is on the closely-spaced multipath scenario, since this situation is generally the most challenging, however, a successful algorithm should provide good performance both in the presence and absence of multipath.

3.1 Problem Formulation

The received signal in a multipath environment is represented by an *M*-path model, composed of the LOS signal and (*M*-1) reflected rays corrupted by additive Gaussian noise with zero mean, $n(t)$, and can be represented by

$$r(t) = \sum_{k=1}^{M} A_k s(t - \tau_k) e^{j\phi_k} + n(t) \tag{3.1}$$

In this model A_k, ϕ_k and τ_k are the amplitude, phase shift and time delay parameters corresponding to the *k*-th path relative to the direct path ($A_1 = 1, \phi_1 = 0, \tau_1 = 0$) and $s(t)$ being the direct baseband spread spectrum signal which carries the navigation data bits. Considering the above signal model, the received baseband signal after being correlated with a local replica of the spreading code, coherently integrated over c and sampled at the rate of $\frac{1}{T_s}$, can be expressed as

$$y(\tau)=\sum_{k=1}^{M} a_k g(\tau-\tau_k)+w(\tau), \qquad \tau=0,T_s,\ldots,(N-1)T_s \tag{3.2}$$

where $a_k = A_k e^{j\phi_k}$ is the complex path coefficient corresponding to the *k*-th path and $g(\tau)$ is the ideal autocorrelation function of the PN code with the period of T_p and $w(\tau)$ is the noise term at the output of the correlator with a variance of σ_w^2. The path parameters are assumed to be unchanged during the integration time. Eq. (2) can be written in matrix form as

$$\mathbf{y}=\mathbf{G}\,\mathbf{a}+\mathbf{w}, \tag{3.3}$$

where **y** is the vector of the samples of $y(\tau)$ with a length of $N=\left\lfloor \frac{T_p}{T_s} \right\rfloor$ and

$$\mathbf{a}=[a_1\ a_2\ \ldots\ a_M] \tag{3.4}$$

The vector **w** with a length of *N* is the vector of noise samples with a covariance matrix of **Q** and **G** is an $N\times M$ matrix that can be represented as

$$\mathbf{G}=\left[\mathbf{g}_{\tau_1}\ \ \mathbf{g}_{\tau_2}\ \ldots\ \mathbf{g}_{\tau_M}\right] \tag{3.5}$$

where $\mathbf{g}_{\tau_m}$ is sampled version of $g(\tau-\tau_m)$ and can be represented by

$$\mathbf{g}_{\tau_m}=\left[g(0-\tau_m)\ g(T_s-\tau_m)\ldots g\left((N-1)T_s-\tau_m\right)\right]^{\mathrm{T}} \tag{3.6}$$

3.2 Maximum Likelihood Channel estimation

Given the fact that the true multipath delays are unknown to the receiver beforehand, a search region around the global maximum of the correlation function is considered. Thus,

if T is the length of the search region (which is usually selected as a few chips around the correlation function peak), there are $L = \left\lfloor \frac{T}{T_\delta} \right\rfloor$ equally spaced search points, where T_δ is the delay between two adjacent points. Considering this fact, (3.3) can be rewritten as

$$\mathbf{y} = \bar{\mathbf{G}}\,\bar{\mathbf{a}} + \mathbf{w}, \tag{3.7}$$

where $\bar{\mathbf{G}}$ is now an $N \times L$ matrix and is defined as

$$\bar{\mathbf{G}} = \left[\mathbf{g}_{\bar{\tau}_1} \;\; \mathbf{g}_{\bar{\tau}_2} \;\; \cdots \;\; \mathbf{g}_{\bar{\tau}_L} \right], \tag{3.8}$$

with $\bar{\tau}_i = (i-1)T_\delta$; $\bar{\mathbf{a}}$ has a length of L and can be described by

$$\bar{\mathbf{a}}[i] = \begin{cases} \mathbf{a}[m] & \text{if} \quad \bar{\tau}_i = \tau_m \in \{\tau_1, \tau_2, ..., \tau_M\} \\ 0 & \text{elsewhere} \end{cases}. \tag{3.9}$$

where $\bar{\mathbf{a}}[i]$ is the i$^{\text{th}}$ entry of $\bar{\mathbf{a}}$. Considering (3.7), the maximum likelihood (ML) estimate of $\bar{\mathbf{a}}$ will be (Kay 1993)

$$\hat{\mathbf{a}} = \left(\bar{\mathbf{G}}^{\mathrm{H}} \mathbf{Q}^{-1} \bar{\mathbf{G}} \right)^{-1} \bar{\mathbf{G}}^{\mathrm{H}} \mathbf{Q}^{-1} \mathbf{y}. \tag{3.10}$$

Since the system model in (3.7) is a linear model and the noise component follows the Gaussian distribution, the performance of ML estimate in (3.10) attains the Cramer-Rao Lower Band (CRLB) (Kay 1993). Hence, the covariance matrix of the estimate in (3.10) can be expressed as

$$\mathbf{C}_{\bar{\mathbf{a}}} = \left(\mathbf{I}(\bar{\mathbf{a}}) \right)^{-1}. \tag{3.11}$$

where $\mathbf{I}(\bar{\mathbf{a}})$ is the Fisher information matrix and can be represented by

$$\mathbf{I}(\bar{\mathbf{a}}) = \bar{\mathbf{G}}^{\mathrm{H}}\mathbf{Q}^{-1}\bar{\mathbf{G}}\,. \tag{3.12}$$

In the case where the noise process is white ($\mathbf{Q} = \sigma_w^2\mathbf{I}$), (3.12) can be written in a simpler form as

$$\left\{\mathbf{I}(\bar{\mathbf{a}})\right\}_{ij} = \frac{\left(\mathbf{g}_{\tau_i}^{\mathrm{H}}\mathbf{g}_{\tau_j}\right)}{\sigma_w^2}\,. \tag{3.13}$$

Increasing the number of parameters to be estimated (L) expands the Fisher information matrix by adding similar elements to the matrix and this does not affect the previous members. However, as it is proven in Appendix A, when this matrix is inverted to form the estimation covariance matrix ($\mathbf{C}_{\bar{\mathbf{a}}}$), the expansion of $\mathbf{I}(\bar{\mathbf{a}})$ results in an increase in the diagonal elements of $\mathbf{C}_{\bar{\mathbf{a}}}$ which are equivalent to the variance of the estimation of individual elements of $\bar{\mathbf{a}}$. Therefore, since in the MLE solution of (3.10) all of the elements of $\bar{\mathbf{a}}$ are estimated at once, the performance of the estimation of the parameters of interest is adversely affected by increasing the number of search points. In Figure 3-1, the diagram of variations of the normalized CRLB of the estimation of each of the elements of a vector $\mathbf{a}$ with 3 elements versus different values of the length of $\bar{\mathbf{a}}$, *m*, is shown using the results described in APPENDIX A. The vertical axis represents the ratio of CRLB for a certain value of *m* to CRLB for *m* = 3.

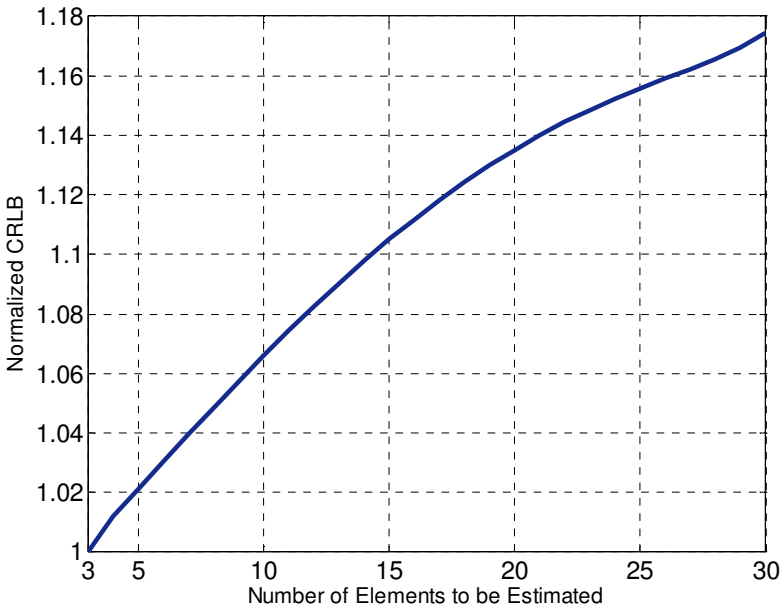

Figure 3-1: Normalized CRLB of estimation as a function of the number of elements to be estimated

To enhance the estimation performance of the solution in (3.10), which we refer to as vector ML, at low SNRs it is usually combined with some post processing techniques. This post processing includes considering some constraints based on some prior knowledge about the distribution or range of the multipath delays or amplitudes (Kostic & Pavlovic 1999). In the case where the Probability Distribution Function (PDF) of a path parameter is priori known, some goodness of fit (GOF) evaluation can be applied to the estimated paths to find the LOS (Kim 2004).

3.3 Multipath estimation Delay Lock Loop

To accommodate the problem of decreasing estimation performance discussed in the previous section, a new ML-based algorithm, namely the Multipath Estimation Delay Lock Loop (MEDLL), was proposed (Van Nee 1992, Van Nee et al 1994, Townsend 1995, Van Nee 1997, Lohan et al 2005). In this ML based algorithm, instead of

estimating all of the multipath components at once, which results in the estimation of some undesired parameters, major multipath channel components are estimated one by one.

In the original MEDLL algorithm (Van Nee 1992), the parameters of the i-th multipath signal are estimated as

$$\hat{\tau}_i = \max_{\overline{\tau}_i} \left\{ y\left(\overline{\tau}_i\right) - \sum_{\substack{j=0 \\ j\neq i}}^{M} \hat{a}_j g\left(\overline{\tau}_i - \hat{\tau}_j\right) \right\}. \tag{3.14}$$

$$\hat{A}_i = \left\| y\left(\hat{\tau}_i\right) - \sum_{\substack{j=0 \\ j\neq i}}^{M} \hat{a}_j g\left(\hat{\tau}_i - \hat{\tau}_j\right) \right\| \tag{3.15}$$

$$\hat{\theta}_i = \angle \left(y\left(\hat{\tau}_i\right) - \sum_{\substack{j=0 \\ j\neq i}}^{M} \hat{a}_j g\left(\hat{\tau}_i - \hat{\tau}_j\right) \right) \tag{3.16}$$

where the notation $\hat{x}$ denotes the estimation x. Solving the equations (3.14) to (3.16) is equivalent to performing a nonlinear curve fit to find a set of reference correlation functions with certain parameters that give the best possible fit on the input correlation function. However, when estimating the parameters of the entire multipath components at once by using a large search space, the same problem that was discussed in the previous section will arise, in addition to the implementation being too costly. To deal with this problem, Van Nee (1997) proposed an Interference Cancellation (IC) technique with the following steps in MEDLL:

Step 1) Set $y^{(i)}(\tau)$ to $y(\tau)-\sum_{k=0}^{i-1}\hat{A}_k e^{j\hat{\theta}_k} g(\tau-\hat{\tau}_k)$.

Step 2) Find the global maximum of $y^{(i)}(\tau)$ and estimate $\hat{\tau}_i$, $\hat{A}_i$ and $\hat{\theta}_i$.

Step 3) Re-estimate $\hat{\tau}_k$, $\hat{A}_k$, and $\hat{\theta}_k$ for $k<i$ by finding the global maximum of

$$y^{(ik)}(\tau)=y(\tau)-\sum_{\substack{l=0\\ l\neq k}}^{i}\hat{A}_l e^{j\hat{\theta}_l} g(\tau-\hat{\tau}_l).$$

Step 4) If not converged go back to step 2.

Step 5) If $i<m$ increment i and go back to step 1.

In step 5, *m* is the desired number of paths to be estimated.

In the approach discussed above, the parameters corresponding to the maximum of the correlation function are directly selected as the path parameters. However, in the presence of multipath, there is no independent relationship between the delay, amplitude and phase of the peak of the correlation function and the parameters of each individual multipath component. Therefore, when the number of paths is large, there is no guarantee that the iterative procedure converges. In Figure 3-2, the steps of MEDLL in estimating a simulated channel are shown. For the case of this figure, the number of components to be estimated has been set to 4 (this value is chosen based on the statistical parameters of an urban channel presented in Table 3-1).

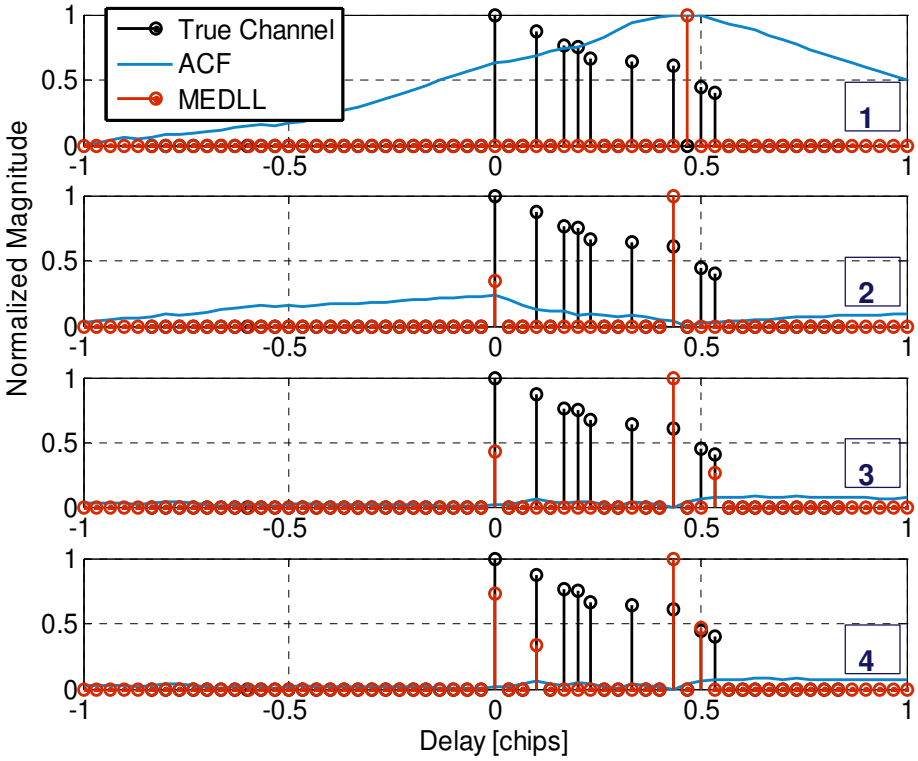

Figure 3-2: An example of different stages of MEDLL in estimating a simulated channel (C/N_0 =35 dB-Hz)

3.4 Sequential ML

Another noteworthy ML-based algorithm, proposed in (Sahmoudi & Amin 2009), is referred to as the sequential ML (SML) Algorithm. The SML algorithm estimates the parameters of the paths sequentially using the following set of ML-based equations:

$$\hat{\tau}_i = \arg\max_{\bar{\tau}_k} \frac{\mathbf{g}_{\bar{\tau}_k}^{\mathrm{H}} \mathbf{Q}^{-1} \mathbf{y}}{\mathbf{g}_{\bar{\tau}_k}^{\mathrm{H}} \mathbf{Q}^{-1} \mathbf{g}_{\bar{\tau}_k}}, \tag{3.17}$$

$$\hat{a}_i = \frac{\mathbf{g}_{\hat{\tau}_i}^{\mathrm{H}} \mathbf{Q}^{-1} \mathbf{y}}{\mathbf{g}_{\hat{\tau}_i}^{\mathrm{H}} \mathbf{Q}^{-1} \mathbf{g}_{\hat{\tau}_i}}. \tag{3.18}$$

Equations (3.17) and (3.18) are based on the assumption that there is only a single signal component in the received signal. Similar to MEDLL, the structure of the SML algorithm can be summarized by the following steps:

Step 1) Set $y^{(i)}(\tau)$ to $y(\tau)-\sum_{k=0}^{i-1}\hat{A}_k e^{j\hat{\theta}_k} g(\tau-\hat{\tau}_k)$.

Step 2) Substitute $y^{(i)}(\tau)$ into Eq. (15-16) to find $\hat{\tau}_i$, $\hat{A}_i$ and $\hat{\theta}_i$.

Step 3) Re-estimate $\hat{\tau}_k$, $\hat{A}_k$, and $\hat{\theta}_k$ for $k<i$ by substituting

$y^{(ik)}(\tau)=y(\tau)-\sum_{\substack{l=0\\ l\neq k}}^{i}\hat{A}_l e^{j\hat{\theta}_l} g(\tau-\hat{\tau}_l)$ into (3.17) and (3.18).

Step 4) If not converged go back to step 2.

Step 5) If $i<m$ increment i and go back to step 1.

It should be noted that for this algorithm, since the values of delays and complex coefficients are computed from an ML estimate of the channel, the required number of iterations to meet the convergence will be smaller than that of the MEDLL. In Figure 3-3, different steps of SML in estimating a simulated channel are shown. In this case, the LOS to residual power ratio is greater than the SNR after estimating the three paths. It is clear, however, that due to the low accuracy of the algorithm, the estimated components are not exactly located at positions of the true multipath components.

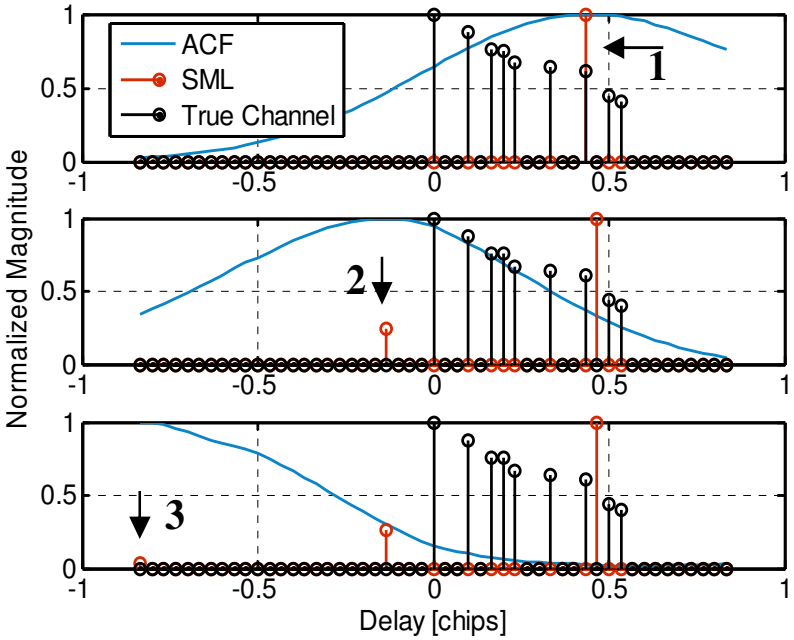

Figure 3-3: An example of different stages of SML in estimating a simulated channel

3.5 Proposed Algorithm

The sequential ML algorithm discussed in the previous section is able to find optimum estimates for the parameters of individual paths by considering the estimation of only one path at the time. However, there are still some problems that need to be considered.

Firstly, in the MEDLL algorithm, the number of signal paths is considered fixed and known. However, considering a fixed number of paths may result in underestimation or overestimation of the true number of paths which, in turn, may lead to a bias in the final ranging solution due to the unresolved multipath components or trusting on noise peaks respectively. Furthermore, in the SML algorithm, a threshold equal to the receiver's signal to noise ratio (SNR) is compared with the LOS-to-residual signal power ratio to find an estimate for the number of paths. This requires an exact knowledge of the SNR and results in a lack of system robustness. Secondly, for both of these algorithms,

iterations are required for refining the estimates of the path coefficients. In this section, we propose a modified sequential ML algorithm (MSML) that targets these problems and can be described by the following steps:

Step 1) Sequential ML estimation

Step 2) Refinement of estimated parameters

Step 3) Detection of new paths

Step 4) Update of the noise covariance matrix

In estimating each multipath component, all the above four steps are repeated once. In the rest of this section, the above steps are explained in detail. The flowchart of the algorithm is shown in Figure 3-4.

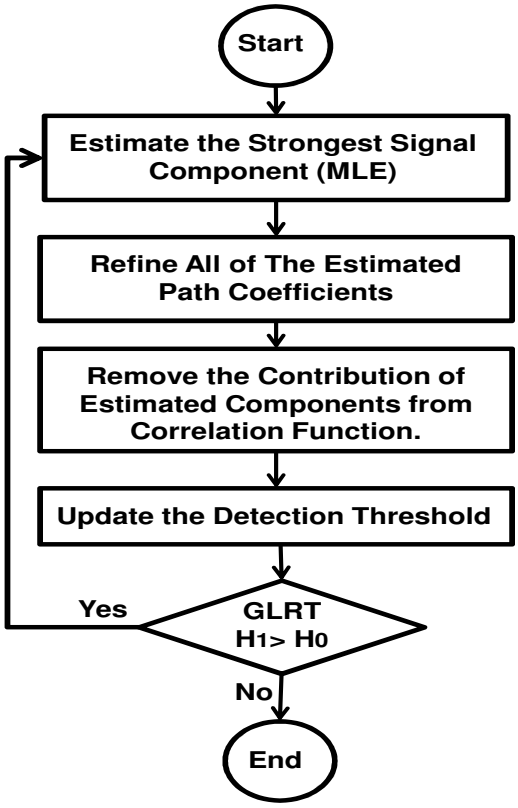

Figure 3-4: Flowchart of MSML algorithm

3.5.1 A. Sequential ML

In the first step of the MSML algorithm, the vector $\hat{\mathbf{a}}$ is computed from (3.10) and the maximum element of the estimated vector and its corresponding delay and complex coefficients are determined as the initial estimates of the parameters of the current path. The reason for using (3.10) instead of (3.17) in finding the delay of the current strongest path is that, since the pair of (3.17) and (3.18) is based upon the assumption that only one signal component is present, when there are more than one signal path (which it is the case in a multipath channel), it is no longer an efficient ML estimate. In Figure 3-5, the functionalities of these two approaches in estimating the delay of the first path of a simulated 5-path channel profile are compared wherein "ML" refers to (3.10) and "SML" refers to (3.17). This figure shows that although, and as was expected, the channel estimated by (3.10) is not perfectly matched to the true channel, it is a better option for finding the first path than (3.17). Similar to the two previous techniques, after estimating the parameters of each new path, its contribution is subtracted from the correlation function to yield a new approximation of the correlation function and the residual correlation function is substituted in (3.10) to estimate the parameters of the next path using the maximum element of the estimated vector. This step of the algorithm is then followed by refining the parameters of all of the estimated paths, as explained in the next sub-section.

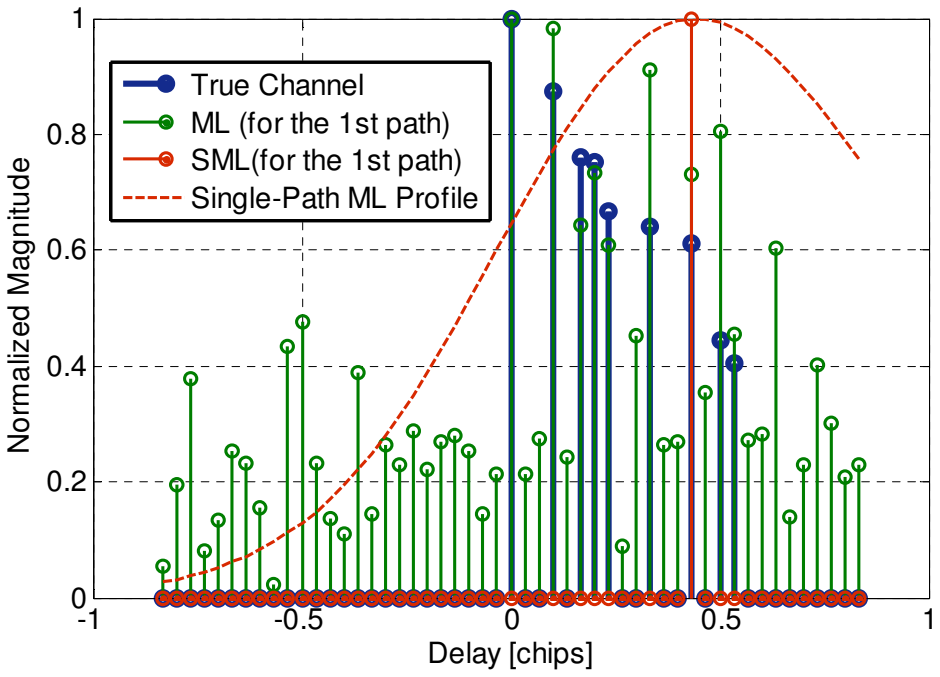

Figure 3-5: A comparison of the functionality of Eq. (3.10) and (3.17) when finding the first path (C/N_0 = 35 dB-Hz)

3.5.2 B. Refinement

In general, in the MSML algorithm, after detecting each new path (m^{th} path), the estimated parameters for all of the previously detected paths are refined as follows:

$$\hat{\mathbf{a}}_m = \begin{bmatrix} \hat{a}_1 \\ \hat{a}_2 \\ \vdots \\ \hat{a}_m \end{bmatrix} = \left(\bar{\mathbf{G}}_m^T \mathbf{Q}^{-1} \bar{\mathbf{G}}_m\right)^{-1} \bar{\mathbf{G}}_m \mathbf{Q}^{-1} \mathbf{y}\,, \tag{3.19}$$

where

$$\bar{\mathbf{G}}_m = \left[\mathbf{g}_{\hat{\tau}_1}\ \mathbf{g}_{\hat{\tau}_2}\ \cdots\ \mathbf{g}_{\hat{\tau}_m}\right]. \tag{3.20}$$

The difference between $\bar{\mathbf{G}}_m$ and $\bar{\mathbf{G}}$ is that $\bar{\mathbf{G}}_m$ only includes those columns of $\bar{\mathbf{G}}$ that correspond to the m estimated paths by that time. Therefore, since *m* is much smaller than *L*, the estimation performance in the refinement stage is considerably better than that in the first step. The solution in (3.19) is the ML estimate of the channel under the assumption that there are *m* multipath components present in the received signal. As opposed to the SML and MEDLL algorithms, the solution in (3.19) considers the mutual effects of these *m* signal components on each other (since multipath components are correlated) (Li & Pahlavan 2004). The other advantage of the proposed refinement stage is that it does not require iterations since it solves a linear equation.

3.5.3 C. Detection of New Paths

As opposed to the MEDLL and the SML, in the MSML algorithm the number of paths is not considered fixed. Instead, after each cycle of estimating a new path component and performing the refinement stage, the existence of a possible new path is detected through the Generalized Likelihood Ratio Test. In order to accomplish this goal, two different strategies can be considered in determining the threshold of detection. The first strategy is to consider the estimated parameters of all of the previously detected paths as deterministic known parameters when trying to examine the possibility of existence of a new path. The second strategy is to consider these parameters as nuisance parameters (Kay 1993). Herein, we explain the problem of detecting the (m+1)-th (possible) multipath component considering the parameters of all the m previously detected components as nuisance parameters since this assumption is more realistic. The first strategy is developed in Appendix B.

A new path (path m+1) is considered present if the following test ratio passes the threshold (hypothesis H_1):

$$L(\mathbf{y}) = \frac{p\left(\mathbf{y};\, \hat{a}_{m+1}, \hat{a}_m \left| \mathrm{H}_1, ..., \hat{a}_1 \right| \mathrm{H}_1\right)}{p\left(\mathbf{y};\, \hat{a}_m \left| \mathrm{H}_0, ..., \hat{a}_1 \right| \mathrm{H}_0\right)} > \gamma . \tag{3.21}$$

(3.21) can be expanded as

$$L(\mathbf{y}) = \frac{\frac{1}{(2\pi)^{\frac{N}{2}} \det^{\frac{1}{2}}(\mathbf{Q})} \exp\left(-\frac{1}{2}\left(\mathbf{y} - \bar{\mathbf{G}}_{m+1}\hat{\mathbf{a}}_{m+1}\right)^{\mathrm{H}} \mathbf{Q}^{-1}\left(\mathbf{y} - \bar{\mathbf{G}}_{m+1}\hat{\mathbf{a}}_{m+1}\right)\right)}{\frac{1}{(2\pi)^{\frac{N}{2}} \det^{\frac{1}{2}}(\mathbf{Q})} \exp\left(-\frac{1}{2}\left(\mathbf{y} - \bar{\mathbf{G}}_{m}\hat{\mathbf{a}}_{m}\right)^{\mathrm{H}} \mathbf{Q}^{-1}\left(\mathbf{y} - \bar{\mathbf{G}}_{m}\hat{\mathbf{a}}_{m}\right)\right)} > \gamma , \tag{3.22}$$

where vectors $\hat{\mathbf{a}}_m$ and $\hat{\mathbf{a}}_{m+1}$ are obtained from (3.19). By taking the logarithm of both sides of (3.22), it reduces to

$$\mathbf{y}^{\mathrm{H}}\mathbf{Q}^{-1}\bar{\mathbf{G}}_{m+1}\hat{\mathbf{a}}_{m+1} - \mathbf{y}^{\mathrm{H}}\mathbf{Q}^{-1}\bar{\mathbf{G}}_{m}\hat{\mathbf{a}}_{m} - \frac{1}{2}\left(\hat{\mathbf{a}}_{m+1}^{\mathrm{H}}\bar{\mathbf{G}}_{m+1}^{\mathrm{H}}\mathbf{Q}^{-1}\bar{\mathbf{G}}_{m+1}\hat{\mathbf{a}}_{m+1} - \hat{\mathbf{a}}_{m}^{\mathrm{H}}\bar{\mathbf{G}}_{m}^{\mathrm{H}}\mathbf{Q}^{-1}\bar{\mathbf{G}}_{m}\hat{\mathbf{a}}_{m}\right) > \gamma' , \tag{3.23}$$

where $\gamma' = \log\gamma$. After substituting $\hat{\mathbf{a}}_m$ and $\hat{\mathbf{a}}_{m+1}$ from (3.19) into (3.21), the above can be represented as

$$\mathbf{y}^{\mathrm{H}}\mathbf{Q}^{-1}\left[\bar{\mathbf{G}}_{m+1}\left(\bar{\mathbf{G}}_{m+1}^{\mathrm{H}}\mathbf{Q}^{-1}\bar{\mathbf{G}}_{m+1}\right)^{-1}\bar{\mathbf{G}}_{m+1}^{\mathrm{H}} - \bar{\mathbf{G}}_{m}\left(\bar{\mathbf{G}}_{m}^{\mathrm{H}}\mathbf{Q}^{-1}\bar{\mathbf{G}}_{m}\right)^{-1}\bar{\mathbf{G}}_{m}^{\mathrm{H}}\right]\mathbf{Q}^{-1}\mathbf{y} > \gamma'' , \tag{3.24}$$

where $\gamma'' = 2\gamma'$. Furthermore, $\bar{\mathbf{G}}_{m+1}$ and $\bar{\mathbf{G}}_{m+1}^{\mathrm{H}}$ is given by

$$\bar{\mathbf{G}}_{m+1} = \left[\bar{\mathbf{G}}_{m} \;\; \mathbf{g}_{\hat{\tau}_{m+1}}\right] , \tag{3.25}$$

and $\bar{\mathbf{G}}_{m+1}^{\mathrm{H}}\mathbf{Q}^{-1}\bar{\mathbf{G}}_{m+1}$ can be represented as

$$\bar{\mathbf{G}}_{m+1}^{\mathrm{H}}\mathbf{Q}^{-1}\bar{\mathbf{G}}_{m+1}=\begin{bmatrix}\mathbf{A} & \mathbf{B}\\ \mathbf{B}^{\mathrm{H}} & \alpha\end{bmatrix}, \tag{3.26}$$

where $\mathbf{A}=\bar{\mathbf{G}}_{m}^{\mathrm{H}}\mathbf{Q}^{-1}\bar{\mathbf{G}}_{m}$, $\mathbf{B}=\bar{\mathbf{G}}_{m}^{\mathrm{H}}\mathbf{Q}^{-1}\mathbf{g}_{\hat{\tau}_{m+1}}$ and $\alpha=\mathbf{g}_{\hat{\tau}_{m+1}}^{\mathrm{H}}\mathbf{Q}^{-1}\mathbf{g}_{\hat{\tau}_{m+1}}$ is a constant scalar. Taking advantage of Equation (A.2) in Appendix A, the inverse of the block matrix in (3.26) results in

$$\left(\bar{\mathbf{G}}_{m+1}^{\mathrm{H}}\mathbf{Q}^{-1}\bar{\mathbf{G}}_{m+1}\right)^{-1}=\begin{bmatrix}\left(\mathbf{A}-\dfrac{\mathbf{B}\mathbf{B}^{\mathrm{H}}}{\alpha}\right)^{-1} & \dfrac{-\mathbf{A}^{-1}\mathbf{B}}{\alpha-\beta}\\ -\dfrac{1}{\alpha}\mathbf{B}^{\mathrm{H}}\left(\mathbf{A}-\dfrac{\mathbf{B}\mathbf{B}^{\mathrm{H}}}{\alpha}\right)^{-1} & \dfrac{1}{\alpha-\beta}\end{bmatrix}, \tag{3.27}$$

where $\beta=\mathbf{B}^{\mathbf{H}}\mathbf{A}^{-1}\mathbf{B}$. Applying *Woodbury's identity* (Noble & Daniel 1977) to $\left(\mathbf{A}-\dfrac{\mathbf{B}\mathbf{B}^{\mathrm{H}}}{\beta}\right)^{-1}$ it can be shown that

$$\left(\mathbf{A}-\frac{\mathbf{B}\mathbf{B}^{\mathrm{H}}}{\alpha}\right)^{-1}=\mathbf{A}^{-1}+\frac{\mathbf{A}^{-1}\mathbf{B}\mathbf{B}^{\mathrm{H}}\mathbf{A}^{-1}}{\alpha-\beta}. \tag{3.28}$$

After applying (3.28) into (3.27) and then substituting (3.25) and (3.27) into (3.24), and applying some simplifications, the inequality of (3.24) can be re-written as

$$\mathbf{y}^{\mathrm{H}}\mathbf{Q}^{-1}\left[\mathbf{D}\mathbf{g}\left(\tau-\hat{\tau}_{m+1}\right)\mathbf{g}^{\mathrm{H}}\left(\tau-\hat{\tau}_{m+1}\right)\mathbf{D}^{\mathrm{H}}\right]\mathbf{Q}^{-1}\mathbf{y}>\gamma''', \tag{3.29}$$

where $\gamma'''=\gamma''\left(\alpha-\beta\right)$ and $\mathbf{D}$ is a constant $N\times N$ matrix that can be represented as

$$\mathbf{D}=\bar{\mathbf{G}}_{m}\left(\bar{\mathbf{G}}_{m}^{\mathrm{H}}\mathbf{Q}^{-1}\bar{\mathbf{G}}_{m}\right)^{-1}\bar{\mathbf{G}}_{m}^{\mathrm{H}}\mathbf{Q}^{-1}-\mathbf{I}, \tag{3.30}$$

where $\mathbf{I}$ is the $N \times N$ identity matrix. Using the variable change of $z = \mathbf{y}^{\mathrm{H}} \mathbf{Q}^{-1} \mathbf{D}\,\mathbf{g}\left(\tau - \hat{\tau}_{m+1}\right)$, the sufficient statistics in (3.30) can be represented as

$$T(z) = zz^{\mathrm{H}} > \gamma''' . \tag{3.31}$$

The variable z in (3.31) is a complex Gaussian scalar random variable and its statistics under the two hypotheses can be expressed as

$$z \sim \begin{cases} \mathrm{N}\left(0, \sigma_{m+1}^2\right) & \text{under } \mathrm{H}_0 \\ \mathrm{N}\left(\mu_{m+1}, \sigma_{m+1}^2\right) & \text{under } \mathrm{H}_1 \end{cases}, \tag{3.32}$$

Where $\mu_{m+1} = \hat{\mathbf{a}}_{m+1}^{\mathrm{H}} \bar{\mathbf{G}}_{m+1}^{\mathrm{H}} \mathbf{Q}^{-1} \mathbf{D}\,\mathbf{g}\left(\tau - \hat{\tau}_{m+1}\right)$ and σ_{m+1}^2 can be obtained by

$$\begin{aligned} \sigma_{m+1}^2 &= E\left\{z^H z\right\} \\ &= \mathbf{g}^{\mathrm{H}}\left(\tau - \tau_{m+1}\right) \mathbf{D}^{\mathrm{H}} \mathbf{Q}^{-1} E\left\{\mathbf{y}\mathbf{y}^{\mathrm{H}}\right\} \mathbf{Q}^{-1} \mathbf{D}\mathbf{g}\left(\tau - \tau_{m+1}\right), \\ &= \mathbf{g}^{\mathrm{H}}\left(\tau - \tau_{m+1}\right) \mathbf{D}^{\mathrm{H}} \mathbf{Q}^{-1} \mathbf{D}\mathbf{g}\left(\tau - \tau_{m+1}\right) \end{aligned} \tag{3.33}$$

Thus, $T(z)$ follows a chi-square distribution with two degrees of freedom and can be expressed as

$$\frac{T(z)}{\sigma_{m+1}^2} \sim \begin{cases} \chi_2^2(0) & \text{under } \mathrm{H}_0 \\ \chi_2'^2\left(\lambda_{m+1}\right) & \text{under } \mathrm{H}_1, \end{cases} \tag{3.34}$$

where $\lambda_{m+1} = \mu_{m+1} \mu_{m+1}^*$. Finally, the probability of false-alarm can be expressed as

$$P_{FA} = \Pr\left\{\frac{T(z)}{\sigma_{m+1}^2} > \frac{\gamma'''}{\sigma_{m+1}^2}; \mathrm{H}_0\right\} = Q_{\chi_2^2}\left(\frac{\gamma'''}{\sigma_{m+1}^2}\right) = \exp\left(-\frac{\gamma'''}{2\sigma_{m+1}^2}\right). \tag{3.35}$$

Therefore, for a certain probability of false-alarm, the threshold of detection can be determined as

$$\gamma'' = -2\mathbf{g}^{\mathrm{H}}(\tau - \tau_{m+1})\mathbf{D}^{\mathrm{H}}\mathbf{Q}^{-1}\mathbf{D}\mathbf{g}(\tau - \tau_{m+1})\ln(P_{FA}). \tag{3.36}$$

It is shown in Appendix B that the first strategy introduced at the beginning of this section also results in a sufficient statistics of Chi-squared distribution with two degrees of freedom but with a different threshold that is given by (B-12).

Finally, in order to set a reasonable value for the probability of false-alarm, two important points must be considered. First, the probability of existence of each new signal path is smaller than the one of the previous path. Urban channel characterization work (Jahn et al 1996, Fontan et al 2001) has shown that the probability density function (PDF) of the number of paths in urban and suburban channels follows the Poisson distribution. Therefore, the level of the probability of false-alarm in setting the threshold of detection for each new signal path should be inversely proportional to the cumulative distribution function (CDF) of the Poisson distribution. The other factor that must be considered in setting a value for P_{FA} is that, as the number of paths to be detected increases, since the number of nuisance parameters and consequently the level of uncertainty increases, the probability of detection of the new path is decreased accordingly. However, in Figure 3-6 (which is a Monte-Carlo simulation) it is shown that when the number of paths to be

detected (m) is larger than two (which is usually the case in urban and suburban channels), this adverse effect is insignificant and can therefore be ignored. This figure shows the Receiver Operating Characteristic (ROC) curves of the system which are the diagrams of P_D versus P_{FA} (as the threshold of detection is varied) for different values of the number of multipath components to be detected.

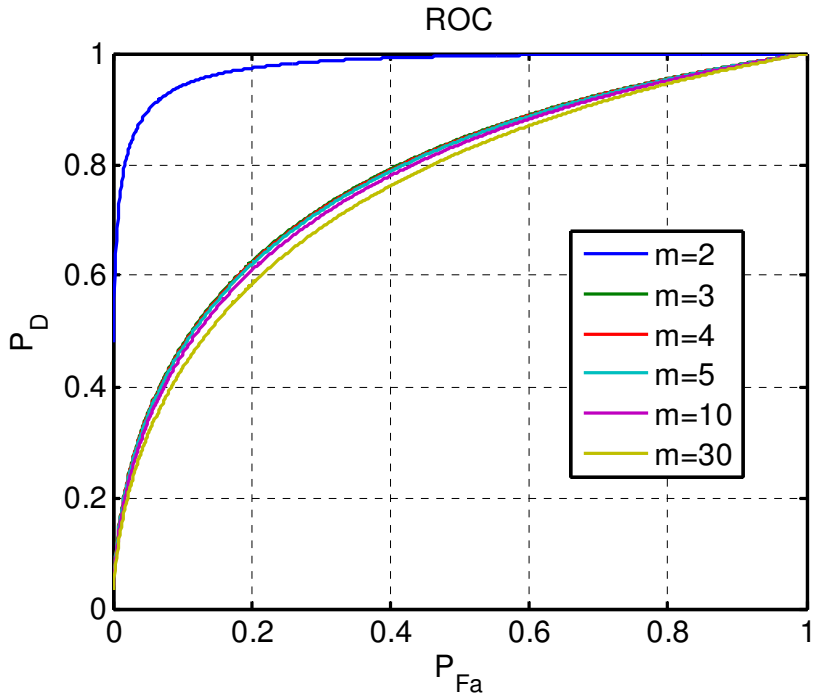

Figure 3-6: Performance of detector (Receiver Operating Characteristic (ROC)) for different values of m (number of parameters to be estimated) at C/N_0 = 35 dB-Hz

3.5.4 Updating the Noise Covariance Matrix

The covariance matrix of the colored noise is updated by averaging (moving average) the remaining signal after the sufficient statistics computed via (3.25) falls below the adaptive threshold (the reason of using a moving average was to be able to track the changes in the channel). This step can be expressed as

$$\mathbf{Q}_n = \mathbf{Q}_{n-1} + \left(\mathbf{y}_n^{(M')}\right)^{\mathrm{H}} \mathbf{y}_n^{(M')} - \mathbf{Q}_{n-K} \,. \tag{3.37}$$

where n, n-1 and n-K are time indices, K is the length of the moving average window, M' is the final number of estimated paths at the current time epoch and $\mathbf{y}_n^{(M')} = \mathbf{y}_n - \sum_{l=0}^{M'} \hat{A}_l e^{j\hat{\theta}_l} \mathbf{g}\left(\tau - \hat{\tau}_l\right)$. In Figure 3-7, an example of the steps of MSML in estimating a simulated channel is shown. For the case of this figure, after estimating four multipath components, the applied GLRT has failed and the algorithm has stopped estimating new components.

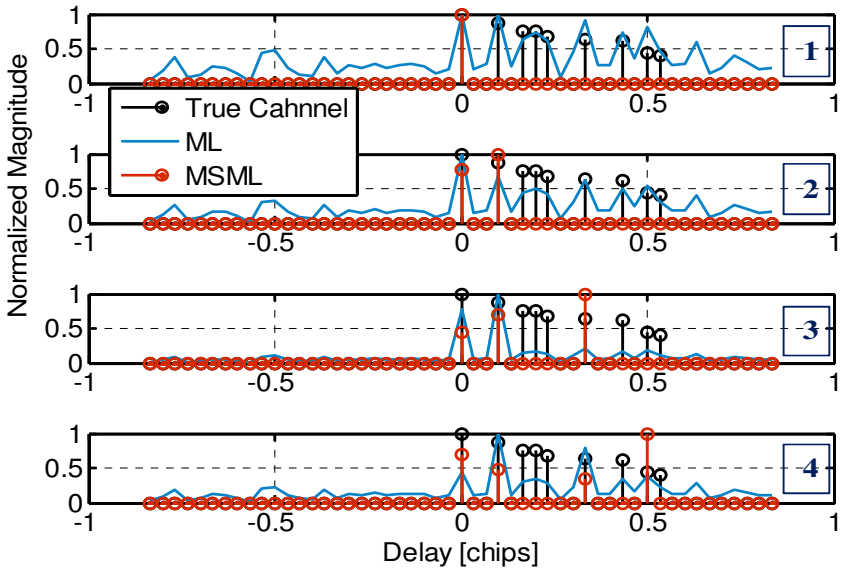

Figure 3-7: An example of different stages of MSML in estimating a simulated channel (C/N_0=35)

3.6 Simulation Results

To evaluate the effectiveness of the proposed multipath estimation/detection approach and compare its performance to the three other ML-based techniques, a set of realistic

simulation scenarios was considered. In these simulations, an intermediate frequency (IF) GPS L1 C/A signal with a sampling rate of 20 MHz was used. The coherent integration time was 10 ms. The reason for selecting this value for T_c is that the choice of coherent integration time should be larger than 1 ms (one epoch of the C/A code) and smaller than 20 ms (since we considered a non-data-aided scenario). Within this range, the performance of the receiver is insensitive to the choice of T_c and 10 ms is a value used for high sensitivity receivers operating in urban canyons and indoors. Since the maximum excessive delay of the channel for near echoes, which are the stronger echoes and therefore of more concern, is less than one chip in most environments (Jahn et al 1996), the focus here is to search for those components with sub-chip level delays. Therefore we consider the search region to be ± 1 chip around the correlation peak. Herein, only one signal from one of the satellites is considered whereas the contribution of the signals from other satellites is modeled as AWGN due to the weakness of their interference. Three different simulation scenarios including urban, suburban and rural were considered. For these simulation scenarios, it was assumed that the channel follows a Rician fading model with a mean of μ and a standard deviation of σ, the number of multipath components follows a Poisson distribution with a mean of λ_p and the relative multipath delays follow an exponential distribution with a mean of b. The parameters used to characterize the simulated channels are given in Table 3-1 (Jahn et al 1996).

Table 3-1: Parameters of the simulated channels

Scenario	Elevation	λ_p	Max	b Exp. [μs]	μ [dB]	σ [dB]

	[degrees]	Poisson	Delay [ns]			
Urban	$45^\circ - 55^\circ$	3.7	600	0.08	-3	2.7
Suburban	$45^\circ - 55^\circ$	1.6	400	0.03	-7.5	2.9
Rural	$45^\circ - 55^\circ$	1.7	400	0.05	-6.3	3.1

Figure 3-8 to 3-10 compare the root mean square (RMS) values of the LOS delay estimation errors produced by the four vector ML, MEDLL, SML and MMSL techniques under the three different simulation scenarios (the title "ML" in the legend of the figures refers to the "vector ML" approach). The applied Monte Carlo simulations were run over 4000 epochs of data for each value of carrier to noise ratio (C/N_0) and the simulated channel was altered every 100 ms. The value of the number of paths to be estimated (m) for the MEDLL and SML was set to 3 for the three figures. Since the estimated profile by the vector ML method has non zero values at all the delays within the search region, in order to select the LOS peak for this algorithm, a goodness of fit value was attributed to each peak in the profile and the one with the maximum value was selected. The considered GOF function correlates the histogram of the delays corresponding to all of the peaks coming after each candidate peak with the PDF of the exponential distribution that was used in simulating the channel to evaluate the level of fit.

As can be seen in the figures, under all of the simulation scenarios, the MSML outperforms the MEDLL in the sense of LOS delay estimation RMS error for C/N_0 values smaller than 35 dB-Hz. This improvement in the performance under weak signal conditions is a result of enhanced noise rejection at the detection step of the algorithm.

Among the four approaches compared, the MEDLL appears to be the most sensitive to multipath parameters and noise. The number of paths to be estimated is another factor that greatly affects the performance of the MEDLL. In Figure 3-11 the performance of the MEDLL for two different values of *m* are compared; increasing *m* actually increases the risk of relying on spurious peaks.

It is also evident from Figures 3-8 to 3-10 that the SML algorithm is biased, even for high C/N_0 values, especially under more severe multipath scenarios where the number of multipath components and their relative power is larger. Also increasing *m* has the same adverse effect on the SML as it has on the MEDLL. Since the MSML selects its first path from the vector ML profile in (3.10), under LOS conditions, the performances of the two techniques are very similar.

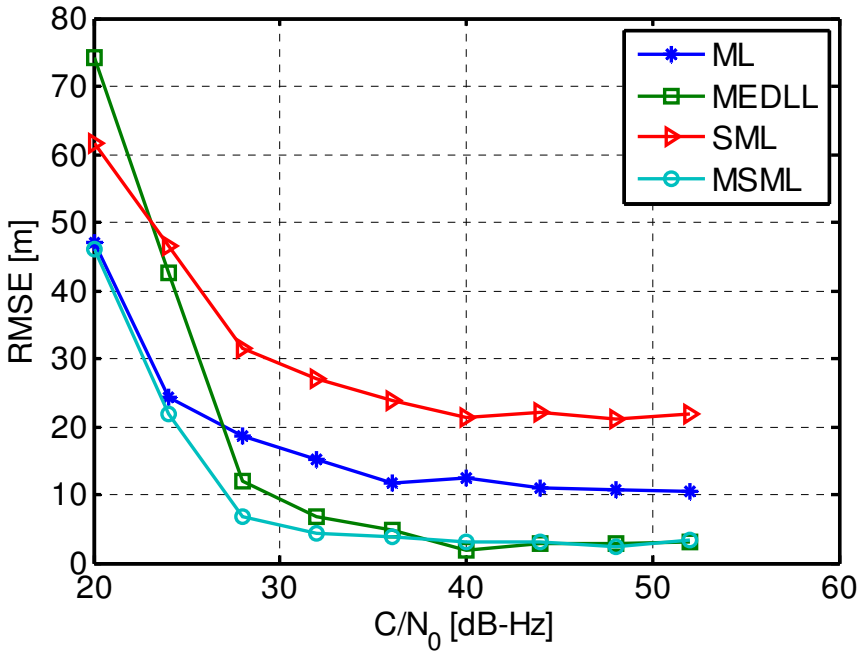

Figure 3-8: Comparison of ML-based estimation algorithms in the sense of LOS delay estimation for a fading channel with urban model characteristics

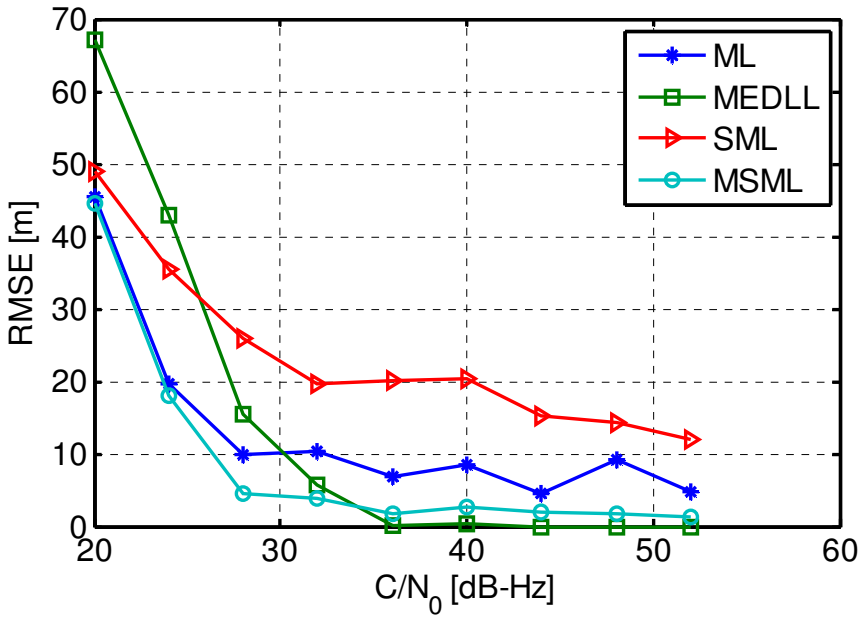

Figure 3-9: Comparison of ML-based estimation algorithms in the sense of LOS delay estimation for a fading channel with suburban model characteristics

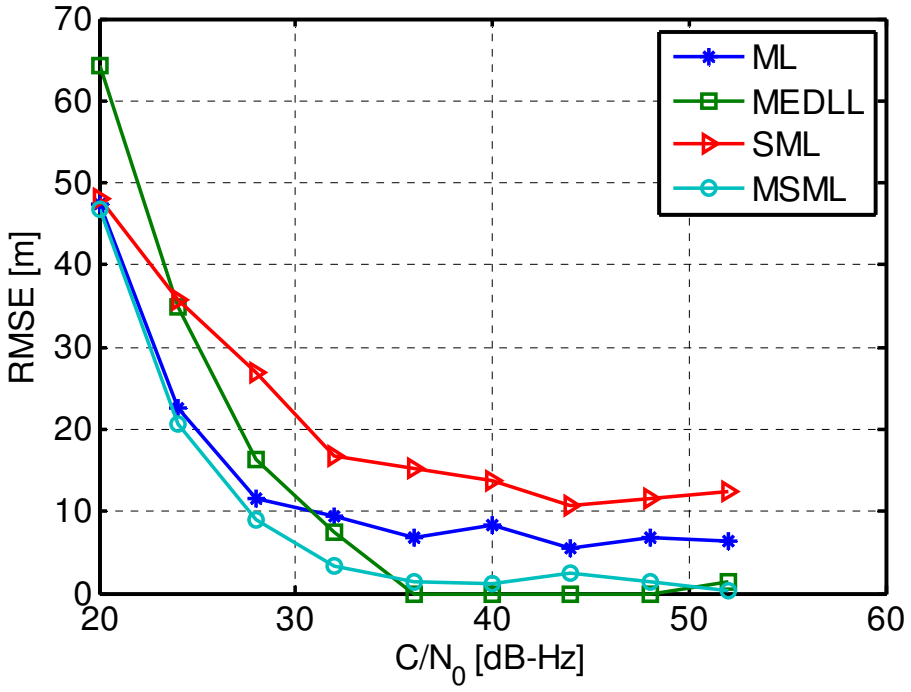

Figure 3-10: Comparison of ML-based estimation algorithms in the sense of LOS delay estimation for a fading channel with rural model characteristics

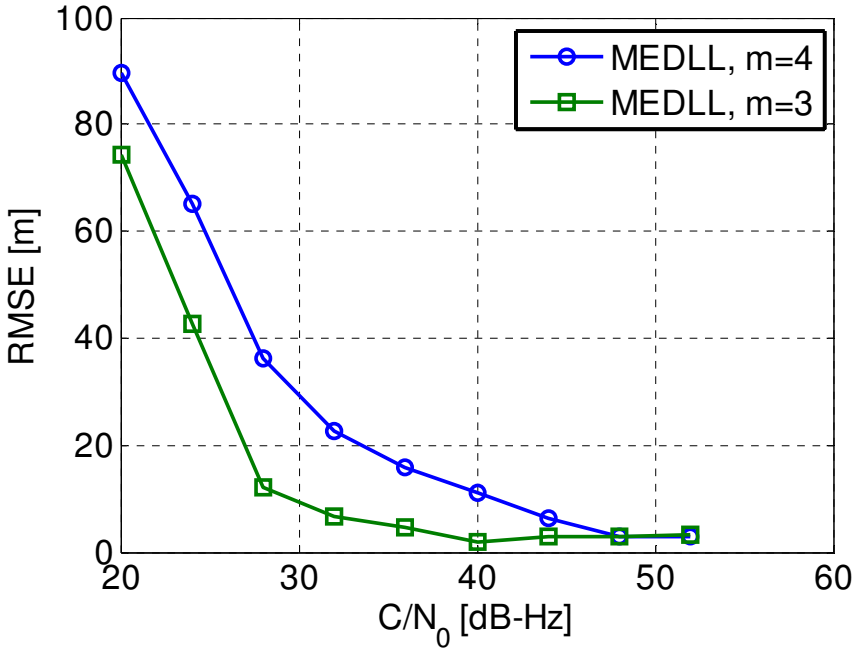

Figure 3-11: Comparison of performance of MEDLL for two different values of m under urban simulation scenario

In the previous set of figures (3-8 to 3-10) the performances of different approaches was compared in the sense of LOS delay estimation RMS error. However, the performance of the algorithm in this sense is heavily dependent on the strategy that it used to select the LOS index. It is also of interest to compare the performance of the studied approaches in the sense of their ability to estimate the entire channel correctly. In this sense, the error metric can be defined as the mean square of the difference between the estimated channel and the true one and can be represented as

$$\text{Channel MSE}=\frac{1}{N_t}\sum_{N_t}\left(\mathbf{h}_{\text{true}}-\mathbf{h}_{\text{estimated}}\right)\left(\mathbf{h}_{\text{true}}-\mathbf{h}_{\text{estimated}}\right)^{\text{H}}, \tag{3.38}$$

where N_t is the length of the observation period. Figure 3-12 and Figure 3-13 show the performance of the four approaches in the sense of channel MSE under urban and suburban channel simulation scenarios respectively. The vertical axis represents the channel MSE introduced in (3.38) divided by $\rho=\frac{1}{N_t}\sum_{N_t}\mathbf{h}_{\text{true}}\mathbf{h}_{\text{true}}^{\text{H}}$ and therefore it is unit-less.

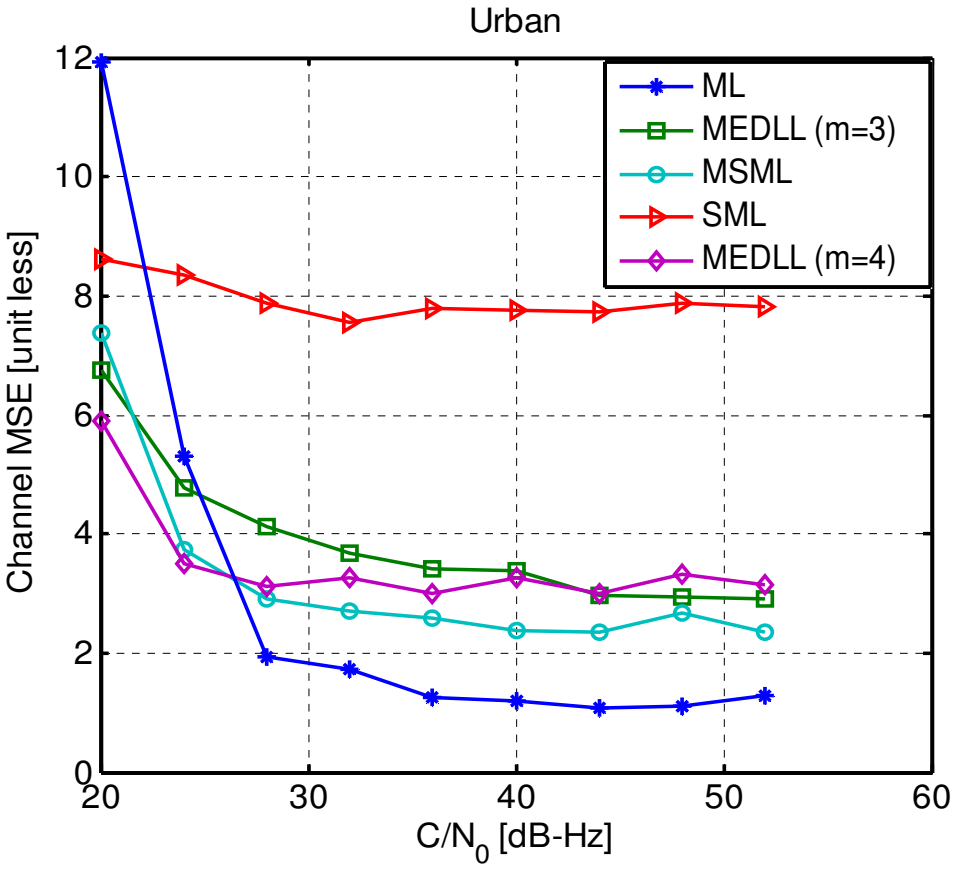

Figure 3-12: Comparison of ML-based estimation algorithms in the sense of channel MSE for a fading channel with urban model characteristics

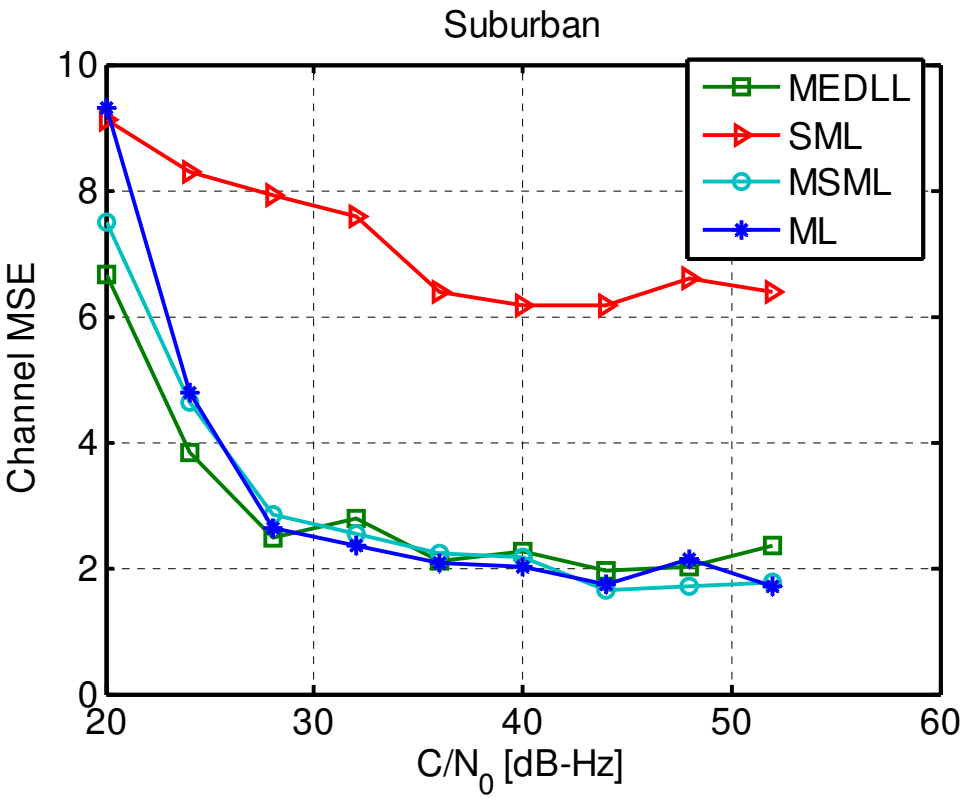

Figure 3-13: Comparison of ML-based estimation algorithms in the sense of channel MSE for a fading channel with suburban model characteristics

As opposed to the other three techniques that attempt to select a few peaks among all the components of the true channel, the vector ML profile has an estimate of the entire channel and therefore has the best channel MSE performance. Selecting the channel paths carefully and refining the estimates of the detected components, MSML performs better than the MEDLL and the SML and more poorly than the vector ML. The performance of MEDLL is still sensitive to the choice of m but this time, increasing m to a value close to the true number of paths increases the chance of estimating more channel components and improves the performance.

As it was shown in Figure 3-3, the estimated channel indices by the SML are rarely located at the exact delays corresponding to the multipath components due to the low resolution. Therefore, it generally performs the poorest of the four algorithms.

To further support the simulation results, a set of related data processing results will be presented in Chapter 4.

3.7 Summary and Conclusions

A novel sequential ML-based multipath parameter estimation technique was proposed herein. The novel algorithm was compared to some of the well-known ML-based techniques in the same context in both theory and simulation.

It was shown that the basic vector ML estimation suffers from decreasing performance as the estimation resolution increases through a higher number of search points. The SML algorithm provides inaccurate and biased estimates of the multipath delays. The MEDLL algorithm, in addition to requiring iterations and being computationally complex, considers a fixed number of paths; this may result in underestimation or overestimation of the true number of paths, which in turn may lead to a bias in the final ranging solution. Conversely, the proposed MSML algorithm includes a detection step to avoid considering a fixed number of paths and a refinement step to improve the estimation accuracy of the detected paths.

The simulation results show that the performance of MEDLL is very sensitive to the choice of the number of paths to be estimated and a pessimistic choice (depending on the type of environment) can result in a better performance and, for high values of C/N_0, it can even outperform MSML in some cases. It was also shown that the SML is almost always biased, except under LOS conditions, due to its low resolution and its attempt to

find the center of power of the delay profile. However the robustness of this algorithm in dealing with noise is better than the MEDLL. The results show that the proposed MSML algorithm outperforms the other techniques in the sense of LOS delay estimation RMSE, in particular for lower values of signal-to-noise ratios under all simulation scenarios examined. The comparison of the performance of the algorithms in the sense of channel MSE shows that the conventional raw ML technique still has the best performance in this sense and that the MSML performance is comparable to it for most C/N_0 values.

Chapter Four: Bayesian Tracking of the ML-Based Algorithm

4.1 Introduction

In Chapter 3, a set of optimal ML-based algorithms were introduced that can estimate the parameters of the channel impulse response with no prior knowledge. Without *a-priori* information, the receiver must perform a full multipath estimation procedure, a process which can be computationally expensive. When provided with an initial estimate of the multipath channel, however, the receiver need only to incur a small computational overhead to track changes in the channel. In this Chapter, a receiver design is proposed which adaptively alternates between full channel characterization and recursive channel refinement, depending on the severity of the variations of the channel to provide a robust and efficient multipath mitigating GNSS receiver.

To perform multipath estimation with no *a-priori* information, the sequential maximum-likelihood channel estimation technique (MSML) introduced in Chapter 3 is used. Once an initial estimate of the channel has been generated, the receiver can employ a sequential Bayesian algorithm, a linear minimum mean square error (LMMSE) technique also referred to as Wiener filter (Haykin 2001), to track small changes in the channel. This approach has been designed to accurately mitigate the effects of multipath at a low computation cost and is effective provided the channel does not change rapidly. To accommodate this eventuality, a method of detecting sudden channel variations has been developed which can instigate a reversion to the MSML algorithm.

The performance of the proposed scheme has been tested using several simulated data and real data collected in a downtown environment. The performance metrics are based upon pseudorange and positioning errors. The computed range and position solutions by

the proposed techniques will be compared to the reference trajectory achieved with a combined GNSS-INS system, namely the Novatel SPAN LCI system, that is not affected by multipath in these conditions.

4.2 Sequential Linear Minimum Mean Square Error Estimation

In addition to taking advantage of prior information, there is still another key difference between the Bayesian and non-Bayesian approaches introduced in Chapter 3 in their estimation strategies. Whereas the ML-based approaches introduced in Chapter 3 consider the parameters of interest as deterministic but unknown constants, the Bayesian approaches assume that they are random variables and their prior probability distribution is somehow known. The Bayesian estimators aim to estimate a particular realization of the unknown random variable using the prior data and the available measurements.

To proceed with a sequential Linear Minimum Mean Square Error (LMMSE) estimation, the following considerations and assumptions should be taken into account:

1) The system model is linear. This is the case since the system model in (3.7) is a linear model which is repeated here for convenience:

$$\mathbf{y} = \bar{\mathbf{G}}\,\bar{\mathbf{a}} + \mathbf{w} \ . \tag{4.1}$$

2) The channel coefficients are assumed to be zero-mean complex Gaussian random variables with a covariance matrix $\mathbf{Q}_{\bar{\mathbf{a}}}$.

3) The noise process is a zero-mean complex Gaussian random process with a covariance matrix $\mathbf{Q}$. It is also assumed that the channel coefficients and the noise samples are statistically independent.

4) Taking into account the discussed jointly-Gaussian linear model which is referred to as the *Bayesian general linear model*, the LMMSE estimator is an optimal estimator in terms of Bayesian Minimum Mean Square Error (BMMSE) (Kay 1993) that can be represented by

$$\mathrm{BMMSE}\left(\hat{\mathbf{a}}[i]\right) = E\left[\left|\bar{\mathbf{a}}[i] - \hat{\mathbf{a}}[i]\right|^2\right] \tag{4.2}$$

for the i-th entry of the estimated vector. In a same way, the error covariance matrix can be represented by

$$\mathbf{M}_{\hat{\mathbf{a}}} = E\left[\left(\bar{\mathbf{a}} - \hat{\mathbf{a}}\right)\left(\bar{\mathbf{a}} - \hat{\mathbf{a}}\right)^{\mathrm{H}}\right] \tag{4.3}$$

which includes the BMMSE of the entries of $\bar{\mathbf{a}}$ on its main diagonal.

4.3 Combined MSML-LMMSE Algorithm

As discussed in the introduction, although the ML-based algorithms discussed in Chapter 3 provide near optimal multipath estimation performance, they are computationally demanding since they operate on a large search space at each signal interval to find a set of multipath parameters that give the best possible fit on the input correlation function. For this reason, as a means to decrease the overall computation burden of the system, a combined algorithm is introduced in this section. Once an initial estimate of the channel has been generated by applying the MSML technique (first mode of operation) for a certain number of time epochs, N_{ML}, the receiver employs the sequential LMMSE

technique (second mode of operation) to track small variations in the channel and slightly modify the estimated channel at a low computation cost provided that the channel does not change rapidly. N_{ML} is selected as a value smaller than the ratio of the channel coherence time and the coherent integration time of the receiver. In this tracking loop, the multipath delays and complex coefficients are sequentially updated from one epoch to the next one and the objective is to minimize the Bayesian minimum mean square error. The procedure of the loop can be described as follows (Kay 1993):

Initialization: The initial estimate of the channel coefficients vector ($\hat{\mathbf{a}}_0$) is obtained by averaging the N_{ML} channel estimates computed by the MSML algorithm. Furthermore, the initial estimate of the error covariance matrix ($\mathbf{M}_0$) is selected as

$$\mathbf{M}_0 = \hat{\mathbf{Q}}_{\tilde{\mathbf{a}}} = \frac{1}{N_{ML}} \sum_{i=1}^{N_{ML}} \left(\hat{\mathbf{a}}_i^{ML} - \hat{\mathbf{a}}_0 \right) \left(\hat{\mathbf{a}}_i^{ML} - \hat{\mathbf{a}}_0 \right)^{\mathrm{H}} \tag{4.4}$$

where $\hat{\mathbf{a}}_i^{ML}$ is the i$^{\text{th}}$ estimated channel coefficient vector in the most recent referral to the MSML stage.

Estimator Update: The estimated channel is updated using the following equation:

$$\hat{\mathbf{a}}_k = \hat{\mathbf{a}}_{k-1} + \mathbf{K}_k \left(\mathbf{y}_k - \bar{\mathbf{G}}_{M'} \hat{\mathbf{a}}_{k-1} \right) . \tag{4.5}$$

In the above equation, k and k-1 are time indices and $\mathbf{K}_k$ is the Kalman gain matrix which can be represented as

$$\mathbf{K}_k = \mathbf{M}_{k-1} \bar{\mathbf{G}}_{M'}^{T} \left(\mathbf{Q} + \bar{\mathbf{G}}_{M'}^{T} \mathbf{M}_{k-1} \bar{\mathbf{G}}_{M'} \right)^{-1} . \tag{4.6}$$

Bayesian Mean Square Error Matrix Update: The error covariance matrix is updated using the following recursive formula:

$$\mathbf{M}_k = \left(\mathbf{I} - \mathbf{K}_k \bar{\mathbf{G}}_{M'}\right)\mathbf{M}_{k-1} \ , \tag{4.7}$$

Decision Making:

The moving average of the MSE of the correlation function is used as a parameter to decide when it is the time to switch back to the ML-base mode of operation and can be expressed as

$$q_k = \frac{1}{N_{ML}} \sum_{i=k-N_{ML}+1}^{k} \left(\mathbf{y}_i - \hat{\mathbf{a}}_i \bar{\mathbf{G}}_{M'}\right)^{\mathrm{H}} \left(\mathbf{y}_i - \hat{\mathbf{a}}_i \bar{\mathbf{G}}_{M'}\right) . \tag{4.8}$$

This parameter is compared to a threshold that is computed using the following equation every time the MSML algorithm is performed:

$$\gamma = \frac{1}{N_{ML}} \sum_{i=1}^{N_{ML}} \left(\mathbf{y}_i - \hat{\mathbf{a}}_i^{ML} \bar{\mathbf{G}}_{M'}\right)^{\mathrm{H}} \left(\mathbf{y}_i - \hat{\mathbf{a}}_i^{ML} \bar{\mathbf{G}}_{M'}\right) . \tag{4.9}$$

Any rapid change in the multipath channel will result in a sudden increase in the estimation error. The system will revert to the MSML algorithm if the moving average MSE of the correlation function passes the computed threshold which is adaptively set using (4.9). The reason for using this threshold is that, unless a sudden change happens in the parameters of the channel being tracked as it will be shown in the simulation results, the MSE of the correlation function when the channel is being tracked by the LMMSE method is smaller than when it is estimated by the MSML algorithm without using any prior information.

The block diagram of the system is shown in Figure 4-1.

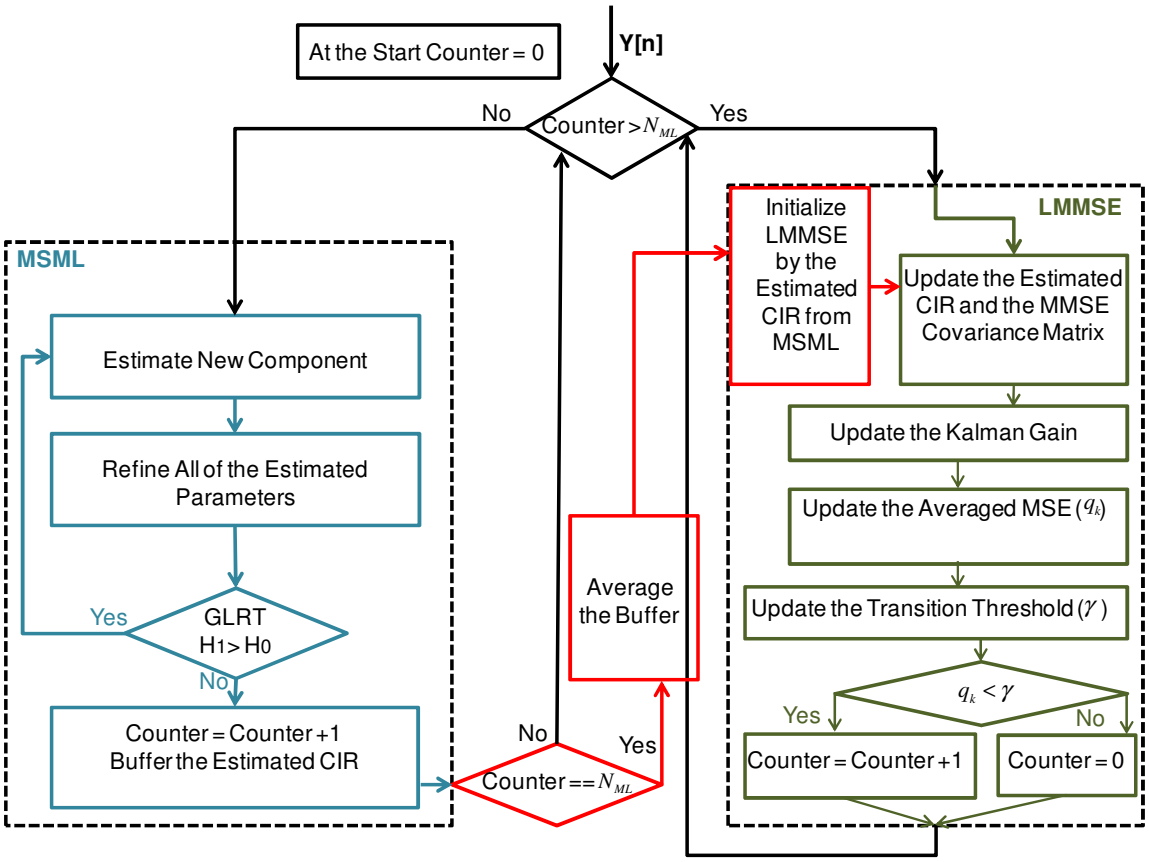

Figure 4-1: The block diagram of the proposed system

4.4 Simulation Results

In this section, some simulation results are presented to analyze the performance of the MSML-LMMSE algorithm.

In Figure 4-2, the estimated CIR is compared to the true CIR at four different instants of a simulation. In this simulation N_{ML} is set 6, therefore at k=7, the average of the 6 estimated channels in the MSML stage is used as the initial estimate for the LMMSE recursion and it is shown in the first subplot. It can be observed that this initial estimate is not perfectly matched to the true CIR. However, the second subplot shows that after 50 ms of applying the LMMSE, the estimated channel is quite close to the true CIR. At

k=100, the true channel has been changed. Therefore at k=101, q_k passes the threshold and the system is switched back to the MSML. Again 6 CIRs are estimated and averaged. The averaged CIR is shown in the fourth subplot and is relatively similar to the true CIR. The updated CIR by the LMMSE after 50 ms is shown in the first plot on the second row. The true channel is again changed at k=200 and the system reverts back to the MSML mode of operation and the same procedure is repeated.

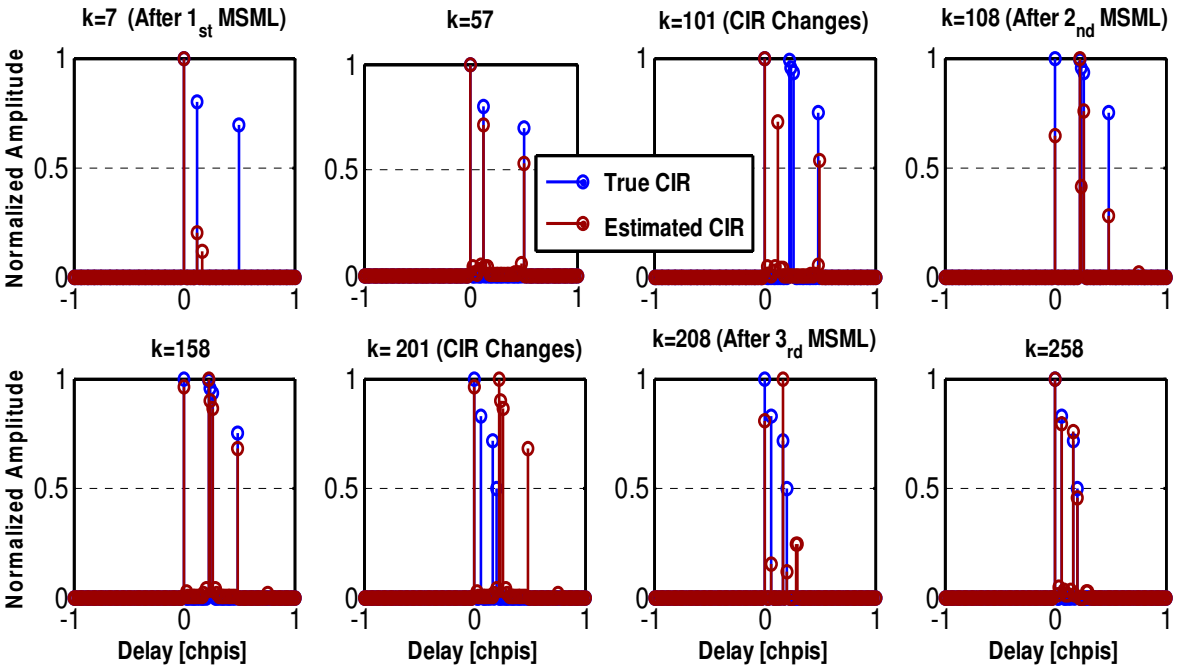

Figure 4-2: Estimated CIRs and the true CIR at different stages of the algorithm

In order to show how the transitions between the two modes takes place, in Figure 4-3 the moving average of the MSE, q_k, and the transition threshold, γ, are shown when the simulated channel changes with different periods. This simulation scenario does not necessarily represent a realistic scenario and the only objective is to examine the response

of the system to sudden changes in the channel since these are the situations when the system switches between the two modes of operation. In the first subplot the simulated channel varies every 100 ms while in the second one, it changes every 500 ms and the third subplot zooms on a transition edge. In both cases, when the channel changes the moving averaged MSE passes the threshold and the MSML routine is called. In the third subplot, the blue arrow approximately shows the area that corresponds to MSML stage. It can be observed that the average MSE when the MSML stage is operating is considerably larger than in the LMMSE stage. The reason is that the LMMSE method uses the initial estimate of the channel and smoothly modifies it and therefore the corresponding MSE smoothly decreases.

Figure 4-4 and Figure 4-5 show the LOS delay estimated RMSE and MSE, respectively, for the urban channel simulation scenario with the parameters introduced in Chapter 3 for three different processing methods, namely MSML-only, MSML-LMMSE and LMMSE-only.

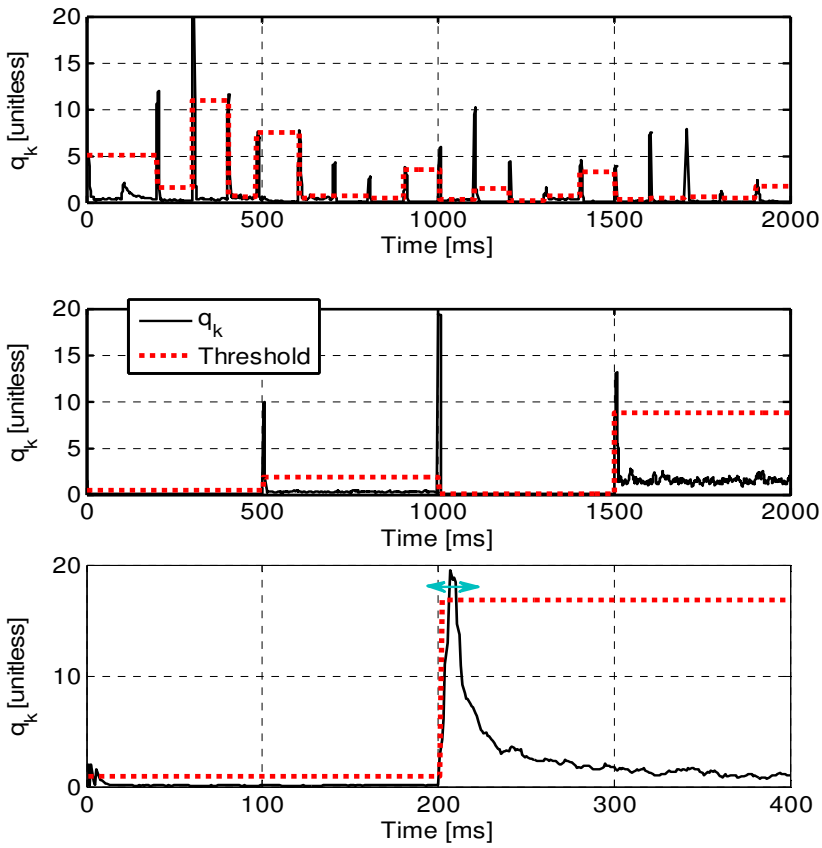

Figure 4-3: Moving averaged MSE and adaptive transition threshold when the simulated channel changes at some specific instances

It can be observed in Figure 4-4 that for C/N_0 values greater than 32 dB-Hz, the RMSE values corresponding to the MSML-LMMSE method are very close to those corresponding to the MSML-only method. However, the diagram corresponding to MSML-only algorithm drops faster as the C/N_0 increases and therefore, for smaller values of C/N_0, it corresponds to slightly smaller RMSE values. The RMSE values corresponding to the LMMSE algorithm however are significantly biased for most parts of the simulated data. The reason is that the LMMSE algorithm is not able track the fast variations of the channel that sometimes occur in an urban environment. In other words,

even if the channel estimated by LMMSE at some specific time is in a good agreement with the true channel, when one considerably large path is added to or removed from the received signal because of obstacles, this algorithm is not able to deal with the large change and therefore a large bias appears in the estimated LOS delay. For the same reason, the channel MSE corresponding to the LMMSE method (Figure 4-5) is also significantly biased at some time intervals. It is also observed in Figure 4-5 that the MSE corresponding to MSML-LMMSE is smaller than both the MSM-only and LMMSE-only methods. This observation can be justified by two causes. Firstly, as explained before, the MSE corresponding to the LMMSE-only method is biased when the channel changes. Secondly, the MSE corresponding to the MSML-only method is larger than the MSML-LMMSE since, as shown in Figure 4-5, the MSML algorithm does not use any initial estimates and results in relatively larger MSE values.

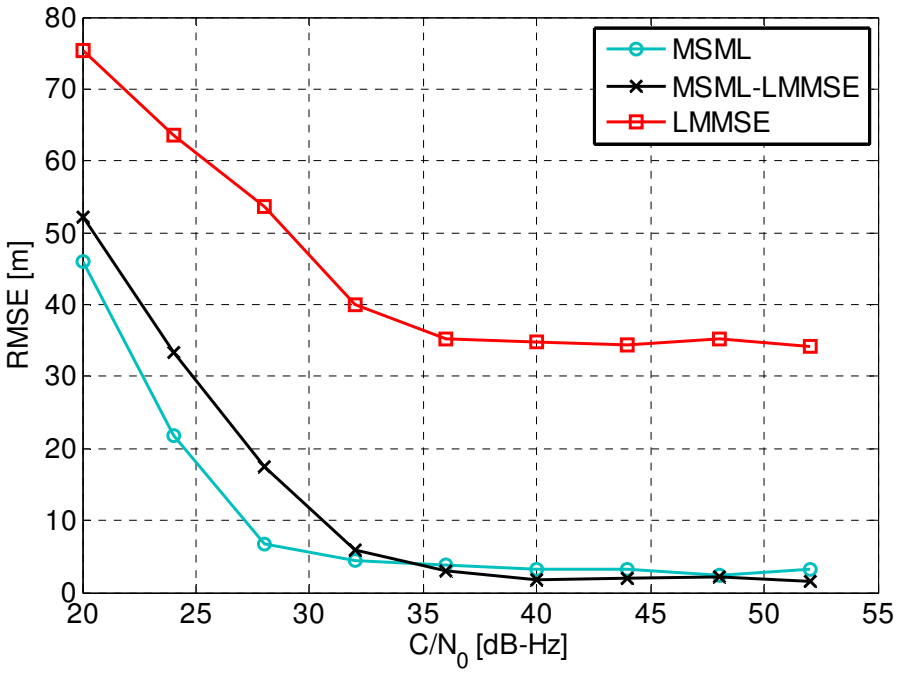

Figure 4-4: Diagrams of LOS time of arrival estimation RMSE with three processing methods: (1) MSML, (2) MSML-LMMSE, and (3) LMMSE

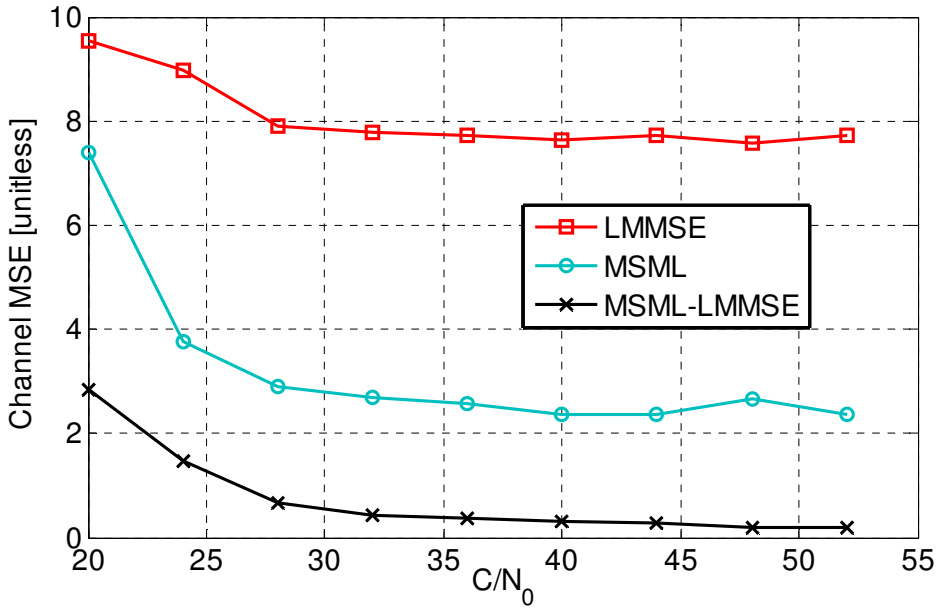

Figure 4-5: Diagrams of the channel MSE for the three processing methods used in Figure 4-4

4.5 Experimental Results

In this section, the performance of the proposed estimation technique is assessed by processing real GPS L1 C/A signals captured in downtown Calgary (this data was collected on August 19, 2011). The environment is an example of an urban canyon with buildings ranging in height from one to 50 stories. Figure 4-6 shows the test trajectory (red curve), the sky plot of the constellation at the beginnings of the test, the data collection set-up, and the vehicle speed versus time. The part with high buildings is inside the yellow rectangle shown in Figure 4-6 (a). In order to eliminate the effect of correlated error sources other than multipath, a differential GPS setup was utilized. Furthermore, an integrated GPS-INS (Inertial Navigation System) was used on the vehicle to obtain continuous reference positions at the 1-m accuracy level. The accuracy of the reference trajectory as function of time is shown in Figure 4-8. The most challenging part of the

trajectory was during its first 600 m due to the building arrangement, is shown in Figure 4-7. However the reference trajectory components are still better than 1 m, which is sufficient for the current analysis. These reference positions were employed to independently assess the positions obtained by the proposed techniques. The computed delay and Doppler parameters from the estimated reference data were then passed to a block processing software receiver (GNSRx.ss) (Petovello et al 2008, Lin et al 2011) and were used to define the centre of the search space.

A block diagram of the equipment configuration is shown in Figure 4-9. The GPS signal received by the vehicle-mounted antenna was split into two branches. The first branch was fed into a National Instrument (NI) RF front-end to be amplified, filtered, down-converted and sampled at a rate of 12.5 MHz. The second branch was connected to an integrated GNSS-INS SPAN^{TM} system to generate the reference positions. Data from the GNSS portion of the SPAN system was collected by an NI data acquisition board with a sampling rate of 100 Hz. The antenna and the INS unit were mounted on the vehicle's roof. GPS data was also collected under LOS conditions with another receiver at a base station (reference) for differential processing.

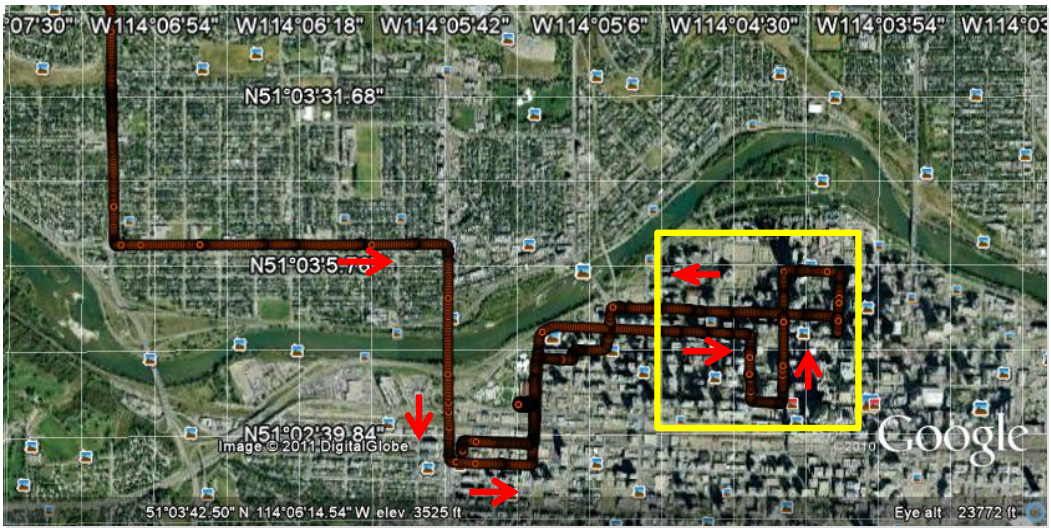

(a)

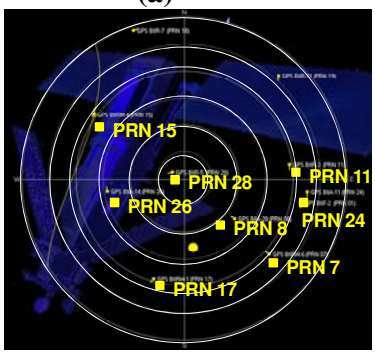

(b)

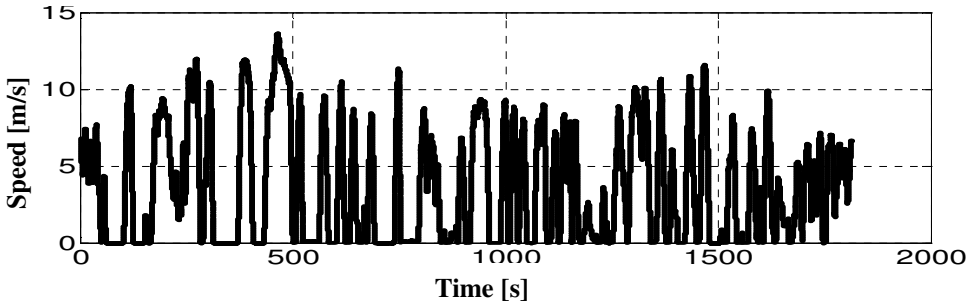

(c)

(d)

Figure 4-6: (a) Reference trajectory (b) Sky plot of the constellation (c) Speed of the vehicle (d) Data collection set up

Figure 4-7: An urban area with tall buildings (5 Avenue, Calgary)

The raw GPS samples were then processed using GSNRx-ss. In this software receiver, assistance information in the form of broadcast ephemeris, raw data bits and a reference trajectory are utilized to improve tracking sensitivity. The data bits are wiped off using the known data bit information. The signal parameters estimated from the reference trajectory are used to reduce the search space. At each epoch, the reference data, which includes position and velocity components, are used to generate the nominal code phase and carrier Doppler which are then passed to the signal processing channels where a grid of correlators is evaluated. The duration of the coherent integration time and the range

and resolution of the delay and Doppler values within the correlation grid can be set and the output correlation grids are centered on the true LOS delay that is provided by the aiding process. This prior knowledge of the true LOS delay was used to evaluate the performance of the approaches discussed. For all of the data processing results in this chapter, the coherent integration time was 40 ms.

Figure 4-10 shows a specific example of different steps of the MSML technique in estimating the channel impulse response for the signal of PRN 17.

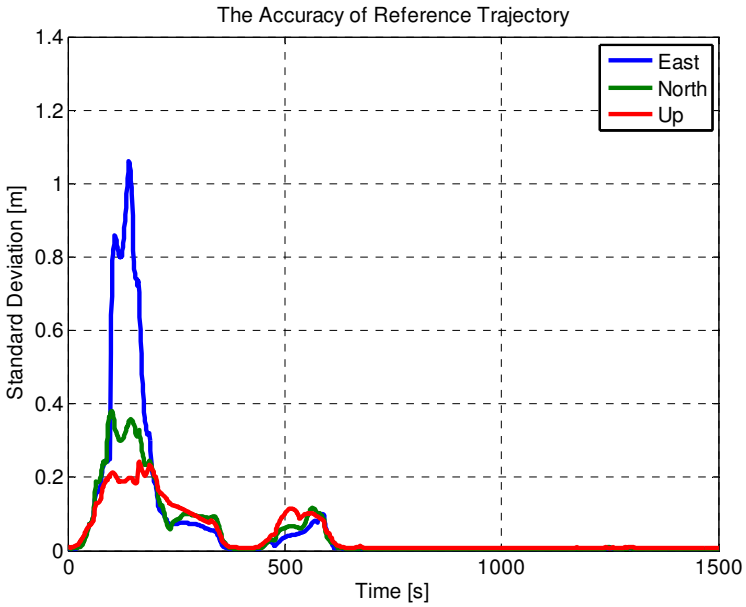

Figure 4-8: Accuracy of reference trajectory

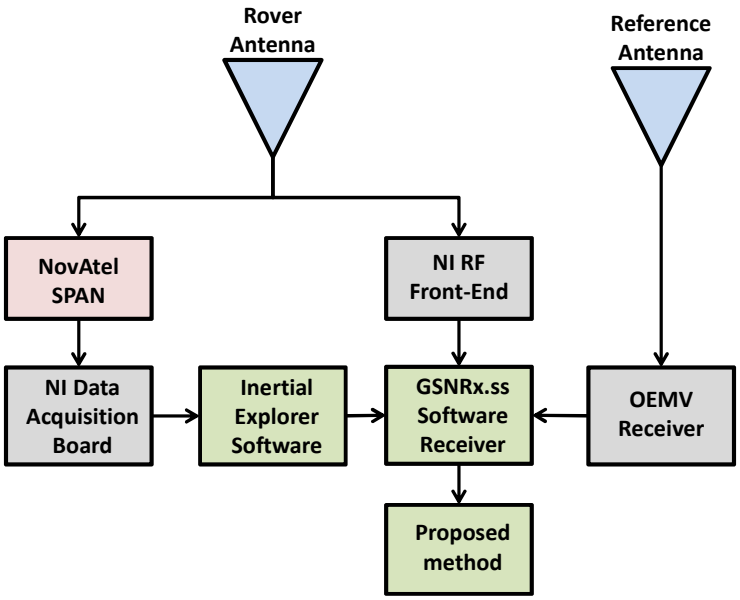

Figure 4-9: Data collection architecture

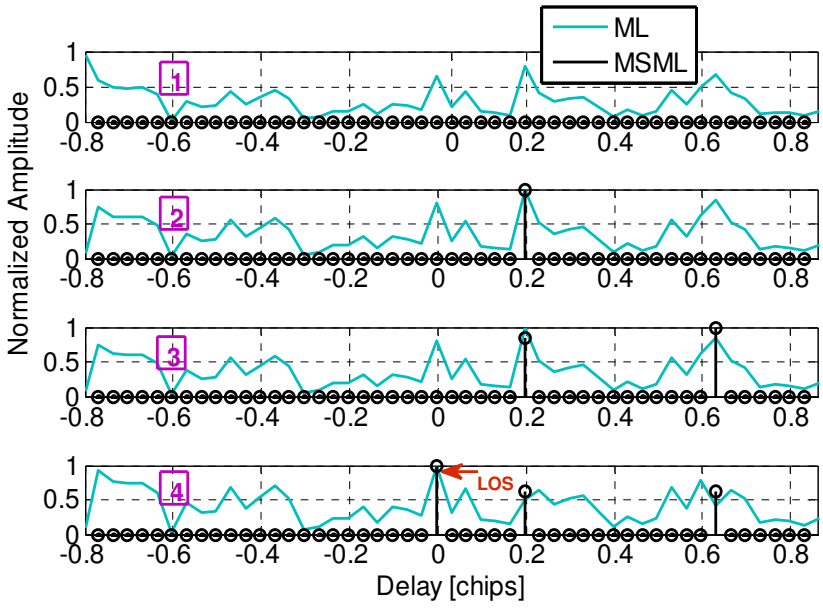

Figure 4-10: MSML steps in estimating CIR, PRN 17, C/N_0 = 25 dB-Hz

Since the value of the signal to noise ratio for this time period was small (6 dB), the first estimated peak (the highest peak in the ML profile) was actually a noise peak (since the delay value corresponding to LOS is known from the reference data, any peak that corresponds to smaller delay values is a noise peak). This peak is identified as a noise peak when GLRT is run (subplot 1). Since the estimation procedure is run only for visible PRNs, the algorithm attempts to find at least one signal component. Therefore, when the GLRT failed for the first peak, the algorithm removed this peak and found the next highest peak in the ML profile (subplot 2) and then the GLRT was assessed for the second peak. Since the GLRT performed successfully passed, the refinement procedure was run to estimate the amplitude and phase of the first signal path. As observed in subplot 2, it has a 0.2 chips lag from the LOS. At the next step, the effect of the recently updated CIR was removed from the signal ACF and the ML profile was formed for the second time. The highest peak of the updated profile, which is at a delay of 0.63 chips from the reference LOS, was then identified. This candidate also passed the GLRT successfully. The refinement stage was again applied to the two detected signal components and the refined CIR is shown in subplot 3. Finally, at the fourth run of the estimation/detection procedure, the third signal component, which turned out to be the LOS, was detected and its parameters were estimated. The final channel after the refinement stage is shown in subplot 4. After this refinement, the GLRT test was again performed but it failed, which resulted in the termination of the procedure for this part of data.

For each PRN, the discussed MSML algorithm was applied over N_{ML}=6 successive time snapshots (each equal to the coherent integration time) and, after that, the N_{ML} estimated

CIRs were averaged to provide an initial estimate for the second mode of processing the data which is LMMSE tracking.

Figure 4-11 shows the estimated ACF, the received ACF and their difference in addition to the estimated CIR for PRN 24 after tracking 200 ms of data with the LMMSE algorithm.

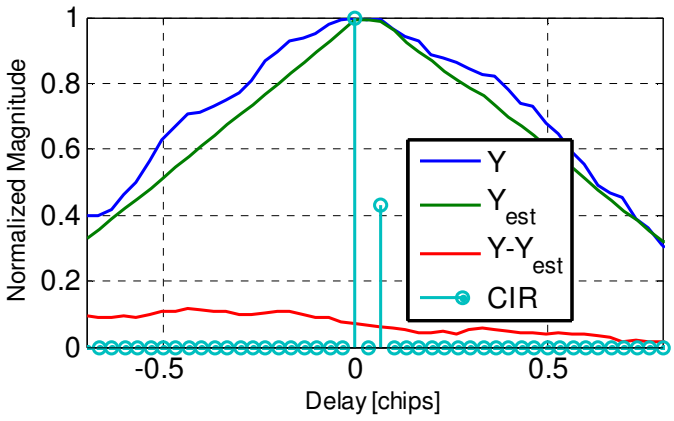

Figure 4-11: Example of the estimated CIR and ACF for PRN 24

The system keeps processing the data by tracking the channel using the LMMSE technique until the moving averaged MSE of the estimate ACF in (4.8) is greater than the adaptively computed transition threshold in (4.9). Figure 4-12 shows these two parameters as a function of time for some of the visible PRNs.

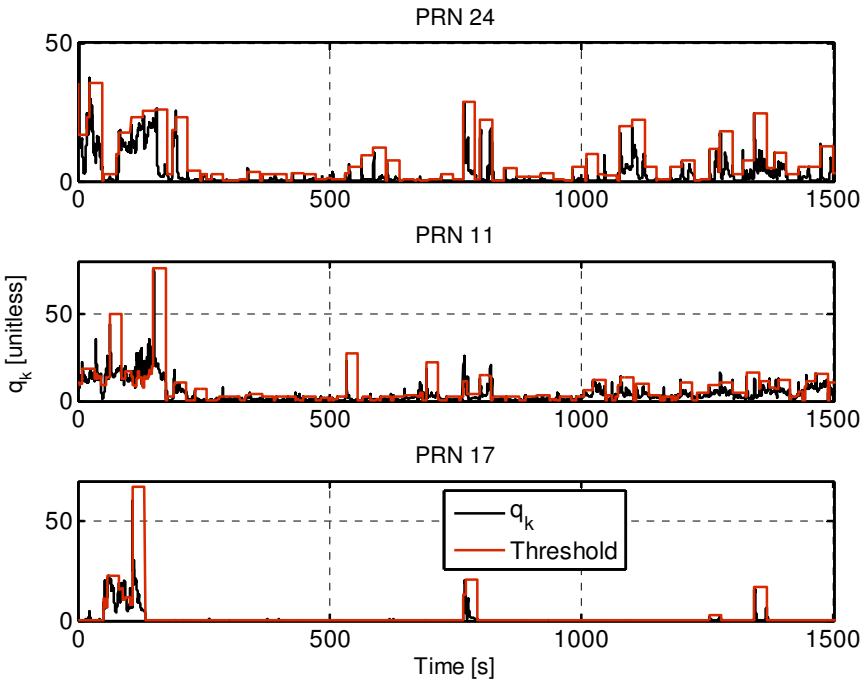

Figure 4-12: Moving average MSE and adaptive transition threshold for some of the visible PRNs

It can be observed in Figure 4-12 that the trend of variation of q_k and γ is very different for different PRNs. For example, the number of transitions between the two algorithms for PRN 17 is considerably smaller than PRN 11. Moreover, it can be inferred from this figure that fast variations in the wireless channel are quite common in a vehicular application in urban areas.

As the number of times that the system switches back to the MSML stage in a certain observation interval increases, the accuracy of the system increases and at the same time its computational load grows and the system becomes slower. Therefore, a trade off should be made between the accuracy and the processing time of the system. The length of the sliding window, which is used in the moving average, is one of the parameters that can affect this trade off. The number of times that the control parameter passes the

defined threshold is equal to the number of times that the system switches back to the MSML stage. In Table 4-1, the percentage of the total time that has been spent in the MSML stage (T_{MSML}) during the test time is shown for all visible PRNs.

Table 4-1: Percentage of the total time that is spent in the MSML stage for different PRNs

PRN	7	8	11	15	17	24	26	28
T_{MSML} [Percentage]	17.1	9.75	9.50	10.31	3.01	12.43	13.79	1.67

A long time being spent in total in the MSML stage for a specific PRN compared to the other PRNs (such as PRN 7) indicates a poor signal quality for that PRN (low signal to noise ratio or large number of multipath components).

Figure 4-13 shows the histogram of the number of detected paths for different PRNs during the test time. To each histogram, the approximately closest Poisson PDF curve has been fitted (using a second order curve fit). The corresponding mean values of the Poisson PDFs (λ_p) are shown in Table 4-2.

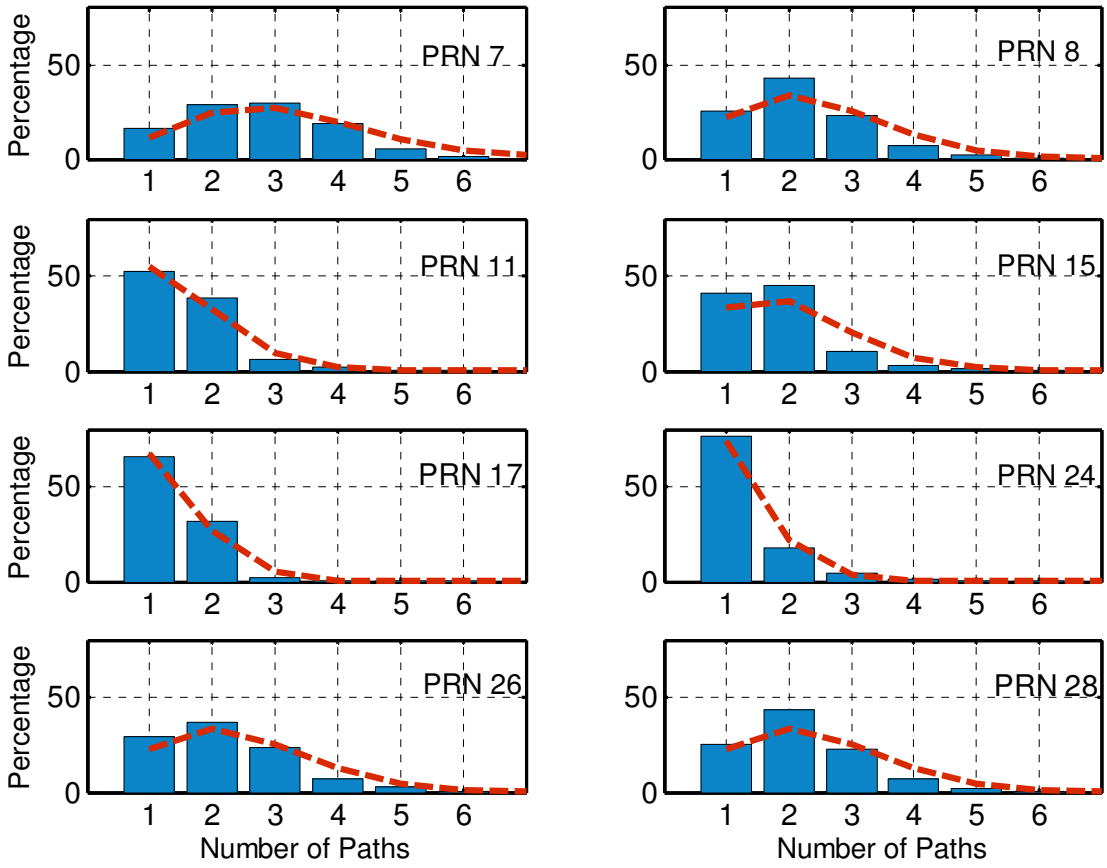

Figure 4-13: Histogram of the number of detected paths during the MSML procedure for different PRNs

Table 4-2: Mean of fitted Poisson distribution curve for different PRNs

PRN	7	8	11	15	17	24	26	28
λ_p	3.3	2.6	1.6	2.1	1.4	1.2	2.5	2.6
Elevation [degrees]	20-25	50-55	30-35	25-30	30-35	25-30	45-50	80-90

The first observation that can be inferred from this set of histograms and PDFs is that the distribution of the number of paths for all of the PRNs can be well fitted to a Poisson

distribution PDF curve. However the corresponding values of the PDF mean parameter is different for different PRNs.

Table 4-3 tabulates the Poisson distribution mean values measured by Jahn et al (1996) for urban environments as a function of satellite elevation angles.

Table 4-3: Measured Poisson distribution mean values for the number of paths in urban areas as a function of satellite elevation angles

Elevation [degrees]	15	25	35	45	55
λ_p	1.2	4	3.5	3.6	3.8

Comparing Table 4-2 to Table 4-3, it can be observed that although there seems to be a relation between the elevation angles and the number of paths, perhaps this parameter is not the only parameter that affects the distribution of the number of paths. For example, PRNs 11, 17 and 24 are very close to each other in elevation angle and their corresponding detected numbers of paths are also very close. On the other hand, PRN 28 is very close to zenith and the detected number of paths for this PRN is very close to PRN 26 which is located at a very different elevation angle. Therefore, the azimuth of the satellites and the orientation of the streets with respect to the surrounding buildings also affect these statistical results. Table 4-3 does not include elevation angels above 55° and therefore it is not possible to compare the two tables for PRN 28. In general, for most PRNs, except PRN 7, the mean of detected number of paths is smaller than the measured values by Jahn et al (1996). The reason is that the very weak multipath components are

not detectable by the estimation/detection algorithms discussed in this chapter and in Chapter 3. However, the effect of these very weak components on the final ranging error is normally insignificant.

Since the center of the delay range corresponds to the true LOS delay obtained from the reference trajectory, the distance of the estimated LOS to the center of the delay range obtained by the proposed algorithm in unit of metre determines the pseudorange error for the corresponding PRN at the current epoch. Figure 4-14 shows the pseudorange estimation errors computed by the proposed algorithm for all visible PRNs and the results are compared with the estimation errors produced by some of the classical DLLs introduced in Chapter 2, such as narrow correlator (NC), early-late-slope (ELS) or double delta correlator and high resolution correlator (HRC). In Figure 4-15, the RMS values of these pseudorange estimation errors are compared.

The comparison of the pseudorange estimation errors computed by different techniques from Figure 4-15 shows that the RMS values of the estimation errors produced by the MSML-LMMSE algorithm is considerably smaller than the ones produced by the correlation-shape based DLLs for all of the PRNs. This improvement in estimation accuracy is at the cost of the additional computation load for estimating the CIR in the MSML stage of the algorithm. In fact, the three correlation-based DLLs have lost lock on the signal in most parts of the data during the first 600 m of the trajectory due to high buildings and severe multipath. Among the three conventional DLLs, the HRC has almost the best performance (for all of the PRNs except PRN17). The correlator spacing parameters for the DLLs were set to 0.13 and 0.26 chips. The RMS values of the

estimation error produced by the two double delta correlator techniques (HRC and ELS) are slightly smaller than the ones produced by NC.

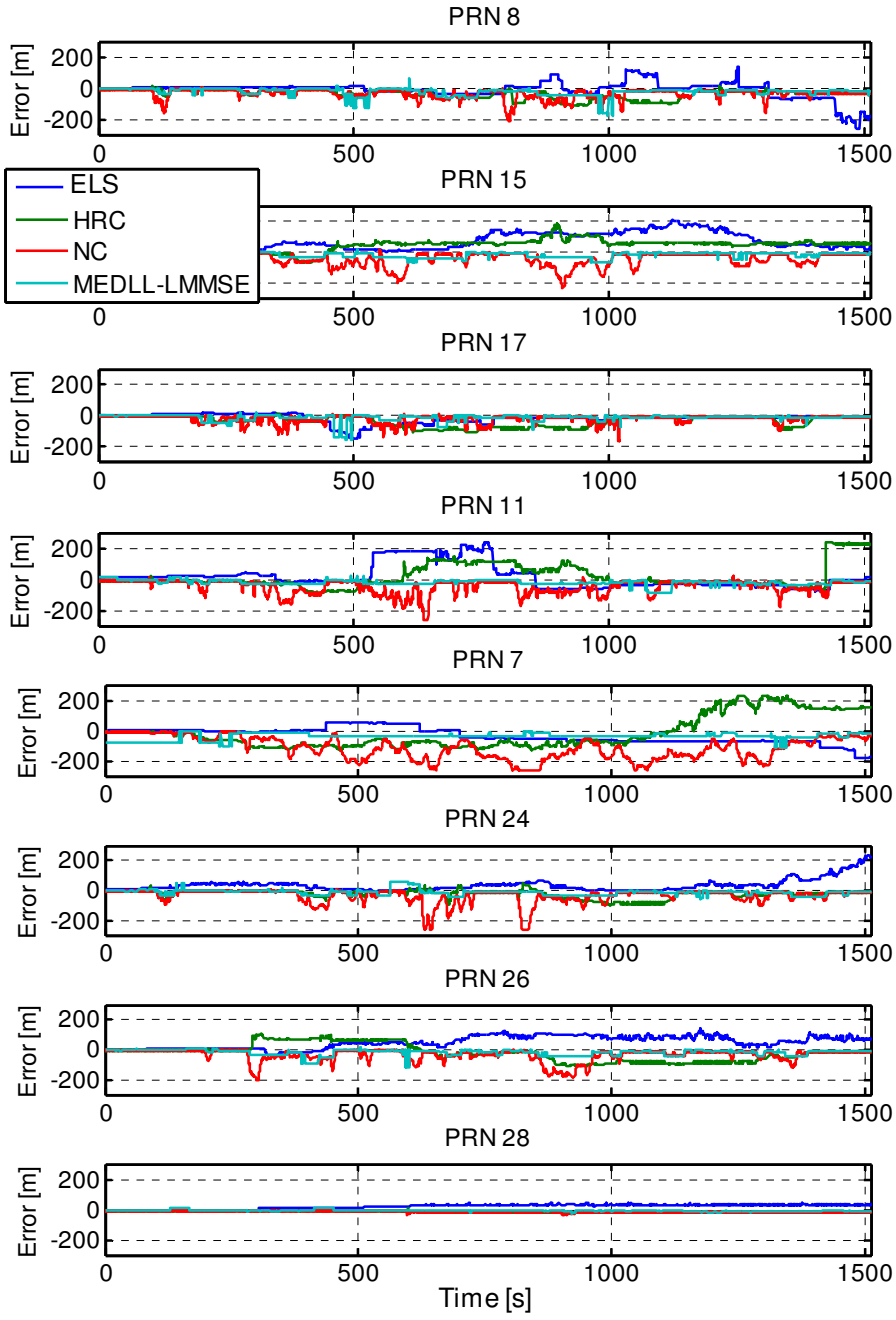

Figure 4-14: Comparison of pseudorange estimation errors

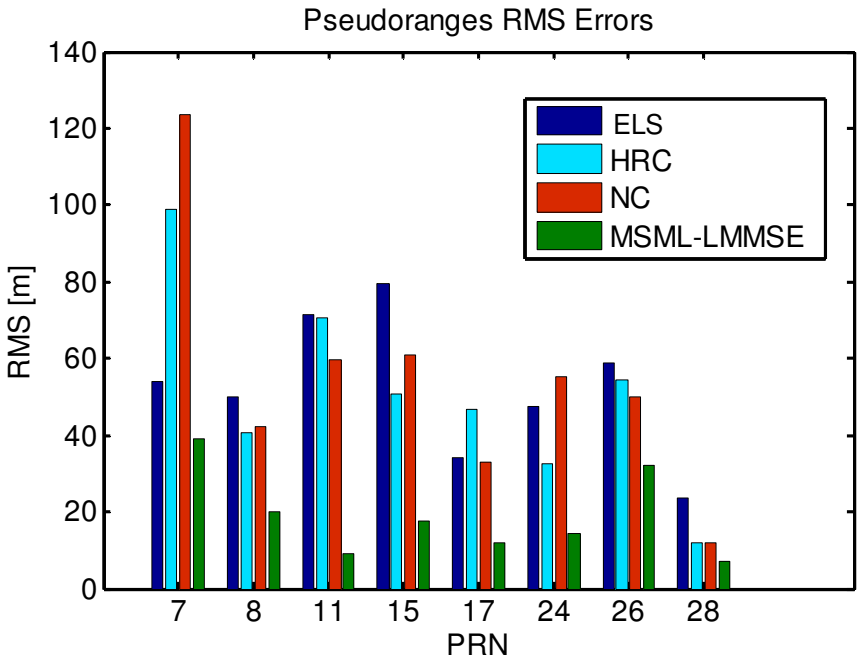

Figure 4-15: RMS values of pseudorange estimation errors

The estimated pseudoranges for all visible satellites were then used in the computation of the positions of the receiver (trajectory). Figure 4-16 shows the position errors for the four discussed techniques and the corresponding RMS values are compared in Figure 4-17. As it was expected from the pseudorange error diagrams, the position solution produced by the MSML-LMMSE algorithm is considerably improved compared to the conventional techniques. It is important to mention again that this improvement is obtained at the cost of a large computational load. Although the complexity of the MSML algorithm is slightly smaller than similar ML-based methods, it is still much larger than conventional DLLs such as the ones in Figures 4-14 to 4-17.

In Chapter 5 a new class of estimation algorithms will be introduced to impose a considerably smaller computational load to receiver but they are comparable in terms of estimation performance to the ML-based techniques.

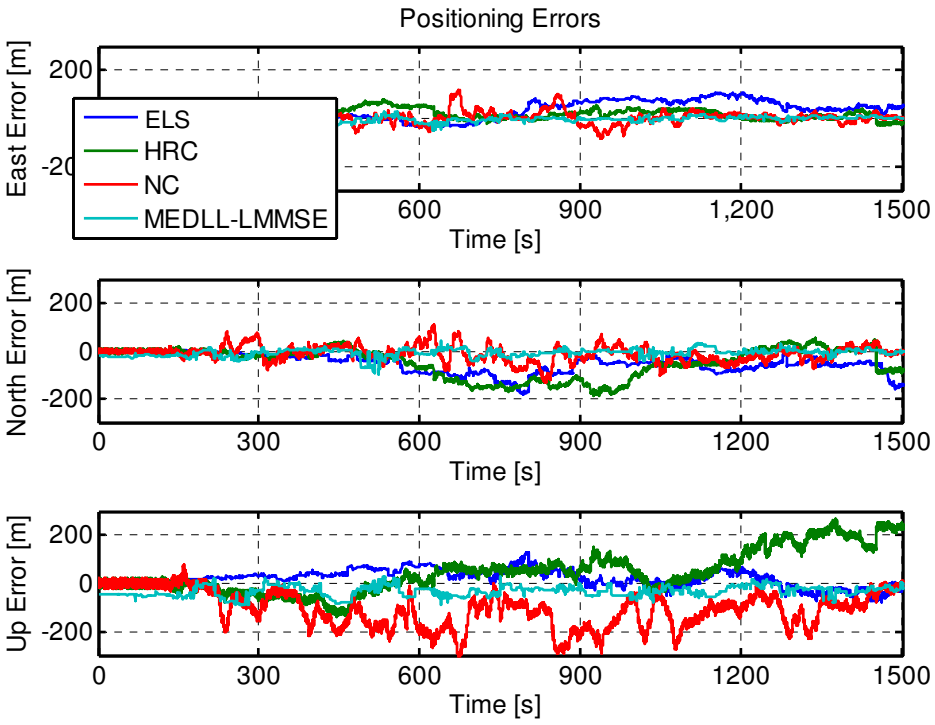

Figure 4-16: Position errors

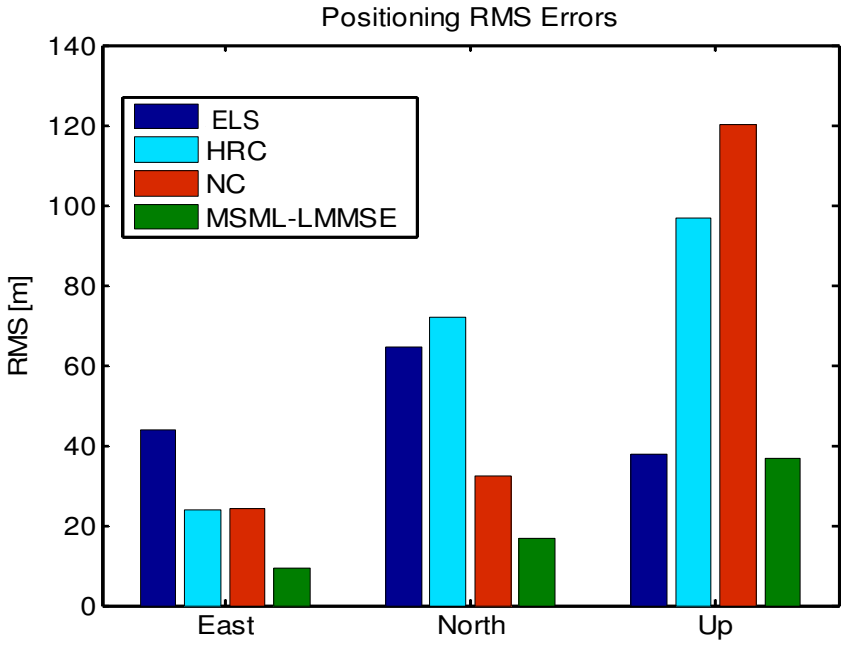

Figure 4-17: Comparison of position errors RMS values

4.6 Summary

A real-time channel estimation /tracking receiver structure was introduced to compensate for the effect of multipath in urban navigation applications. The proposed algorithm changes the mode of the operation of the receiver adaptively based on the severity of the variations of the wireless channel to make a trade-off between the complexity and reliability of the system. The simulation and data processing results demonstrated the effectiveness of the proposed algorithm in reducing the values of bias in estimated ranging and position solutions compared to the conventional delay lock loops.

Chapter Five: Adaptive Equalizers

5.1 Introduction

In the previous chapters, the problem of LOS delay estimation was pursued through direct estimation of the multipath channel by means of some optimal estimation techniques. In this chapter, however, this problem is investigated through a different class of techniques based on adaptive equalization of the multipath channel. Using this class of techniques, instead of direct estimation of the multipath channel, its resulting distortion on the received GNSS signal is compensated for by passing the signal through an adaptive filter and then the LOS delay is estimated from the equalized signal.

The optimal algorithms introduced in Chapters 3 and 4 have large computational complexities as a result of performing matrix inversion procedures. In some applications, this level of computational complexity may be expensive or impossible to implement. The channel equalization approaches that are introduced in this Chapter are sub-optimal techniques that employ a filter structure with relatively small computational complexities.

5.2 Linear Estimation Problem

The linear filter which is most often used for equalization has the structure shown in Figure 5-1 where c_j's are the equalizer coefficients. These equalizers are usually used to remove the effect of ISI (Inter-Symbol Interference) introduced by the multipath channel on the data symbols as a part of the bit detection procedure of digital communication systems. For such an application, the input to the filter is the received signal sequence

$\{v_k\}$ and its output, the estimate of the transmitted symbol $\{I_k\}$ which can be expressed as

$$\hat{I}_k = \sum_{j=-K}^{K} c_j v_{k-j}, \tag{5.1}$$

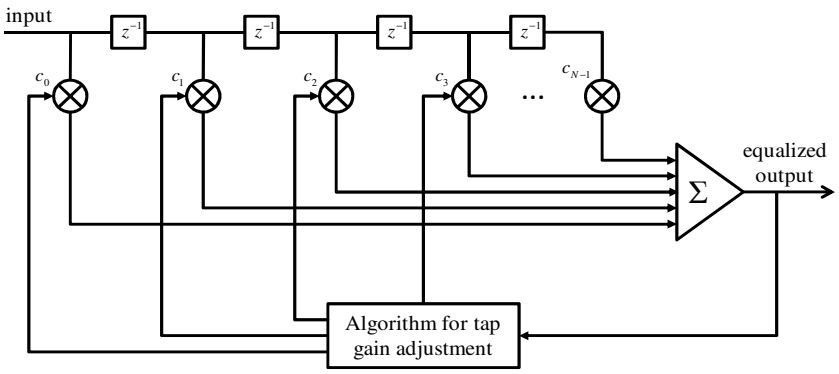

Figure 5-1: Linear equalizer

In this thesis, however, the equalizer filters are employed to compensate for the multipath distortion on the autocorrelation sequence of the received signal. Therefore, for the case of this application, the input to the filter is the vector of the autocorrelation sequence of the received signal ($\mathbf{y}_k$) which is a row vector with a length of *N* and its output is the estimate of the ideal autocorrelation function of the LOS signal ($\hat{\mathbf{y}}_k$) which is a vector with the same size as $\mathbf{y}_k$, which can be expressed as

$$\hat{\mathbf{y}}_k = \mathbf{y}_k \mathbf{C}, \tag{5.2}$$

where **C** is an N by N matrix of the equalizer coefficients. Thus, the problem is to find an optimum value for the equalization matrix.

In the case of linear equalizers, there are two different criteria for determining the equalizer coefficients. These criteria are the peak distortion and the mean square error at the output of the equalizer and are introduced in the next sections.

5.2.1 Peak Distortion Criterion

To solve (5.1), the minimization of the worst case of ISI at the output of the equalizer is called peak distortion criterion. This cost function can be expressed as (Proakis 1983)

$$D(c) = \sum_{\substack{n=-K \\ n\neq 0}}^{n=K+L-1} \left| \sum_{j} c_j h_{n-j} \right|, \tag{5.3}$$

where h_n are channel impulse response tap coefficients. Consequently, the peak distortion cost function for (5.2) can be defined as

$$D(\mathbf{C}) = \left\| \mathbf{h}' \bar{\mathbf{G}}^{\mathrm{T}} \mathbf{C} \right\|, \tag{5.4}$$

where $\mathbf{h}'$ is a row vector with a length of L that contains the CIR tap coefficients on its elements except that it has zero on the element corresponding to LOS and the $\bar{\mathbf{G}}$ matrix was introduced by (3.8). The cost functions of (5.3) and (5.4) are based on the idea that in a distortionless system, the cascade of the channel and the equalizer are equivalent to a delta function. The solution to these optimization problems is the so called linear zero-forcing equalizer which introduces the disadvantage of enhancing the additive noise at the output of the equalizer in its effort to compensate for the nulls in the channel frequency response (Ding & Li 2001). Hence, this criterion is not commonly used in practical systems.

5.2.2 Mean Square Criterion

In the MSE criterion, the equalizer coefficients are adjusted so that to minimize the mean square value of the error at the output of the equalizer. Optimization based on this criterion is the focus of this chapter.

For the problem of (5.2) the cost function for this criterion can be represented by

$$\begin{aligned} J(\mathbf{C}) = E\left\|\mathbf{d}-\hat{\mathbf{y}}\right\|^2 &= E\left[\left(\mathbf{d}-\mathbf{y}\mathbf{C}\right)\left(\mathbf{d}-\mathbf{y}\mathbf{C}\right)^{\mathrm{H}}\right] \\ &= tr\left\{E\left[\left(\mathbf{d}-\mathbf{y}\mathbf{C}\right)^{\mathrm{H}}\left(\mathbf{d}-\mathbf{y}\mathbf{C}\right)\right]\right\} \\ &= tr\left\{E\left[\boldsymbol{\varepsilon}^{\mathrm{H}}\boldsymbol{\varepsilon}\right]\right\}, \end{aligned} \tag{5.5}$$

where $\mathbf{d}_k = a_{LOS,k}\mathbf{g}^{\mathrm{T}}_{\tau_{LOS,k}}$ in which $\mathbf{g}_{\tau_m}$ is the vector of ideal correlation function shifted by τ_m that was introduced by (3.6), $\tau_{LOS,k}$ and $a_{LOS,k}$ are the complex path gain and delay parameters associated to the LOS signal at the k-th signaling interval and $\boldsymbol{\varepsilon}$ is the error vector and is represented by

$$\boldsymbol{\varepsilon} = \mathbf{d}-\mathbf{y}\mathbf{C}. \tag{5.6}$$

The equality in (5.5) implies that in the MSE criterion, the cost function is a quadratic function of the equalizer coefficients and can be easily minimized with respect to $\mathbf{C}$. Substituting (5.2) into (5.5) and taking the derivative with respect to $\mathbf{C}$ results in the orthogonal equation in mean square estimation and can be represented as (Guo et al 2006)

$$E\left[\mathbf{y}^{\mathrm{H}}\left(\mathbf{d}-\mathbf{y}\mathbf{C}\right)\right] = 0. \tag{5.7}$$

The expression in (5.7) can be simplified to

$$\mathbf{RC} = \mathbf{\Gamma}, \tag{5.8}$$

where $\mathbf{R} = E\left[\mathbf{y}^{\mathrm{H}}\mathbf{y}\right]$ is the Hermitian covariance matrix of the received signal and $\mathbf{\Gamma} = E\left[\mathbf{y}^{\mathrm{H}}\mathbf{d}\right]$. The solution of (5.8) is

$$\mathbf{C}_{\mathrm{o}} = \mathbf{R}^{-1}\mathbf{\Gamma}\ , \tag{5.9}$$

and the residual MSE after substituting (5.9) into (5.5) is referred to as $J_{\min}$ and can be represented by

$$J_{\min} = tr\left\{\mathbf{R_d} - \mathbf{\Gamma}^{\mathrm{H}}\mathbf{R}^{-1}\mathbf{\Gamma}\right\}. \tag{5.10}$$

where $\mathbf{R_d} = E\left[\mathbf{d}^{\mathrm{H}}\mathbf{d}\right]$. The solution in (5.9) involves inverting the matrix $\mathbf{R}$ which incurs a considerable computational complexity. In the next sections, some recursive equalization approaches are introduced to avoid this complexity.

5.3 Decision Feedback Equalizer

In an adaptive equalization system with no training data (a blind equalizer), which is the case considered in this chapter, a hard decision is applied to the output of the equalizer. The output of this decision block is considered as a substitute for the training data in evaluating the error sequence. This error sequence is later fed back to the system to update the equalizer coefficients. The use of a decision device makes the equalizer a non-linear device and, thus, susceptible to error propagation.

A Decision Feedback Equalizer (DFE), as shown in Figure 5.2, consists of two filters: a feedforward filter and feedback filter. In a data communication system, the shorter the length of the feedback filter is, the less the error propagation it imposes on the system (Ding & Li 2001).

Herein, the input to the feed forward filter is the correlation sequence of the received signal and the input to the feedback filter is the output of the decision block. DFE uses previously detected data to subtract their contribution to the distortion in the current data to be detected. Therefore, the output of the feedforward filter can be represented by

$$\hat{\mathbf{y}}_k = \mathbf{y}_k \mathbf{C}_f + \tilde{\mathbf{d}}_{k-1} \mathbf{C}_b, \tag{5.11}$$

where $\tilde{\mathbf{d}}_{k-1}$ is the output of the decision block at the (k-1)-th time interval, and $\mathbf{C}_f$ and $\mathbf{C}_b$ are the matrices of the coefficients of feedforward and feedback filters, respectively.

Given (5.11), the MSE cost function for the DFE can be represented by

$$E\left[\left(\tilde{\mathbf{d}}_k - \hat{\mathbf{y}}_k\right)\left(\tilde{\mathbf{d}}_k - \hat{\mathbf{y}}_k\right)^{\mathrm{H}}\right] = E\left\|\varepsilon_k\right\|^2. \tag{5.12}$$

If the channel response changes, this change is reflected in the error signal, $\boldsymbol{\varepsilon}_k$, since it depends on $\hat{\mathbf{y}}_k$ and consequently on $\mathbf{y}_k$ and on the channel response. Hence the filter coefficient matrix will change according to the change in the channel.

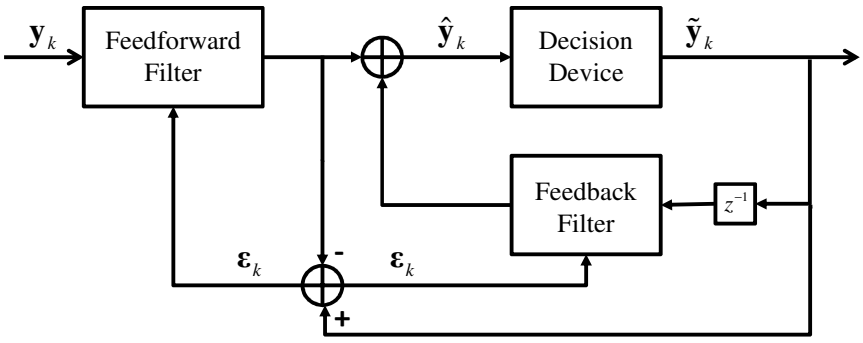

Figure 5-2: Decision feedback equalizer

Before finishing this section, it is important to note that as the equality in (5.11) indicates, the role of the backward filter is to remove the contribution of the last block of data from the equalized estimate of the current block. Although this is an important issue in data communication systems in which data units are short symbols, for GNSS signals the time interval between two consecutive blocks of data is at least one epoch (one code period). As discussed in Chapter 3, the length of the multipath channel is rarely longer than one chip for L1 signal and a few chips for the signals with higher chip rates. Hence, in GNSS systems two adjacent epochs of data do not impose ISI interference on each other and, therefore, the existence of a backward filter is unnecessary in the system.

5.4 Steepest-Descent Technique

The steepest-descent methods can be exploited here to solve the optimal MSE solution in a recursive fashion to avoid matrix inversion (Haykin 2001). This class of techniques can be applied to any other performance criteria as well as MSE, even those that cannot be

described in a closed-form optimal solution. Steepest-descent methods are studied in this section as the launching pad for the development of adaptive filters in the next sections.

5.4.1 Steepest-Descent for MSE Criterion

As represented by (5.5), the MSE cost function is a scalar-valued quadratic function of $\mathbf{C}$ and have a unique global minimum at $\mathbf{C}_{\mathrm{o}} = \mathbf{R}^{-1}\mathbf{\Gamma}$ with the minimum value given by (5.10). The objective of this section is to devise a procedure based on $J(\mathbf{C})$, and with no prior knowledge about the location of its global minimum that starts from an initial guess for $\mathbf{C}_{\mathrm{o}}$ and then recursively improves upon it until converging to $\mathbf{C}_{\mathrm{o}}$. Such a procedure is represented by the following form:

$$\mathbf{C}_k = \mathbf{C}_{k-1} + \mu\mathbf{P}, \tag{5.13}$$

where $\mathbf{C}_k$ and $\mathbf{C}_{k-1}$ denote the guess for $\mathbf{C}_{\mathrm{o}}$ at iterations k and k-1, $\mathbf{P}$ is an *update direction* matrix and μ indicates the step-size parameter which is a positive scalar. In order to lead the recursive procedure in (5.13) to convergence, $\mathbf{P}$ and μ should be selected so that to enforce the following condition:

$$J(\mathbf{C}_k) < J(\mathbf{C}_{k-1}). \tag{5.14}$$

In this way, the value of the cost function will decrease monotonically as the iterations run on. Substituting (5.13) into (5.5) results in

$$
\begin{aligned}
J(\mathbf{C}_k) &= tr\left\{\mathbf{R_d} - \mathbf{\Gamma}^{\mathrm{H}}\mathbf{C}_k - \mathbf{C}_k^{\mathrm{H}}\mathbf{\Gamma} + \mathbf{C}_k^{\mathrm{H}}\mathbf{R}\mathbf{C}_k\right\} \\
&= tr\left\{\mathbf{R_d} - \mathbf{\Gamma}^{\mathrm{H}}\left(\mathbf{C}_{k-1} + \mu\mathbf{P}\right) - \left(\mathbf{C}_{k-1}^{\mathrm{H}} + \mu\mathbf{P}^{\mathrm{H}}\right)\mathbf{\Gamma} + \left(\mathbf{C}_{k-1}^{\mathrm{H}} + \mu\mathbf{P}^{\mathrm{H}}\right)\mathbf{R}\left(\mathbf{C}_{k-1} + \mu\mathbf{P}\right)\right\} \\
&= J(\mathbf{C}_{k-1}) + tr\left\{\mu\left(\mathbf{C}_{k-1}^{\mathrm{H}}\mathbf{R} - \mathbf{\Gamma}^{\mathrm{H}}\right)\mathbf{P} + \mu\mathbf{P}^{\mathrm{H}}\left(\mathbf{R}\mathbf{C}_{k-1} - \mathbf{\Gamma}\right) + \mu^2\mathbf{P}^{\mathrm{H}}\mathbf{R}\mathbf{P}\right\} \\
&= J(\mathbf{C}_{k-1}) + tr\left\{2\mu\,\mathrm{Re}\left[\left(\mathbf{C}_{k-1}^{\mathrm{H}}\mathbf{R} - \mathbf{\Gamma}^{\mathrm{H}}\right)\mathbf{P}\right] + \mu^2\mathbf{P}^{\mathrm{H}}\mathbf{R}\mathbf{P}\right\}.
\end{aligned}
\tag{5.15}
$$

The equality in (5.15) can be further simplified by considering the gradient matrix of $J(\mathbf{C})$ as a function of **C,** which can be expressed as

$$
\nabla_{\mathbf{C}} J(\mathbf{C}) = \mathbf{C}^{\mathrm{H}}\mathbf{R} - \mathbf{\Gamma}^{\mathrm{H}}. \tag{5.16}
$$

Using (5.16), (5.15) can be re-written as

$$
J(\mathbf{C}_k) = J(\mathbf{C}_{k-1}) + 2\mu\, tr\left\{\mathrm{Re}\left[\nabla_{\mathbf{C}} J(\mathbf{C}_{k-1})\mathbf{P}\right]\right\} + \mu^2 tr\left\{\mathbf{P}^{\mathrm{H}}\mathbf{R}\mathbf{P}\right\}. \tag{5.17}
$$

Therefore, since $\mu^2 tr\left\{\mathbf{P}^{\mathrm{H}}\mathbf{R}\mathbf{P}\right\} > 0$, a necessary condition for satisfying (5.14) is

$$
tr\left\{\mathrm{Re}\left[\nabla_{\mathbf{C}} J(\mathbf{C}_{k-1})\mathbf{P}\right]\right\} < 0. \tag{5.18}
$$

There are many choices of **P** that satisfy the inequality in (5.18), among those the steepest-descent methods select the one that follows the general form of

$$
\mathbf{P} = -\mathbf{B}\left[\nabla_{\mathbf{C}} J(\mathbf{C}_{k-1})\right]^{\mathbf{H}}. \tag{5.19}
$$

where B is any Hermitian positive definite matrix. A very common choice is $\mathbf{B} = \mathbf{I}$ and corresponds to the following direction matrix (Sayed 2008)

$$\mathbf{P} = -\left[\nabla_{\mathbf{C}} J\left(\mathbf{C}_{k-1}\right)\right]^{\mathbf{H}} = \boldsymbol{\Gamma} - \mathbf{R}\mathbf{C}_{k-1}. \tag{5.20}$$

The equality in (5.20) chooses the direction matrix to point to the opposite direction of the gradient matrix, hence the name `steepest-descent'. This choice of **P** reduces (5.13) to the recursion

$$\mathbf{C}_k = \mathbf{C}_{k-1} + \mu\left[\boldsymbol{\Gamma} - \mathbf{R}\mathbf{C}_{k-1}\right]. \tag{5.21}$$

As mentioned, the inequality in (5.18) is only a necessary but not a sufficient condition to guaranty the convergence of **C**. Therefore, the convergence of the recursive algorithm also depends on the choice of the step-size μ that will be discussed in the next section.

5.4.2 Condition on Step-Size for Convergence

The recursion equation in (5.21) can be re-written in an alternative form to represent the recursion of the weight error matrix $\Delta\mathbf{C}_k = \mathbf{C}_o - \mathbf{C}_k$. Subtracting both sides of (5.21) from $\mathbf{C}_o$ results in

$$\begin{aligned}\Delta\mathbf{C}_k &= \Delta\mathbf{C}_{k-1} + \mu\left[\boldsymbol{\Gamma} - \mathbf{R}\mathbf{C}_{k-1}\right] \\ &= \Delta\mathbf{C}_{k-1} + \mu\left[\boldsymbol{\Gamma} + \mathbf{R}\Delta\mathbf{C}_{k-1} - \mathbf{R}\mathbf{C}_o\right] \\ &= \Delta\mathbf{C}_{k-1} + \mu\left[\boldsymbol{\Gamma} + \mathbf{R}\Delta\mathbf{C}_{k-1} - \boldsymbol{\Gamma}\right] \\ &= \left[\mathbf{I} - \mu\mathbf{R}\right]\Delta\mathbf{C}_{k-1}\end{aligned}. \tag{5.22}$$

The equation in (5.22) is a homogenous difference equation with coefficient matrix $\left[\mathbf{I} - \mu\mathbf{R}\right]$. On the other hand, since R is a positive definite Hermitian matrix, it has an eigen-decomposition representation as

$$\mathbf{R} = \mathbf{U}\boldsymbol{\Lambda}\mathbf{U}^{\mathbf{H}}, \tag{5.23}$$

where $\boldsymbol{\Lambda}$ is a diagonal matrix with positive entries which are the eigenvalues of **R**, $\boldsymbol{\Lambda} = diag\{\lambda_n\}$ and **U** is a unitary matrix, that means $\mathbf{U}\mathbf{U}^{\mathrm{H}} = \mathbf{U}^{\mathrm{H}}\mathbf{U} = \mathbf{I}$. The columns of **U** are the eigenvectors of **R**. Substituting (5.23) into (5.22) and multiplying the both sides in $\mathbf{U}^{\mathbf{H}}$ from left results in the following expression:

$$\mathbf{Z}_k = [\mathbf{I} - \mu\boldsymbol{\Lambda}]\mathbf{Z}_{k-1}, \tag{5.24}$$

where $\mathbf{Z}_k = \mathbf{U}^{\mathrm{H}}\Delta\mathbf{C}_k$ is the transformed weight matrix. Given that $\mathbf{Z}_k^j$ and $\Delta\mathbf{C}_k^j$ denote the j^{th} column of $\mathbf{Z}_k$ and $\Delta\mathbf{C}_k$ respectively, (5.24) leads to $\mathbf{Z}_k^j = \mathbf{U}^{\mathrm{H}}\Delta\mathbf{C}_k^j$. Therefore, $\mathbf{Z}_k^j$ uniquely determines $\Delta\mathbf{C}_k^j$, since $\left\|\Delta\mathbf{C}_k^j\right\|^2 = \left(\Delta\mathbf{C}_k^j\right)^{\mathbf{H}}\Delta\mathbf{C}_k^j = \left(\mathbf{Z}_k^j\right)^{\mathrm{H}}\mathbf{Z}_k^j = \left\|\mathbf{Z}_k^j\right\|^2$. The same statement is valid about the rows of the two matrices. Furthermore, (5.24) can be re-written as

$$\mathbf{Z}_k[n, j] = (1 - \lambda_n)\mathbf{Z}_{k-1}[n, j], \tag{5.25}$$

where $\mathbf{Z}_k[n, j]$ is the $(n,j)^{th}$ element of $\mathbf{Z}_k$ and consequently

$$\mathbf{Z}_k[n, j] = (1 - \mu\lambda_n)^{k+1}\mathbf{Z}_{-1}[n, j], \ k \geq 0. \tag{5.26}$$

where $\mathbf{Z}_{-1}[n, j]$ is the initial value of $\mathbf{Z}_k[n, j]$. Therefore, the necessary and sufficient condition to enforce the elements of $\mathbf{Z}_k$ and consequently, the elements of $\Delta\mathbf{C}_k$ tend to zero regardless of the initial condition is:

$$\left|1-\mu\lambda_n\right|<1, \qquad \text{for all } j=1,2,...,N\ . \tag{5.27}$$

The condition in (5.27) is equivalent to choosing μ such that (Sayed 2008)

$$0<\mu<2/\lambda_{\max} \tag{5.28}$$

where $\lambda_{\max}$ denotes the largest eigenvalue of **R**. Thus (5.24) and (5.27) indicate that convergence occurs when $\left|1-\mu\lambda_j\right|<1$. However, if the difference between the smallest and the largest eigenvalues of **R** is large, even assigning a value close to the upper bound given by (5.28) to μ does not result in a desirable rapid convergence. The reason is that in this case, the convergence rate of the recursive algorithm will be defined by the smallest eigenvalue. Therefore, the convergence rate of the recursive algorithm depends on the ratio of the largest to smallest eigenvalues ($\rho=\lambda_{\max}/\lambda_{\min}$). At small values of this ratio, a convergence can be obtained by proper selection of μ.

It has been also shown by Widrow (1975) that in order to have the excess MSE introduced by noise, J_Δ, smaller than $J_{\min}$, μ should be smaller than the ratio $\frac{2}{N\left(N_0+p_0\right)}$ where $\left(N_0+p_0\right)$ is the received signal plus noise power. Moreover, time variations of the statistics of the channel incur a third term to the total MSE. The reason is that when channel varies with time, the minimum of $J\left(\mathbf{C}\right)$ surface and the corresponding optimum coefficients will be also time-variant. Therefore, the steepest descent algorithm attempts to follow the moving minimum in the N-dimensional space but it is always

lagging behind due to its use of the estimated gradient matrix (Proakis 1983). This additional MSE due to the variations of the channel statistics, J_I, is referred to as the *lag error* and decreases with an increase in μ (Proakis 1983). Specifically, the effect J_I is considerable when the time variations of the channel occur rapidly. In such a case, since with an increase in the step-size, J_Δ increases while J_I decreases, the optimum choice of μ is where the total error ($J = J_{\min} + J_\Delta + J_I$) is minimum.

It should be noted that for a general cost function, which is not necessarily a quadratic function of the coefficients matrix and it may have both local and global minima, proper selection of the initial value of the coefficients is crucial. It is also important to remember that guaranteed convergence of the SD algorithms regardless of initial values holds only for stationary data. Under non-stationary data conditions, the convergence of the algorithm is a probabilistic process and depends on many parameters.

5.4.3 Newton's Method

In Section 5.2.1 it was mentioned that any positive-definite choice of the matrix **B** in (5.19) can enforce $tr\left\{ \mathrm{Re}\left[\nabla_{\mathbf{C}} J\left(\mathbf{C}_{k-1}\right)\mathbf{P}\right]\right\} < 0$, which was proven to be the necessary condition for convergence. It was also mentioned that setting $\mathbf{B} = \mathbf{I}$ leads to the steepest-descent variant of (5.21). However, there are other choices of **B** that guarantee convergence and lead to other steepest-descent algorithms with different properties. One useful choice is (Sayed 2008)

$$\mathbf{B} = \left[\Delta_{\mathbf{C}}^2 J\left(\mathbf{C}_{k-1}\right) \right]^{-1} = \mathbf{R}^{-1}. \tag{5.29}$$

The resulting steepest-descent recursion would be

$$\mathbf{C}_k = \mathbf{C}_{k-1} + \mu \mathbf{R}^{-1} \left[\mathbf{\Gamma} - \mathbf{R}\mathbf{C}_{k-1} \right]. \tag{5.30}$$

Subtracting both sides of (5.30) from $\mathbf{C}_{\mathrm{o}}$ and using (5.9) results in the following coefficients error matrix recursion:

$$\Delta\mathbf{C}_k = \left(1-\mu\right)\Delta\mathbf{C}_{k-1}. \tag{5.31}$$

In contrast to (5.22), the autocorrelation matrix **R** does not appear in (5.31). For this reason, the convergence of this algorithm is guaranteed for all choices of the step-size that satisfy $0 < \mu < 2$, regardless of the eigenvalues of **R**.

In cases where the covariance matrix is close to singular, it is common to employ regularization, wherein the Newton's recursion is to be modified to the following form (Haykin 2001):

$$\mathbf{C}_k = \mathbf{C}_{k-1} + \mu \left(\mathbf{R} + \varepsilon \mathbf{I} \right)^{-1} \left[\mathbf{\Gamma} - \mathbf{R}\mathbf{C}_{k-1} \right] \tag{5.32}$$

where ε is a small positive scalar which is called the regularization parameter and the corresponding recursion algorithm is called the regularized Newton's method. Similar to the step-size, the regularization parameter can be iteration dependent.

There is no doubt that the complexity of the Newton's method is larger than the steepest descent method since it requires a matrix inversion procedure. However, the usefulness of

this algorithm will become evident in Section 5.7 when it is used to devise some remarkable stochastic gradient variants.

5.5 Transient Behavior

In this section the evolution of the coefficients matrix and the resulting MSE as a function of time is discussed and an expression for the optimal step size is provided.

5.5.1 Modes of Convergence

It can be inferred from (5.26) that the trend of the exponential decay of the element (n, j) of $\mathbf{Z}_k$, $\mathbf{Z}_k^j(n)$, to zero depends on the value of $1-\mu\lambda_n$. For instance, when the sign of $1-\mu\lambda_n$ is positive, the convergence to zero occurs monotonically whereas for negative values of this term, the decay of $\mathbf{Z}_k^j(n)$ to zero is oscillatory. For this reason, the parameters $1-\mu\lambda_n$ are referred to as the modes of convergence. Hence, for each value of μ, there are *N* modes of convergence.

5.5.2 Optimal Step-Size

It is clear from (5.26) that among the *N* modes of convergence, the one with the maximum magnitude exhibits the slowest convergence rate and determines the ultimate convergence rate of the system. Since different choices of μ result in different slowest modes, it is possible to optimally select the value of μ so as to minimize the slowest mode subject to the condition that $|1-\mu\lambda_n|<1$ for all $n=1,...,N$. This optimal value of μ, denoted by μ_o, should satisfy the following equality:

$$1-\mu_o\lambda_{\min}=-\left(1-\mu_o\lambda_{\max}\right), \tag{5.33}$$

which leads to

$$\mu_o=\frac{2}{\lambda_{\min}+\lambda_{\max}}. \tag{5.34}$$

By setting the step-size to the value in (5.34), the system will have two optimal slowest modes with identical values but opposite signs which are equal to

$$\text{optimal slowest modes}=\pm\frac{\lambda_{\max}-\lambda_{\min}}{\lambda_{\max}+\lambda_{\min}}=\pm\frac{\rho-1}{\rho+1}. \tag{5.35}$$

Recall from Section 3.2 that $\Delta\mathbf{C}_k=\mathbf{U}\mathbf{Z}_k$ and hence each element of $\Delta\mathbf{C}_k$ is a linear combination of the elements of $\mathbf{Z}_k$ and can be represented as

$$\Delta\mathbf{C}_k\left[n,j\right]=\sum_{l=1}^{N}\mathbf{U}\left[n,l\right]\mathbf{Z}_k\left[l,j\right]=\sum_{l=1}^{N}\left(1-\lambda_l\right)^k\mathbf{U}\left[n,l\right]\mathbf{Z}_{-1}\left[l,j\right]. \tag{5.36}$$

Therefore, $\Delta\mathbf{C}_k\left[n,j\right]$ also tends to zero as $k\to\infty$ if (5.27) holds and its convergence to zero is determined by the slowest convergence mode among $\left\{1-\mu\lambda_n\right\}$. Furthermore, since the convergence rate of the elements of $\Delta\mathbf{C}_k$ is governed by a combination of modes, the choice of $\mu=\mu_o$ does not guarantee the fastest possible convergence during the entire recursion process. However, after the faster modes die out and the slowest mode is dominant, this choice will provide the fastest convergence compared to any other choice of μ.

It is important to mention here that in some cases it may be desirable to use a time-varying step-size instead of a constant one in order to control the rate of the convergence of the algorithm.

5.5.3 Learning Curves

The convergence performance of a steepest-descent algorithm is usually characterized in terms of its learning curve. Assuming μ is selected so that (5.27) is met, the convergence of $\mathbf{C}_k$ within the steepest-descent recursion provides a converging sequence $\{J(\mathbf{C}_k)\}$ that monotonically tends to $J_{\min}$ (Haykin 2001) or, in other words,

$$\text{as } k \to \infty \text{ and } \mathbf{C}_k \to \mathbf{C}_o,\ J(\mathbf{C}_k) \to J_{\min} = tr\left\{\mathbf{R}_{\mathbf{d}} - \mathbf{\Gamma}^{\mathrm{H}}\mathbf{R}^{-1}\mathbf{\Gamma}\right\}. \tag{5.37}$$

To demonstrate this, $J(\mathbf{C}_k)$ can be re-written as

$$\begin{aligned} J(\mathbf{C}_k) &= J_{\min} + tr\left\{(\mathbf{C}_k - \mathbf{C}_o)^H \mathbf{R}(\mathbf{C}_k - \mathbf{C}_o)\right\} \\ &= J_{\min} + tr\left\{\mathbf{Z}_k^H \mathbf{\Lambda} \mathbf{Z}_k\right\} \\ &= J_{\min} + \sum_{n=1}^{N} \lambda_n \left|\mathbf{Z}_k[n,n]\right|^2 \\ &= J_{\min} + \sum_{n=1}^{N} \lambda_n (1-\mu\lambda_n)^{2(k+1)} \left|\mathbf{Z}_{-1}[n,n]\right|^2 \end{aligned} . \tag{5.38}$$

The last expression in (5.38) confirms that if $\mu < 2/\lambda_{\max}$, (5.37) holds irrespective of the initial values and the convergence of $J(\mathbf{C}_k)$ to $J_{\min}$ is exponential. The evolution of $J(\mathbf{C}_k)$ as a function of *k*, referred to as the learning curve or *a priori* output estimation

error, provides valuable information about the learning behavior of the steepest-descent algorithm.

5.6 Stochastic Gradient Algorithms

In this section, adaptive filters are developed by introducing the *Stochastic Gradient* (SG) algorithms (Benvensite et al 1980), obtained from steepest-descent algorithms by replacing the required autocorrelation and cross-correlation matrices by suitable approximations. Different approximations result in different complexities and different performances. Substituting the actual gradient matrices by their estimates will lead to some random fluctuations in the resultant update directions, referred to as *gradient noise*. However, there are two important advantages in employing the SG algorithms. Firstly, they avoid the need to know the exact signal statistics, which are rarely available in practice. Secondly, these algorithms provide a tracking mechanism that enables them to track the variations in the signal statistics. For these two reasons, the SG algorithms are widely used in many applications. Some of the most well-known algorithms of this class are the Least Mean Square (LMS) algorithm (Widrow 1960), the Normalized LMS (NLMS) algorithm (Haykin 2001), the Affine Projection Algorithm (APA) (Slavakis & Theodoridis 2008) and the Recursive Least Squares (RLS) algorithm (Hayes 1996) that will be discussed in the next sections.

5.6.1 The Least-Mean-Square Algorithm

The simplest approximations to $\{\mathbf{R}, \boldsymbol{\Gamma}\}$ are the instantaneous values as follows:

$$\hat{\mathbf{R}} = \mathbf{y}^{\mathrm{H}}\mathbf{y}\,, \tag{5.39}$$

$$\boldsymbol{\Gamma} = \mathbf{y}^{\mathrm{H}}\mathbf{d}\,. \tag{5.40}$$

This is equivalent to simply dropping the expectation operators in (5.21) and replacing the random variables by their instantaneously observed ensembles. Employing this approximation, the gradient matrix in (5.16) will be replaced by

$$-\left[\nabla_{\mathbf{C}} J\left(\mathbf{C}_{k-1}\right)\right]^{\mathrm{H}} \approx \mathbf{y}_k^{\mathrm{H}}\mathbf{d}_k - \mathbf{y}_k^{H}\mathbf{y}_k\mathbf{C}_k\,, \tag{5.41}$$

and the corresponding recursion equation is

$$\mathbf{C}_k = \mathbf{C}_{k-1} + \mu\mathbf{y}_k^{\mathrm{H}}\left[\mathbf{d}_k - \mathbf{y}_k\mathbf{C}_{k-1}\right]. \tag{5.42}$$

Due to its computational simplicity, the stochastic-gradient approximation in (5.42) is the most widely used adaptive algorithm in practice and is known as the Least Mean Squares (LMS) algorithm (Widrow 1960).

The LMS algorithm in (5.42) can be regarded as the exact solution (not approximate) to a local (as opposed to the global) optimization problem, as described in APPENDIX C. Finally, two estimation errors are defined in this context: the *a priori* estimation error vector

$$\mathbf{e}_k = \mathbf{d}_k - \mathbf{y}_k\mathbf{C}_{k-1}, \tag{5.43}$$

and the *a posteriori* estimation error vector

$$\mathbf{r}_k = \mathbf{d}_k - \mathbf{y}_k \mathbf{C}_{k-1}. \tag{5.44}$$

It is important to note that since the LMS algorithm is a local optimization approach, as opposed to the steepest descent technique which was a global optimization technique, the convergence of the algorithm also depends on the choice of the initial values in addition to the step-size.

5.6.1.1 LMS with Decision Feedback

As mentioned in previous sections, in many practical applications such as the one studied in this thesis, there is no training data available to the system, in other words the value of $\mathbf{d}_k$ is unknown at the receiver side. In Section 5.3, it was shown that DFE-based adaptive algorithms are developed to solve this problem by adding a hard decision block to the system. This block provides an estimate of the transmitted data $\tilde{\mathbf{d}}_k$ which is used as a substitute of $\mathbf{d}_k$ to update the coefficients of the adaptive equalizer filter.

For the problem studied in this chapter, different structures can be considered for the decision block. The simplest choice is to set $\tilde{\mathbf{d}}_k$ as $\tilde{\mathbf{d}}_k = a_{\hat{\tau}_{LOS,k}} \mathbf{g}^{\mathrm{T}}_{\hat{\tau}_{LOS,k}}$ where $\hat{\tau}_{LOS,k}$ is the delay that corresponds to the maximum of the equalizer output, $\hat{\mathbf{y}}_k$. This strategy is the same as the one used as the initial guess of the MEDLL algorithm introduced in Chapter 3. However, since the output of the equalizer is supposed to be multipath-free in its steady state, the best estimate of the LOS peak from this data is the scalar ML estimate that was represented by (3.18) in Chapter 3. When using this strategy, the output of the decision block still has the form of $\tilde{\mathbf{d}}_k = a_{\hat{\tau}_{\mathrm{LOS},k}} \mathbf{g}^{\mathrm{T}}_{\hat{\tau}_{\mathrm{LOS},k}}$ in which $\hat{\tau}_{\mathrm{LOS},k}$ is the delay that

corresponds to the maximum of the equalizer output vector as before, but this time $a_{\hat{\tau}_{\mathrm{LOS},k}}$ is represented by

$$a_{\hat{\tau}_{\mathrm{LOS},k}} = \frac{\mathbf{g}^{\mathrm{H}}_{\hat{\tau}_{\mathrm{LOS},k}} \mathbf{G}^{-1} \hat{\mathbf{y}}_k}{\mathbf{g}^{\mathrm{H}}_{\hat{\tau}_{\mathrm{LOS},k}} \mathbf{G}^{-1} \mathbf{g}_{\hat{\tau}_{\mathrm{LOS},k}}} \ . \tag{5.45}$$

Since **G** is a known matrix, its inverse is also known beforehand and hence the computation in (5.45) does not increase the order of the computational complexity of the system. Therefore, for a DFE-based LMS system the recursion equation can be represented by

$$\mathbf{C}_k = \mathbf{C}_{k-1} + \mu \mathbf{y}^{\mathrm{H}}_k \left\lfloor \tilde{\mathbf{d}}_k - \mathbf{y}_k \mathbf{C}_{k-1} \right\rfloor . \tag{5.46}$$

This DFE structure is considered for all the other stochastic gradient algorithms that are introduced in the next sections.

5.6.1.2 Ensemble-Average Learning Curves

It was mentioned in Section 5.3.4 that the performance of the steepest Descent algorithms is characterized by means of their learning curves. Similarly, the performance of a stochastic gradient algorithm is evaluated by investigating its ensemble average learning curve.

As shown in Section 5.2.2, the evaluation of $J\left(\mathbf{C}_k\right)$ requires knowledge about **R**, **Γ** and $\mathbf{R}_{\mathbf{d}}$. However, in a stochastic gradient implementation this statistical information is not available. In contrast, the learning curve of a stochastic gradient algorithm is computed using the *a priori* estimation error sequence in (5.43) as follows. First, the algorithm is

run for a number of iterations, namely K, so that the convergence is met. The error sequence $\{\mathbf{e}_k\}$ and the corresponding squared error sequence $\left\{\left\|\mathbf{e}_k\right\|^2\right\}$ are then produced. This squared error curve in denoted by

$$\left\{\left\|\mathbf{e}^{(1)}{}_k\right\|^2, 0<k<K\right\}, \tag{5.47}$$

wherein the superscript (1) indicates the results of the first experiment. The same stochastic gradient algorithm is then run for other N_e-1 times using data with the same statistical properties (either simulated data or real static data) and with the same initial condition. The *ensemble average* curve is then obtained by averaging over the experiments as

$$\hat{J}_k = \frac{1}{N_e}\sum_{i=1}^{N_e}\left\|\mathbf{e}^{(i)}{}_k\right\|^2, \tag{5.48}$$

which is an approximation to the true learning curve.

5.7 Normalized LMS Algorithm

In the same way that the LMS algorithm is an approximation to the steepest descent recursion in (5.21), the *Normalized LMS* (NLMS) algorithm is an instantaneous approximation of the regularized Newton's recursion in (5.32). Therefore, replacing the quantities $(\varepsilon\mathbf{I}+\mathbf{R})$ and $(\mathbf{\Gamma}-\mathbf{R}\mathbf{C}_{k-1})$ by their instantaneous approximations $\left(\varepsilon\mathbf{I}+\mathbf{y}_k^{\mathrm{H}}\mathbf{y}_k\right)$ and $\mathbf{y}_k^{\mathrm{H}}\left[\mathbf{d}_k-\mathbf{y}_k\mathbf{C}_{k-1}\right]$, respectively, the following stochastic gradient recursion is obtained:

$$\mathbf{C}_k = \mathbf{C}_{k-1} + \mu\left[\varepsilon\mathbf{I} + \mathbf{y}_k^{\mathrm{H}}\mathbf{y}_k\right]^{-1}\mathbf{y}_k^{\mathrm{H}}\left[\mathbf{d}_k - \mathbf{y}_k\mathbf{C}_{k-1}\right]. \tag{5.49}$$

This form of NLMS recursion requires inverting the $\left(\varepsilon\mathbf{I} + \mathbf{y}_k^{\mathrm{H}}\mathbf{y}_k\right)$ matrix at each iteration. However, this inversion can be avoided using the following matrix inversion lemma (Graybill 1969):

$$\left(\varepsilon\mathbf{I} + \mathbf{y}_k^{\mathrm{H}}\mathbf{y}_k\right)^{-1} = \varepsilon^{-1}\mathbf{I} - \frac{\varepsilon^{-2}}{1+\varepsilon^{-1}\left\|\mathbf{y}_k\right\|^2}\mathbf{y}_k^{\mathrm{H}}\mathbf{y}_k. \tag{5.50}$$

Multiplying both sides of (5.50) by $\mathbf{y}_k^{\mathrm{H}}$ from the right results in

$$\left[\varepsilon\mathbf{I} + \mathbf{y}_k^{\mathrm{H}}\mathbf{y}_k\right]^{-1}\mathbf{y}_k^{\mathrm{H}} = \varepsilon^{-1}\mathbf{y}_k^{\mathrm{H}} - \frac{\varepsilon^{-2}}{1+\varepsilon^{-1}\left\|\mathbf{y}_k\right\|^2}\mathbf{y}_k^{\mathrm{H}}\left\|\mathbf{y}_k\right\|^2 = \frac{\mathbf{y}_k^{\mathrm{H}}}{\varepsilon+\left\|\mathbf{y}_k\right\|^2}. \tag{5.51}$$

Substituting (5.51) into (5.49), a simpler equivalent of the NLMS recursion is obtained as

$$\mathbf{C}_k = \mathbf{C}_{k-1} + \frac{\mu}{\varepsilon+\left\|\mathbf{y}_k\right\|^2}\mathbf{y}_k^{\mathrm{H}}\left[\mathbf{d}_k - \mathbf{y}_k\mathbf{C}_{k-1}\right]. \tag{5.52}$$

This form of the recursion is referred to as ε-NMLS. Comparing ε-NMLS with the LMS algorithm illustrates the fact that in the LMS algorithm the correction term to $\mathbf{C}_{k-1}$ is proportional to the norm of $\mathbf{y}_k^{\mathrm{H}}$. Therefore, an input vector with a larger norm results in a more substantial change to $\mathbf{C}_{k-1}$. Adversely, in the NLMS algorithm the correction term

is normalized to the squared norm of $\mathbf{y}_k$. Moreover, the recursive equation in (5.52) can be considered as an LMS recursion with a time-variant step-size so that $\mu_k = \dfrac{\mu}{\varepsilon + \|\mathbf{y}_k\|^2}$.

5.8 Affine Projection Algorithm

The LMS and ε-NMLS algorithms were obtained by employing instantaneous approximation of autocorrelation and cross-correlation matrixes. However, it is possible to derive more sophisticated approximations for these two matrices, which will result in stochastic gradient approaches with improved convergence properties but at increased computational costs. One such approximation uses the *K* most recent epochs of data in the computation of the correlation matrices in which *K* is a positive integer smaller than *N*. This approximation can be represented by

$$\hat{\mathbf{R}} = \frac{1}{K} \sum_{j=k-K+1}^{k} \mathbf{y}_k^{\mathrm{H}} \mathbf{y}_k \,, \tag{5.53}$$

$$\boldsymbol{\Gamma} = \frac{1}{K} \sum_{j=k-K+1}^{k} \mathbf{y}_k^{\mathrm{H}} \mathbf{d}_k \,. \tag{5.54}$$

The equalities in (5.53) and (5.54) can be represented in a more compact form as

$$\hat{\mathbf{R}} = \frac{1}{K} \mathbf{Y}_k^{\mathrm{H}} \mathbf{Y}_k \,, \tag{5.55}$$

$$\boldsymbol{\Gamma} = \frac{1}{K} \mathbf{Y}_k^{\mathrm{H}} \mathbf{D}_k \tag{5.56}$$

where

$$\mathbf{Y}_k = \begin{bmatrix} \mathbf{y}_k \\ \mathbf{y}_{k-1} \\ \vdots \\ \mathbf{y}_{k-K+1} \end{bmatrix} \quad \text{and} \quad \mathbf{D}_k = \begin{bmatrix} \mathbf{d}_k \\ \mathbf{d}_{k-1} \\ \vdots \\ \mathbf{d}_{k-K+1} \end{bmatrix}. \tag{5.57}$$

Substituting the approximation in (5.57) into the Newton's equation, the following recursion will be obtained:

$$\mathbf{C}_k = \mathbf{C}_{k-1} + \mu\left(\varepsilon\mathbf{I} + \mathbf{Y}_k^{\mathrm{H}}\mathbf{Y}_k\right)^{-1}\mathbf{Y}_k^{\mathrm{H}}\left[\mathbf{D}_k - \mathbf{Y}_k\mathbf{C}_{k-1}\right]. \tag{5.58}$$

The recursion in (5.58) requires inverting a $N\times N$ matrix $\left(\varepsilon\mathbf{I} + \mathbf{Y}_k^{\mathrm{H}}\mathbf{Y}_k\right)$. Alternatively, the matrix inversion lemma can be invoked to verify that

$$\left(\varepsilon\mathbf{I} + \mathbf{Y}_k^{\mathrm{H}}\mathbf{Y}_k\right)^{-1}\mathbf{Y}_k^{\mathrm{H}} = \mathbf{Y}_k^{\mathrm{H}}\left(\varepsilon\mathbf{I} + \mathbf{Y}_k\mathbf{Y}_k^{\mathrm{H}}\right)^{-1}, \tag{5.59}$$

and the corresponding recursion would be

$$\mathbf{C}_k = \mathbf{C}_{k-1} + \mu\mathbf{Y}_k^{\mathrm{H}}\left(\varepsilon\mathbf{I} + \mathbf{Y}_k\mathbf{Y}_k^{\mathrm{H}}\right)^{-1}\left[\mathbf{D}_k - \mathbf{Y}_k\mathbf{C}_{k-1}\right]. \tag{5.60}$$

This form of recursion requires inverting the smaller $K\times K$ matrix $\left(\varepsilon\mathbf{I} + \mathbf{Y}_k\mathbf{Y}_k^{\mathrm{H}}\right)$. This matrix is invertible even when $\varepsilon = 0$ since $K<N$. The recursion in (5.60) is referred to as the Affine Projection Algorithm (APA) (Slavakis & Theodoridis 2008). In particular, it can be verified that when K=1, the APA algorithm reduces to the ε-NMLS algorithm. In general, the integer K is referred to as the order of the APA filter.

5.9 The RLS Algorithm

Another example of a stochastic gradient algorithm that employs a more sophisticated approximation of the covariance and cross-covariance matrices is the Recursive Least Squares (RLS) algorithm (Hayes 1996). This algorithm can be also derived as the exact solution to the problem of optimizing the least-squares cost function. However, in this chapter it is motivated as a stochastic gradient algorithm.

The approximation that the RLS algorithm uses for the covariance matrix can be represented as

$$\hat{\mathbf{R}} = \frac{1}{k+1}\sum_{j=0}^{k} \lambda^{k-j} \mathbf{y}_j^{\mathrm{H}} \mathbf{y}_j \ , \tag{5.61}$$

which are exponentially weighted sample averages of the instantaneous matrices. In the above equalities, λ is a scalar that should be selected in the range of $0 \ll \lambda \leq 1$. For the special case of $\lambda = 1$, the above approximation is equivalent to averaging all the past samples up to the present time. When a value smaller than unity is assigned to λ, the recent samples are associated with larger weights than the previous ones. This strategy enables a tracking mechanism for the adaptive system.

To better fit the approximation in (5.61) into the Newton's equation in (5.32), it is assumed that the step-size and the regularization parameter are chosen as (Sayed 2008)

$$\mu_k = \frac{1}{k+1} \ , \qquad \varepsilon_k = \lambda^{k+1} \frac{\varepsilon}{k+1} . \tag{5.62}$$

With these choices, the regularization disappears as time progresses. Substituting the approximation in (5.61) into the Newton's recursion, the following stochastic gradient recursion is obtained:

$$\mathbf{C}_k = \mathbf{C}_{k-1} + \left[\lambda^{k+1} \varepsilon \mathbf{I} + \sum_{j=0}^{k} \lambda^{k-j} \mathbf{y}_j^{\mathrm{H}} \mathbf{y}_j \right]^{-1} \mathbf{y}_k^{\mathrm{H}} \left[\mathbf{d}_k - \mathbf{y}_k \mathbf{C}_{k-1} \right]. \tag{5.63}$$

In order to represent the above recursion in a simpler form, consider the following variable change:

$$\Phi_k = \left(\lambda^{k+1} \varepsilon \mathbf{I} + \sum_{j=0}^{k} \lambda^{k-j} \mathbf{y}_j^{\mathrm{H}} \mathbf{y}_j \right). \tag{5.64}$$

Then it can be easily verified that

$$\mathbf{\Phi}_k = \lambda \mathbf{\Phi}_{k-1} + \mathbf{y}_k^{\mathrm{H}} \mathbf{y}_k, \qquad \mathbf{\Phi}_{-1} = \varepsilon \mathbf{I}. \tag{5.65}$$

Now let $\mathbf{P}_k = \mathbf{\Phi}_k^{-1}$. Then employing the matrix inversion lemma, the recursion in (5.65) can be represented as

$$\mathbf{P}_k = \lambda^{-1} \left[\mathbf{P}_{k-1} - \frac{\lambda^{-1} \mathbf{P}_{k-1} \mathbf{y}_k^{\mathrm{H}} \mathbf{y}_k \mathbf{P}_{k-1}}{1 + \lambda^{-1} \mathbf{y}_k \mathbf{P}_{k-1} \mathbf{y}_k^{\mathrm{H}}} \right], \qquad \mathbf{P}_{-1} = \varepsilon^{-1} \mathbf{I}. \tag{5.66}$$

Applying (5.65) and (5.66) into (5.63), the RLS recursion equation can be represented as

$$\mathbf{C}_k = \mathbf{C}_{k-1} + \mathbf{P}_k \mathbf{y}_k^{\mathrm{H}} \left[\mathbf{d}_k - \mathbf{y}_k \mathbf{C}_{k-1} \right]. \tag{5.67}$$

Implementing the recursion in (5.67) along with the recursion in (5.66) provides an RLS filter that only requires to have knowledge about $\{\mathbf{y}_k, \mathbf{C}_{k-1}, \mathbf{d}_k, \mathbf{P}_{k-1}\}$ at each time instant

k, in contrast to (5.63) that required the knowledge about all previous samples together at a time. Moreover this form of recursion avoids the matrix inversion in (5.63).

5.10 Other Stochastic Gradient Algorithms

It is important to consider the fact that the idea of employing the instantaneous approximations of the steepest descent methods to devise stochastic gradient algorithms is not restricted to the quadratic cost functions. Some of the well-known stochastic gradient algorithms with non-quadratic cost functions include the Error-Sign LMS (ES-LMS) algorithm (Ding & Li 2001) that minimizes the absolute value of the error vector in (5.6), the Leaky-LMS algorithm (Mayyas & Aboulnasr 2002) that minimizes $\left[\alpha tr\left\{\mathbf{C}\mathbf{C}^{\mathrm{H}}\right\}+\mathrm{E}\left\|\mathbf{d}-\mathbf{y}\mathbf{C}\right\|^{2}\right]$ where is α a positive constant and the Least Mean Fourth (LMF) algorithm (Walach & Widrow 1984) that minimizes $\mathrm{E}\left\|\mathbf{d}-\mathbf{y}\mathbf{C}\right\|^{4}$. Among these algorithms we only compare the performance of the ES-LMS algorithm to the previously introduced SG algorithms in some of the simulations. The recursive equation of this algorithm can be represented by (Sayed 2008)

$$\mathbf{C}_{k}=\mathbf{C}_{k-1}+\mu\mathbf{y}_{k}^{\mathrm{H}}\mathrm{csgn}\left[\mathbf{d}_{k}-\mathbf{y}_{k}\mathbf{C}_{k-1}\right]. \tag{5.68}$$

In the above, the csgn(x) operator outputs the sign of a complex number $\mathrm{x}=\mathrm{x}_{\mathrm{r}}+\mathrm{j}\mathrm{x}_{\mathrm{i}}$ defined as

$$\text{csgn}(x) = \text{sign}(x_r) + j\,\text{sign}(x_i) \quad \text{where} \quad \text{sign}(a) = \begin{cases} +1 & \text{if } a > 0 \\ -1 & \text{if } a < 0 \\ 0 & \text{if } a = 0 \end{cases}. \tag{5.69}$$

and the csgn of a vector is a vector of the csgn of its entries.

5.11 Computational complexities

The computational complexities of the stochastic gradient algorithms introduced above are compared in Table 5-1. For computing costs the following general considerations have been made:

1) The summation/subtraction of two vectors with a length of N and complex entries requires $2N$ real scalar summations
2) The summation/subtraction of two matrices with a size of $N \times N$ and complex elements requires $2\,N^2$ real scalar summations
3) The inner product of two vectors with a length of N and complex entries requires N complex scalar multiplications and N-1complex scalar summations which is equal to $4N$ real scalar multiplications and $4N$-2 real scalar summations
4) The multiplication of two matrices with a size of $N \times L$ and $L \times M$ is equivalent to an $N \times M$ inner product of vectors with the length of L which is equivalent to $4 \times L \times N \times M$ real scalar multiplication and $(4L-2) \times N \times M$ real scalar summations
5) The multiplication of scalar to a matrix with a size of $N \times N$ requires $2N^2$ real scalar multiplications
6) The norm of a vector with a length of N is equal to the inner product of two vectors.

7) The outer product of two vectors with a length of N requires N^2 complex multiplications which is equivalent to $4N^2$ real scalar multiplications and $2N^2$ real scalar summations.

8) The inversion of a matrix with a size of $N \times N$ requires N^3 summations and N^3 multiplications.

Table 5-1: Comparison of the computational cost of different SG algorithms

Algorithm	Real Scalar Summation	Real Scalar multiplication	Real Scalar Division	Real Scalar Sign
LMS	$8N^2$	$10N^2$	-	-
NLMS	$8N^2+4N$	$10N^2+4N-1$	1	-
APA	$K^3+8N^2K+8NK^2-2NK$	$K^3+8N^2K+8NK^2$	-	-
RLS	$4N^3+16N^2+2N-1$	$4N^3+20N^2+4N$	1	-
ELMS	$8N^2+4N$	$10N^2+4N-1$	1	$2N$

5.12 Simulation Results

In this section, a set of simulation results is presented to analyze the behavior of the introduced SG algorithms and compare their performance under different operational conditions.

In Figure 5-3, the correlation function of the received signal, the output of the equalizer and the output of the decision block for four of the most common SG algorithms at three

different time instants of a same simulation are shown. In this simulation, the impulse response of the channel has totally changed at time index k=200 from the one shown in Figure 5-4(a) to the one in Figure 5-4 (b). The first column of the subplots in Figure 5-3 shows that all of the four algorithms are successfully locked at time index k=20 since the decision outputs are correctly aligned to the zero delay lag which here corresponds to LOS. In the second column, the shapes of the correlation functions have changed as a result of the changes in the CIR. The output of the equalizers (green curves) have been adaptively modified in the time duration between k=201 to k=250 so that the decision outputs are again correctly aligned to the true LOS delay at k=250.

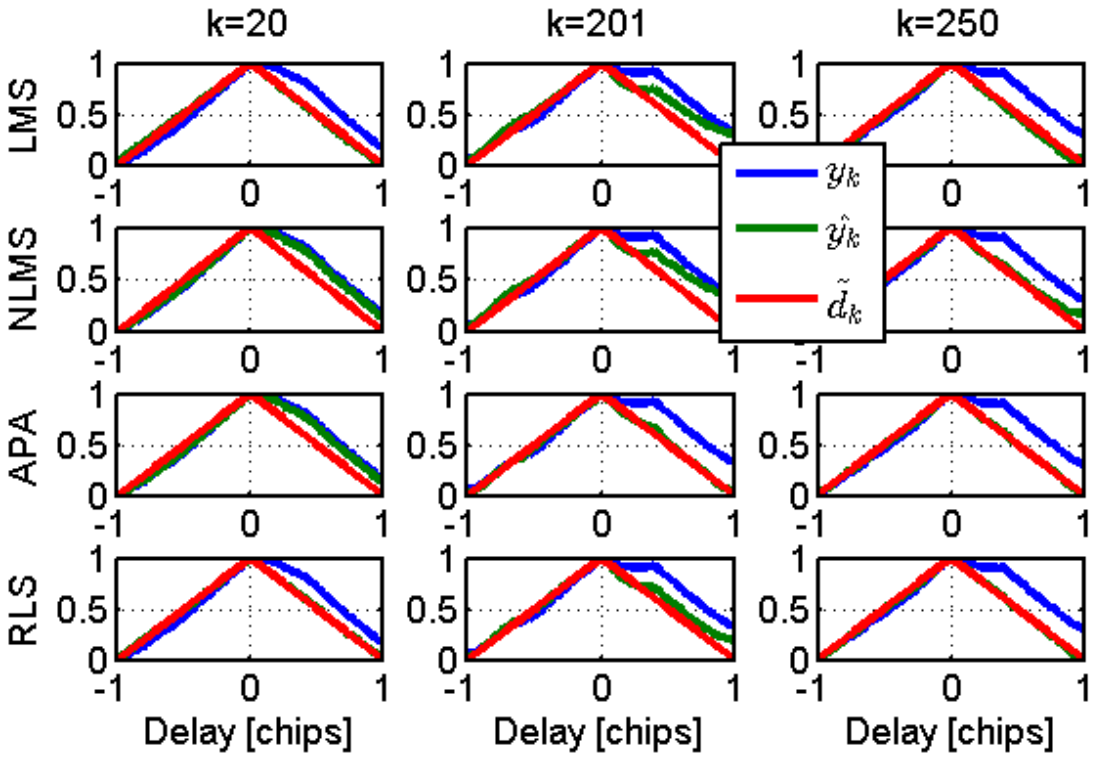

Figure 5-3: Correct equalization of the correlation function by different adaptive algorithms

Figure 5-5 shows an example similar to Figure 5-3. This time the CIR has changed at time index k=600. Again after 50 epochs all algorithms have converged. However, it can be observed in the second column of the figure that in this example, the decision outputs of the LMS and NLMS algorithms are not centered on the true LOS delay. This means that these two algorithms have converged to a local minimum instead of the global minimum. This will result in a bias in LOS delay estimations. This convergence to global minima is possible in SG algorithms because they are indeed approximations to the steepest descent algorithms.

The CIRs associated with Figure 5-5 are shown in Figure 5-6.

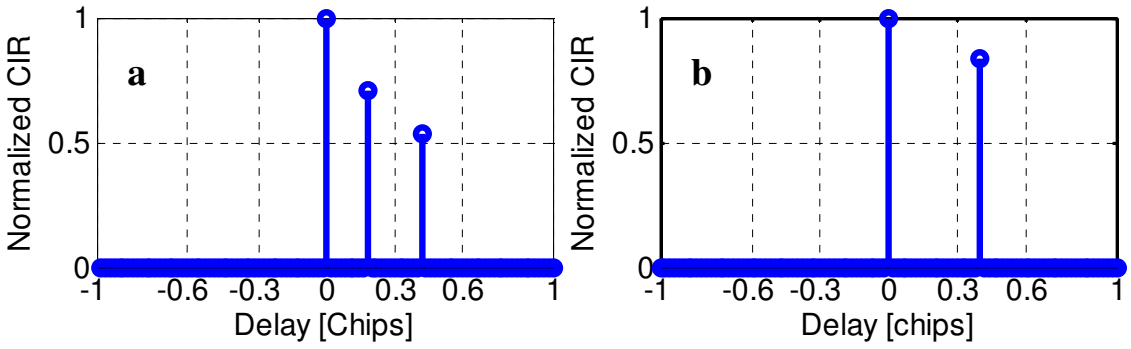

Figure 5-4: CIRs associated to Figure 5-3

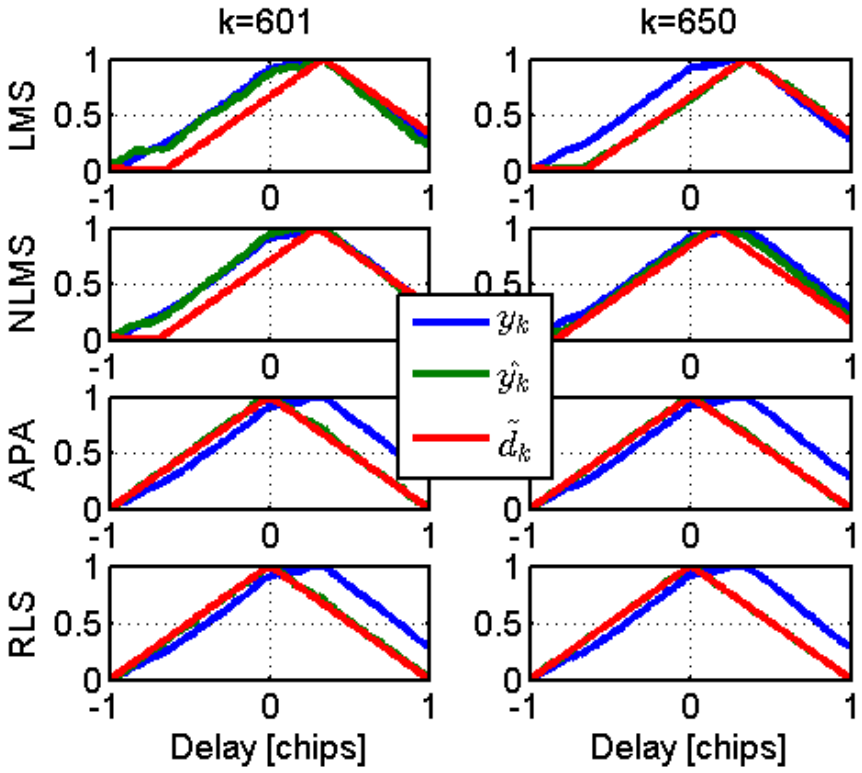

Figure 5-5: Biased equalization of the correlation function by some of adaptive methods

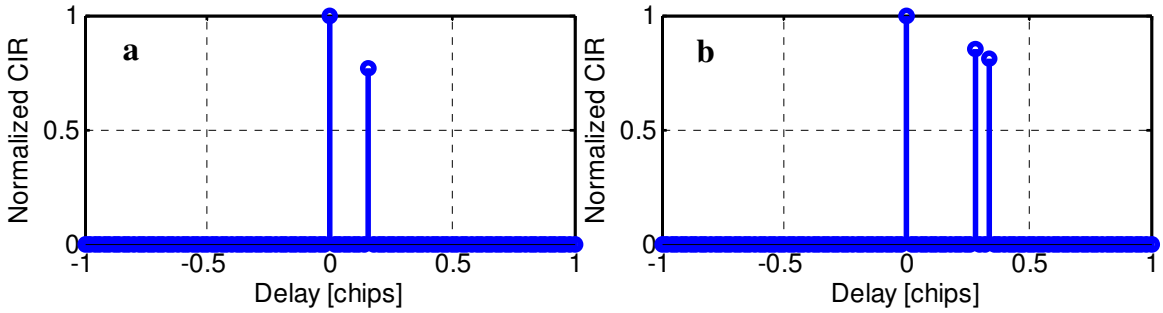

Figure 5-6: CIRs associated to Figure 5-5

5.12.1 The Effects of Different Parameters

In this section, the effects of different design parameters on the performance of the discussed SG algorithms are investigated through simulations.

5.12.1.1 The Effect of the Step-Size

Figure 5-7 shows the learning curves of the LMS algorithm for different values of the step-size which are all selected in a range that leads to convergence of the algorithm. The value of C/N_0 was 40 dB-Hz for this simulation, the integration period was 1 ms, and the sampling rate was 20 MHz. This learning curve has been obtained by averaging over 100 instantaneous curves.

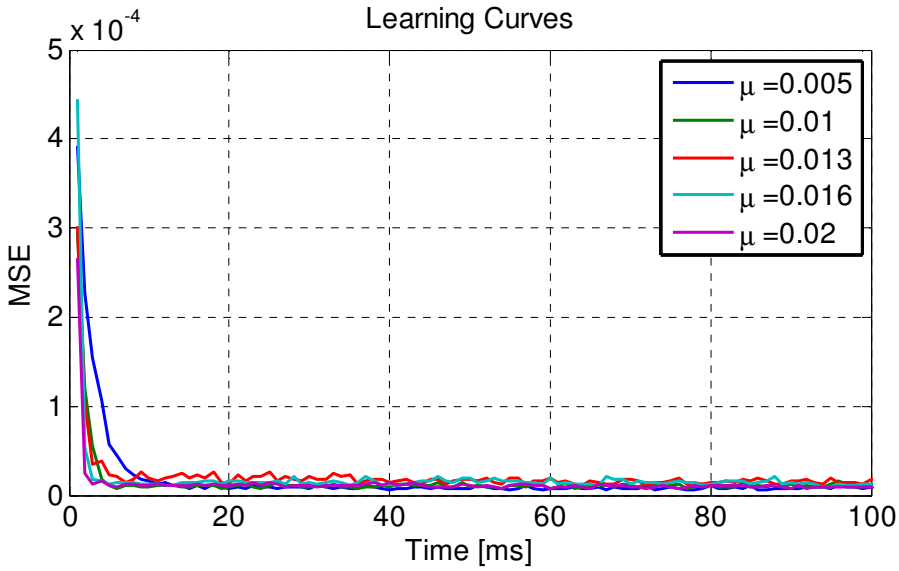

Figure 5-7: Learning curves of the LMS algorithm with different step-size values

It can be observed in this figure that as the selected value for the step-size increases, the convergence rate of the algorithm increases as well. However, any choice of $\mu > 0.023$ would result in divergence of the algorithm.

The time constant of convergence for the LMS algorithm can be approximately computed as (Haykin 2001): $\tau_{msec} \simeq \frac{1}{2\mu tr\{R\}} = \frac{1}{2\mu P_Y}$, wherein P_Y is the tap input power of the filter. For this simulation, the time constant should be 1-3 ms ($P_Y \simeq 35$) which is verified by the learning curves in Figure 5-7.

In Figure 5-8 the RMS errors of LOS delay estimation and the minimum of the cost function for the same simulation as a function of the step-size are shown.

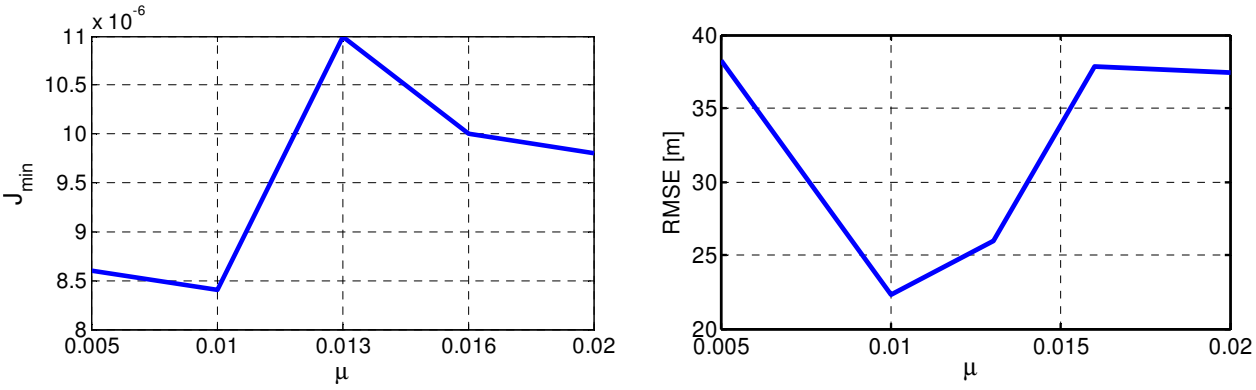

Figure 5-8: Averaged RMSE and $J_{\min}$ as a function of the μ for LMS algorithm

It is obvious that as opposed to steepest descent algorithms, finding an optimum value for the step-size is not quite straightforward in SG algorithms. However, it can be observed that both the $J_{\min}$ and RMSE diagrams have a minimum around $\mu = 0.01$. Therefore, this choice of step-size is used in all simulations in the following sections.

The diagram in Figure 5-9 shows the variations of $J_{\min}$ as a function of μ for the ES-LMS algorithm. This diagram monotonically increases by increasing the value of μ. For a choice of $\mu \geq 0.015$, the ES-LMS algorithm would diverge.

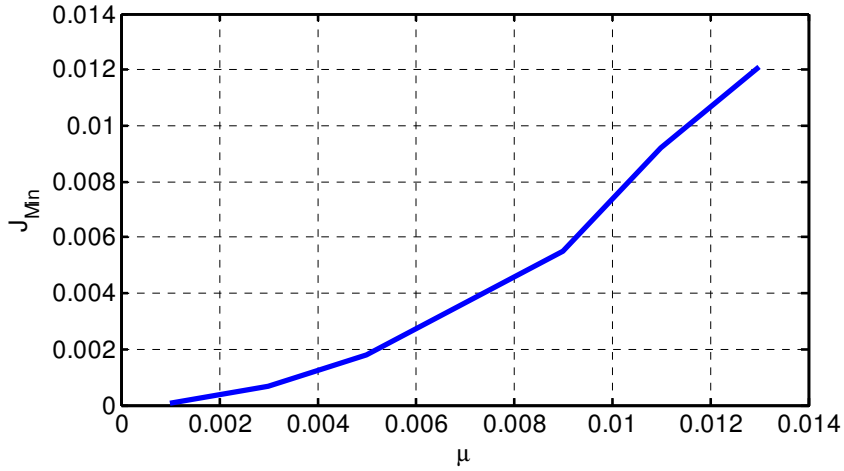

Figure 5-9: Minimum MSE for the sign-error LMS algorithm as a function of step-size

5.12.1.2 Effect of the Regularization Parameter in ε-NMLS

In this section the effect of the regularization parameter on the convergence behavior of the ε-NLMS algorithm is investigated. The simulation scenario is the same as that of Section 5.12.1.1. As before, all the curves have been obtained by averaging over 100 sample learning curves. It is observed that the choice of $\varepsilon = 0.07$ has resulted in the fastest convergence and the choice of $\varepsilon = 0.1$ has led to divergence of the algorithm. In Figure 5-11 the diagrams of the variation of the RMSE and $J_{\min}$ as a function of the regularization parameter are shown. Again it is observed that the minimum $J_{\min}$ is associated to the choice of $\varepsilon = 0.07$. However, the RMSE of the algorithm seems to be monotonically increasing with ε.

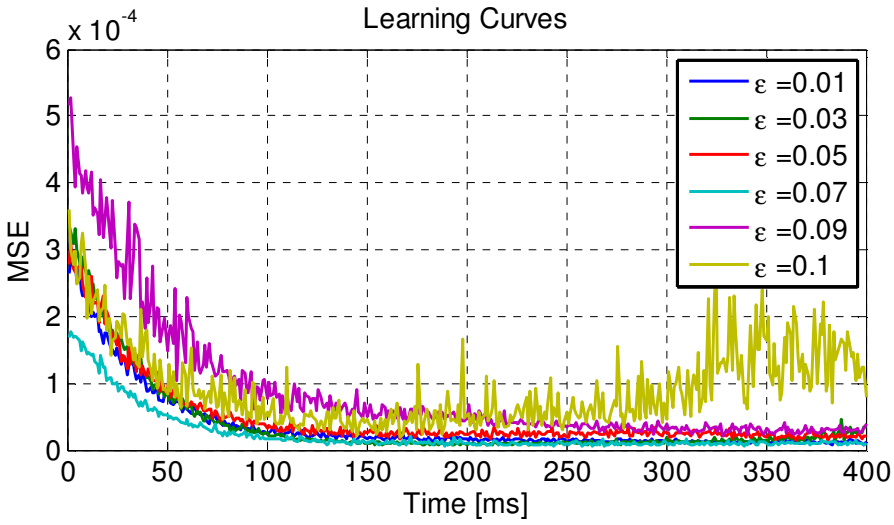

Figure 5-10: Learning curves of the ε-NLMS algorithm for different values of the regularization parameter

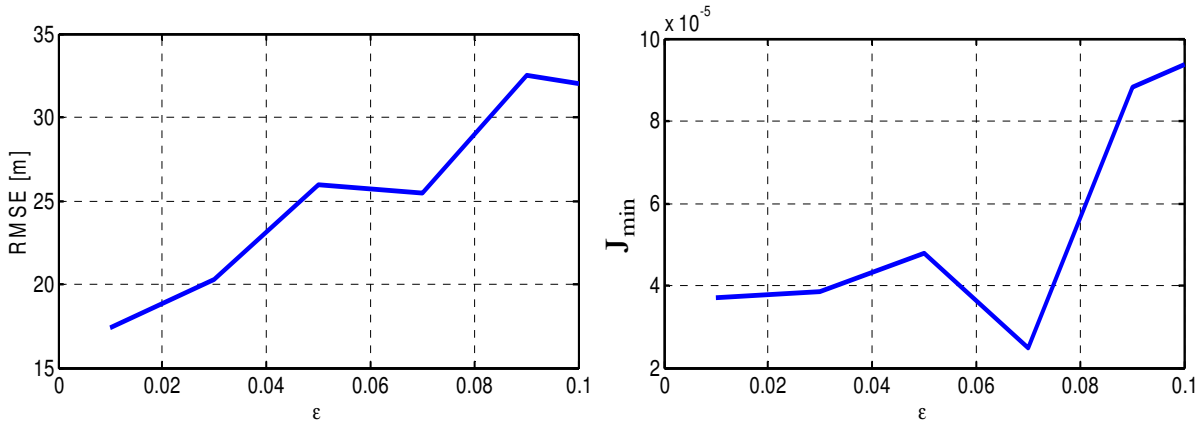

Figure 5-11: Averaged RMSE and J_{min} for ε-NLMS algorithm as a function of the regularization parameter

5.12.1.3 The Effect of *K* in APA

In Figure 5-12 the averaged learning curves of the APA algorithm for different values of *K* are depicted and in Figure 5-13 the corresponding RMSE and J_{min} diagrams are plotted.

It is obvious that in cases where the statistics of the channel does not rapidly change with time, increasing the design parameter K will result in a more accurate approximation of the covariance matrices which in turn results in a smaller RMS estimation error and a smaller $J_{\min}$ at the cost of increased computational complexity and sometimes a slower initial convergence. All of these results can be verified from these two figures.

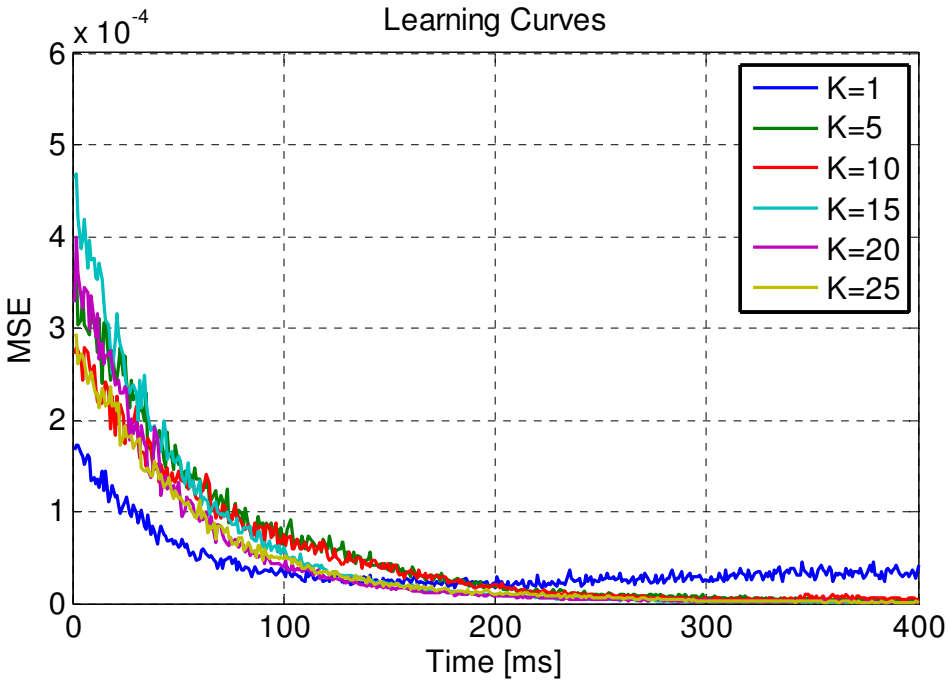

Figure 5-12: Learning curves of the APA algorithm for different values of K

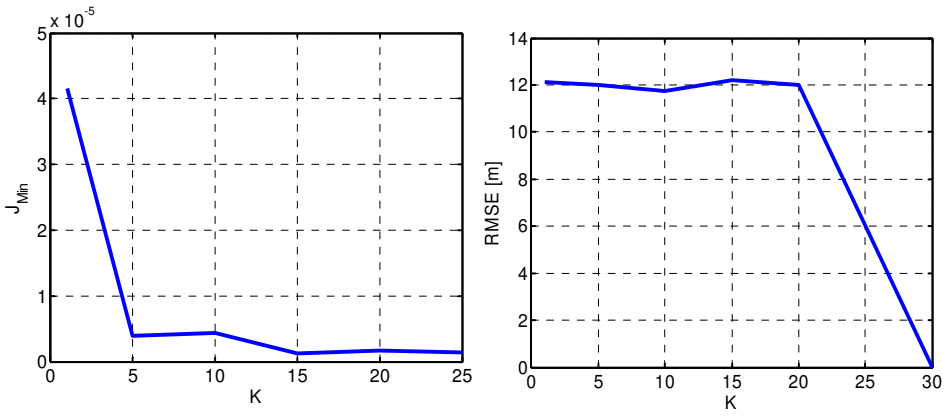

Figure 5-13: Minimum MSE cost function and RMSE diagrams as a function of *K* for the APA algorithm

5.12.1.4 Effect of λ in RLS

Figure 5-14 shows the learning curves of the RLS algorithm for different values of λ and Figure 5-15 shows the corresponding RMSE and $J_{\min}$ diagrams as function of λ. It is observed in this figures that the choice of $\lambda = 0.97$ results in the smallest $J_{\min}$ and slowest convergence. In contrast, the choice of $\lambda = 0.95$ results in the smallest RMSE whereas the corresponding values of averaged $J_{\min}$ and the convergence rate are still relatively small. Therefore, this value of λ will be used in all of the simulations in the upcoming sections. It is important to mention here that in selecting a proper value for λ the rate of the variations of the channel should be also considered. In a slow varying channel, it is possible to set λ very close to unity for improved estimation accuracy. The reason is that smaller values of λ will result in associating smaller weights to the past data. In contrast, in fast varying channels this parameter can be set closer to 0.9. Setting values smaller than 0.85 for λ may result in instability or divergence of the system.

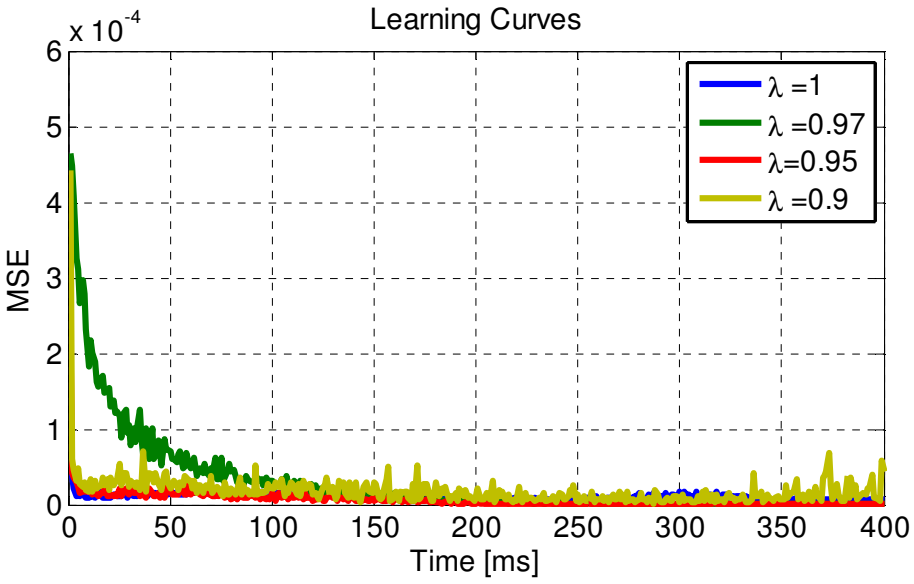

Figure 5-14: Learning curves of the RLS algorithm for different values of λ

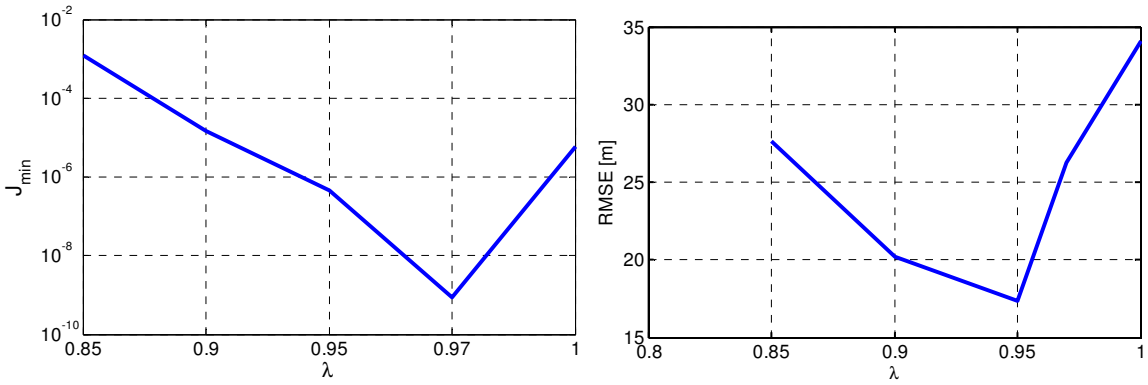

Figure 5-15: Averaged RMSE and MSE for the RLS algorithm as a function of λ

5.12.2 Convergence Comparison

After setting proper values for the design parameters, the learning curves of the different introduced SG algorithms are inter-compared in Figure 5-16 under a slow varying channel condition. The value of *K* was set to 20 for these simulations. The learning curve of the ES-LMS algorithm has been compared to the APA and LMS algorithms in Figure

5-17 (because of the different scales of the diagrams a separate figure has been used). It can be observed from these two figures that the LMS and RLS algorithms converge at considerably faster rates than the other algorithms whereas the ES-LMS algorithm has the slowest convergence rate.

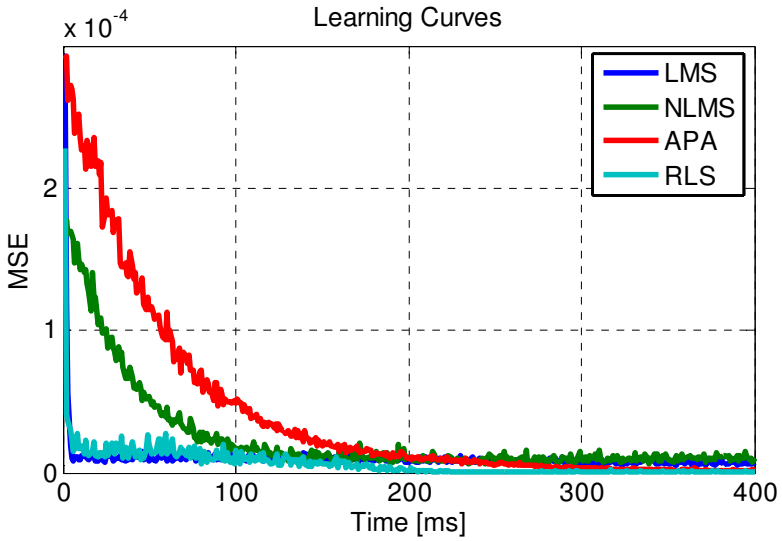

Figure 5-16: Comparison between the learning curves of different stochastic gradient algorithms

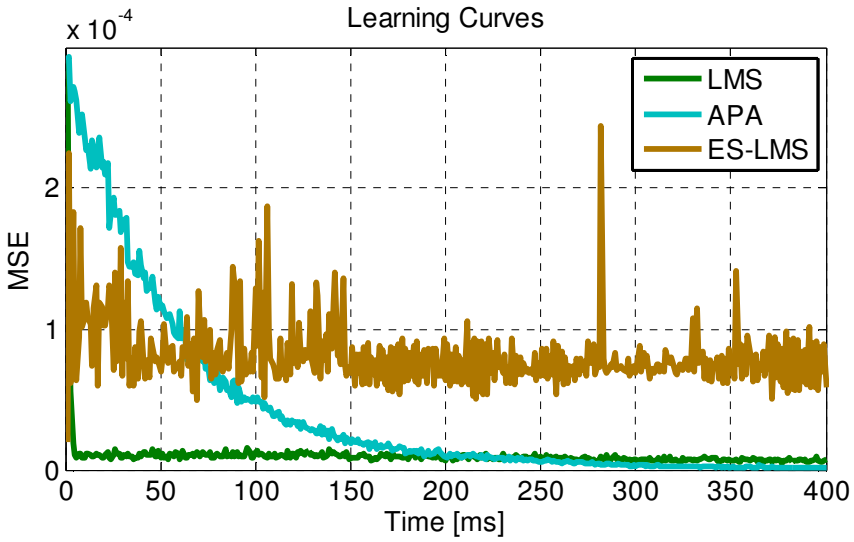

Figure 5-17: Comparison between the learning curve of the error-sign-LMS algorithm and some other SG algorithms

In Figure 5- 18 the corresponding minimum MSE cost function of the above algorithms are compared. It can be observed in this figure that the RLS algorithm has converged to the smallest $J_{\min}$ whereas the ES-LMS algorithm has ended in the largest value of the MSE cost function.

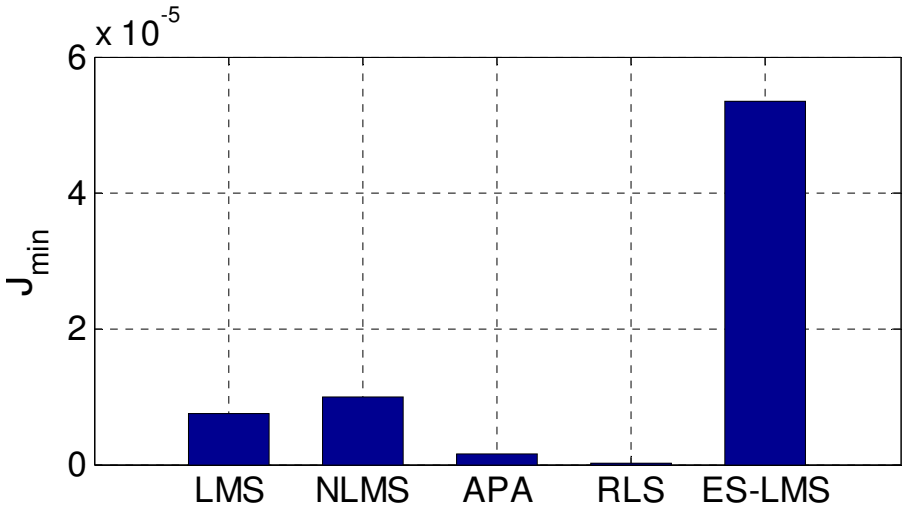

Figure 5- 18: Comparison between the minimum MSE of different SG algorithms

In Figure 5- 19 the learning curves of the algorithms are compared in fast varying channel (Although this simulation does not necessarily represent a realistic fast fading channel; it only changes the channel parameters at certain periods to study the response of the SG algorithms). In this simulation the simulated channel has been subject to serious changes every 200 ms to study if the algorithms are able to go back to convergence after losing lock on the data. It can be observed that all of the algorithms successfully returned to convergence. However, these rapid variations in the channel have led to some jumps in the learning curves of the algorithms. It is also observed that the RLS algorithm shows the smallest jumps in its learning curve and, for this reason, this algorithm is known to be a good option for tracking the signal in fast fading channels.

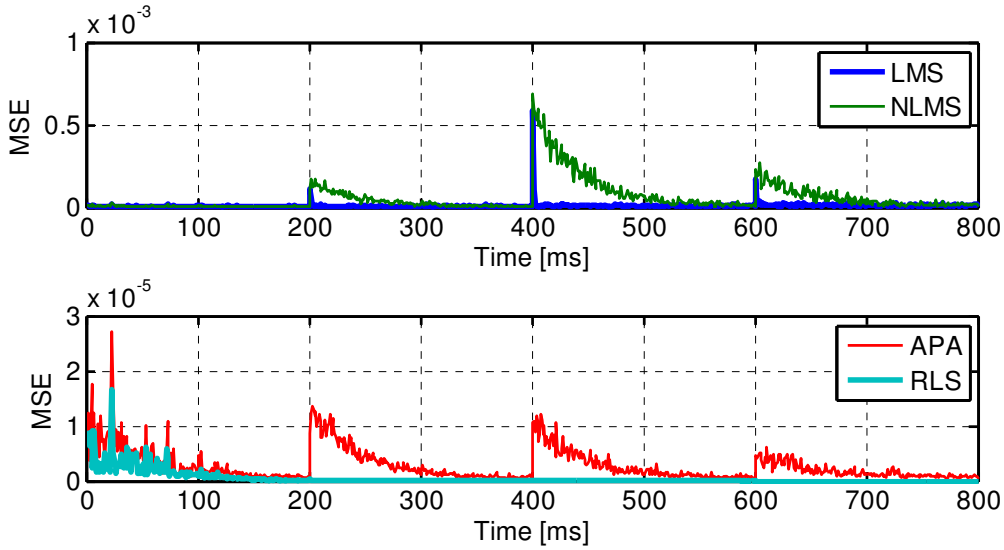

Figure 5- 19: Response of different SG algorithms to rapid changes in the channel

5.12.2.1 Effect of Initial Conditions

The effects of different initial conditions on the behavior of the SG algorithms are shown in Figure 5-20. As before, in this simulation the value of C/N_0 was 40 dB-Hz, the integration period was 1 ms, the sampling rate was 20 MHz and the simulated channel had three multipath components with random amplitudes, phases and Doppler shifts associated with each component. As it was discussed before, with SG algorithms selecting a proper set of initial values for the equalizer coefficients is important since, despite of the steepest descent algorithms, SG algorithms may diverge under improper initial conditions. It is observed that the choice of $\mathbf{C}_{-1} = \mathbf{0}_{N\times N}$ will keep all of the coefficients to zero for all of the algorithms. It is also observed in the figure that any choices in the form of $\mathbf{C}_{-1} = \alpha \mathbf{I}_{N\times N}$ result in the convergence of the algorithm and $\alpha = 1$ corresponds to the fastest convergence rate. It can be also observed that the choices in the

form of $\mathbf{C}_{-1} = \alpha \mathbf{1}_{N\times N}$ can be used to obtain the convergence where $\mathbf{1}_{N\times N}$ is an $N\times N$ all ones matrix.

In all simulations and data processing results in the following section, the choice of $\mathbf{C}_{-1} = \mathbf{I}_{N\times N}$ has been used for all algorithms.

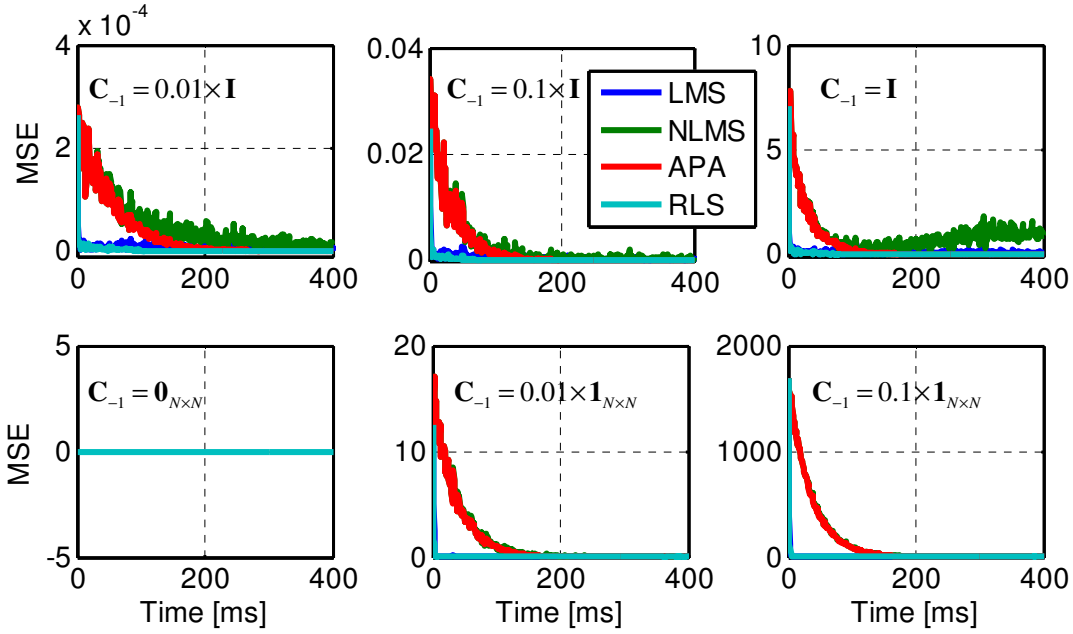

Figure 5-20: Effect of different initial conditions on SG algorithm convergence

5.12.3 Performance Comparison

Finally, in this section the averaged RMS error of LOS delay estimation and the averaged MSE of the discussed SG algorithms are compared as a function of the carrier to noise ratio under a simulated urban channel in Figure 5-21 and Figure 5-22, respectively. The channel parameters are the same as the ones used in Chapter 3 for urban channel.

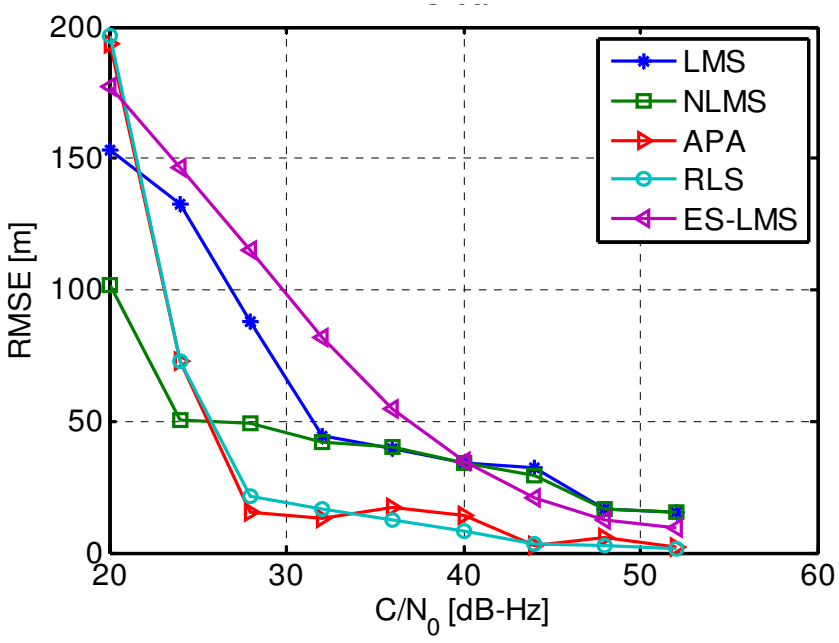

Figure 5-21: Comparison between the LOS estimation RMSE of different SG algorithms as a function of C/N_0 for a simulated urban channel

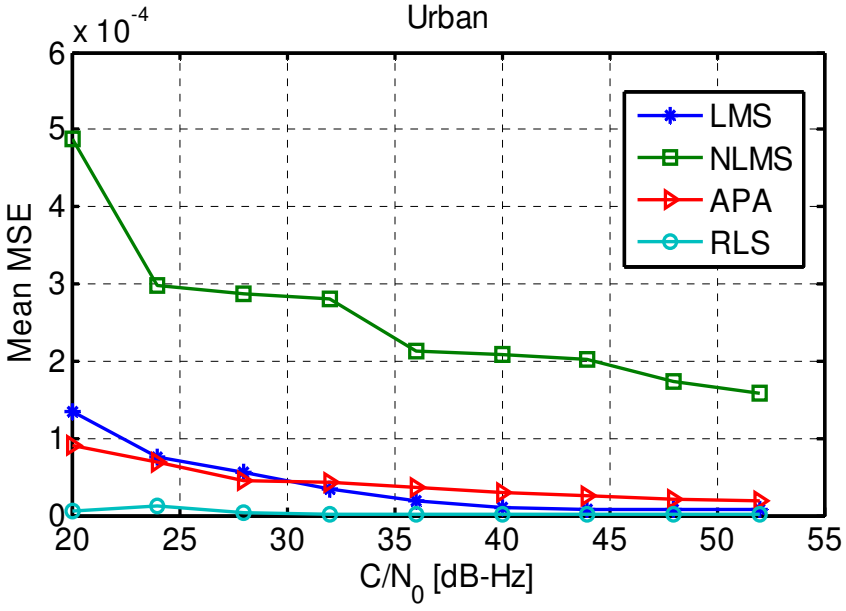

Figure 5-22: Comparison between the mean MSE of different SG algorithms as a function of C/N_0 for a simulated urban channel

The diagrams corresponding to the APA and ALS algorithms in Figure 5-21 show that although the RMSE values of delay estimation for these two algorithms for $C/N_0 < 26\,\text{dB-Hz}$ are very large, when $C/N_0 \geq 26\,\text{dB-Hz}$ these two methods are comparable to MLE-based algorithms. As shown in Table 5-1, the computational costs of these two algorithms are considerably larger than LMS and NLMS algorithms. Moreover, it is observed that the performance of the NLMS algorithm is not as good as the ML-based methods but not too far away from them. However, the computational complexity of this algorithm is much smaller than ML-based methods.

It can be observed in Figure 5-22 that the averaged MSE corresponding to the RLS method is considerably smaller than all of the other methods and the averaged MSE corresponding to NLMS is considerably larger than the other methods.

5.13 Real Data Results

In this section, data processing results are presented to further compare the performance of the introduced SG algorithms under real test field conditions. The data used in this Chapter is the same as that used in Chapter 4.

Figure 5-23 shows the learning curves of the SG algorithms for two visible satellites. Several jumps can be observed in the learning curves of all of the SG algorithms.

Figure 5-24 compares the minimum MSE cost function achieved by different SG algorithms for all of the visible PRNs. It is verified from this figure that the smallest values of $J_{\min}$ correspond to the RLS algorithm and the largest ones correspond to the

NLMS algorithm. Moreover, it can be observed from Figure 5-23 that APA and RLS converge very fast whereas NLMS has the slowest convergence rate.

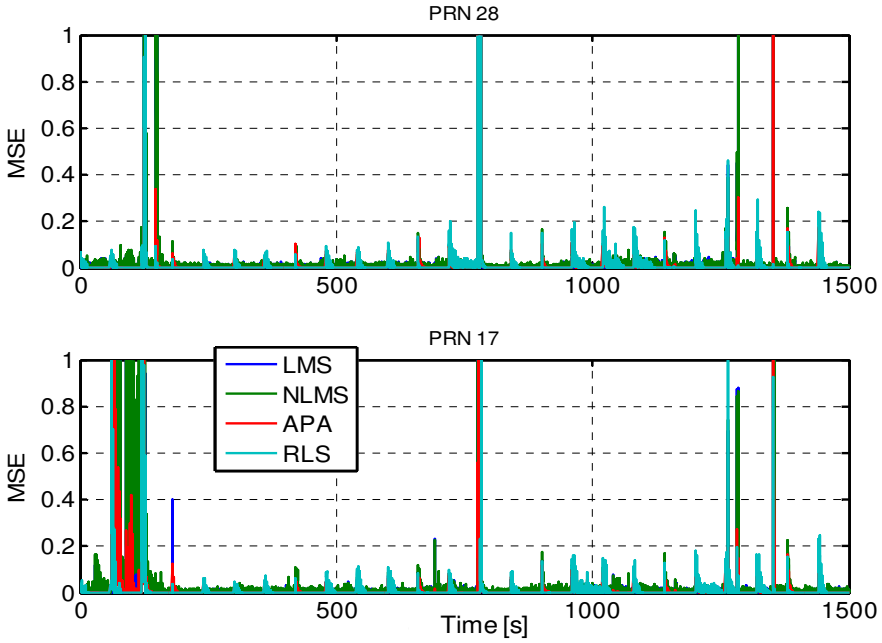

Figure 5-23: Learning curves of different methods in a real urban environment

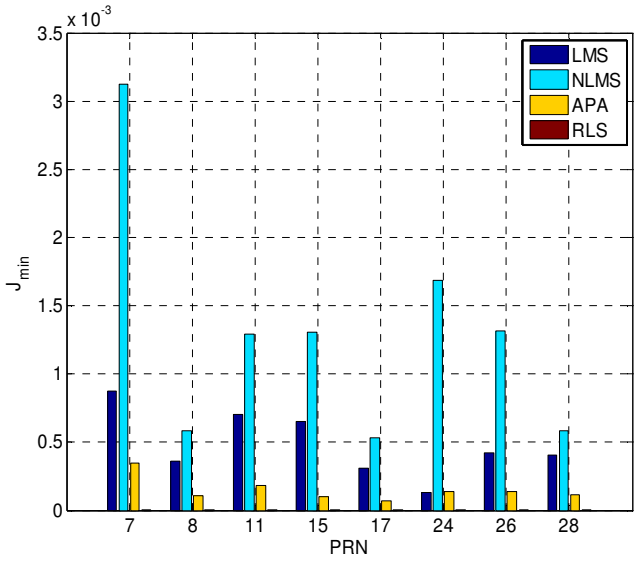

Figure 5-24: Comparison between the minimum MSE cost function for different SG methods under urban conditions

Figure 5-25 pseudorange estimation error diagrams for different SG algorithms for some of the visible PRNs are plotted and in Figure 5-26, their corresponding RMS values are compared.

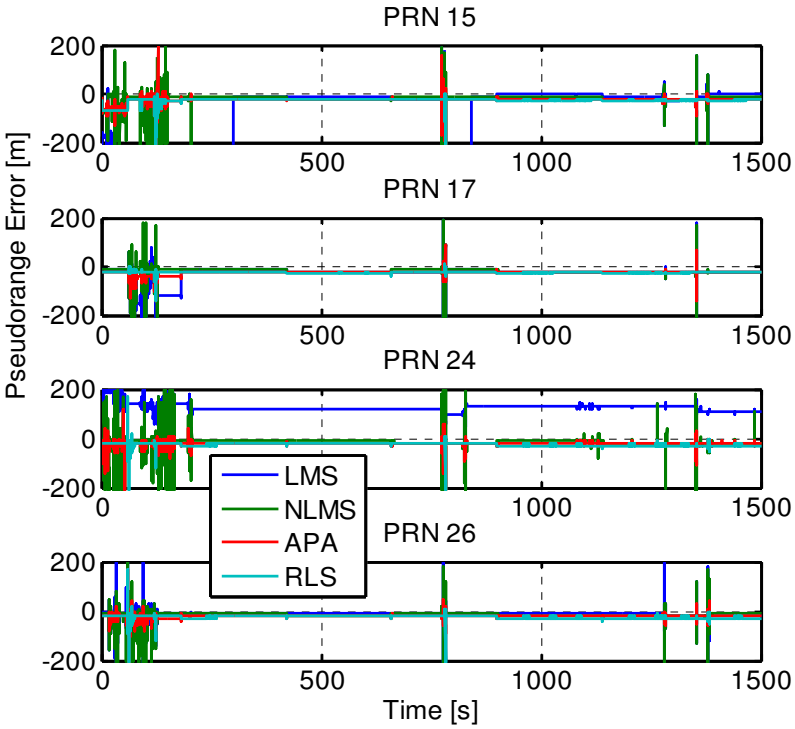

Figure 5-25: Pseudorange estimation errors for different SG algorithm for some of the visible PRNs

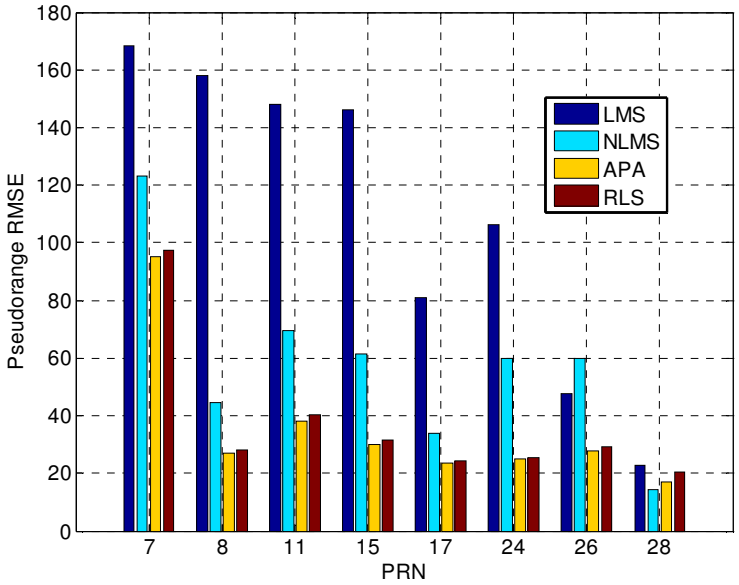

Figure 5-26: Comparison between the RMSE of the pseudorange estimation errors for different SG methods for an urban environment

It can be observed in Figure 5-25 that almost all of the error curves corresponding to the LMS algorithm are biased during some parts of the test duration. The reason is that this algorithm cannot track sudden changes in the signal and, therefore, it is not suitable for equalizing fast varying channels. Figure 5-26 also implies that the performances of the RLS algorithm and APA algorithm with K=25 in terms of RMSE are very similar for all of the visible PRNs. However, for this value of K, the computational complexity of APA is smaller than RLS. In contrast, RLS is much faster than APA in convergence and it converges to a smaller value of the cost function. The NLMS algorithm shows larger RMSE compared to RLS and APA and its convergence is slower but its computational cost is considerably smaller than the two algorithms.

The existence of the jumps in the MSE curves of the SG algorithms in Figure 5-23 implies that the channel encountered in a vehicular application in an urban environment is sometimes a fast varying channel. For example, when the vehicle passes along a tall building with a high speed (54 km/h), the wireless channel from some of the satellites to the receiver instantly changes. One example of such an area with tall buildings corresponds to the time duration between 60 to 120 s of the data in Figure 5-23 and Figure 5-25. This part of data relates to the 5 Avenue in downtown of Calgary and was shown previously in Figure 4-7. It can be observed from these two figures that this duration of data corresponds to large MSE and RMS errors for all of the SG algorithms. However, even for this part of data, the error values produced by APA and RLS are considerably smaller than the ones produced by LMS.

5.14 Summary and Conclusions

In this chapter, some of the algorithms from the class of stochastic gradient approaches were adapted to be used for the purpose of GNSS multipath mitigation. The LOS delay was then estimated from the equalized signal at the output of the filter. An optimum decision block was designed to be used in the feedback loop that adaptively modifies the filter coefficients.

The simulations and data processing results showed that at moderate to high values of C/N_0, two of this SG algortithms, namely RLS and APA, show LOS delay estimation performances that are comparable to ML-based algorithms. Although these two techniques are more complex than LMS and NLMS, but their computational costs are still smaller than the ML-based algorithms. Among the four techniques RLS converges

with the fastest rate and provides smallest steady state cost function error. It was also shown that the convergence of the algorithms in this class is sensitive to the choice of the initial values of the tap coefficients and their convergence rate is dependent to different design parameters such as the step-size parameter.

Chapter Six: High Resolution GNSS Delay Estimation for Vehicular Navigation Utilizing a Doppler Combining Technique

6.1 Introduction

In order to improve the accuracy of the delay estimation in severe multipath scenarios (e.g. urban environments where the number of signal reflections is normally large and some of these might be stronger than LOS), this chapter analyzes high resolution subspace based-TOA estimation techniques in an effort to achieve a higher TOA estimation accuracy. These techniques estimate the multipath delays in two steps. In the first step, a low-resolution channel profile, e.g., a PN correlation profile (Bouchereau et al 2001) or a frequency response (Li & Pahlavan 2004) is obtained and used to compute the signal covariance matrix. Next, the resolution of the channel profile is enhanced by a high resolution technique, such as the MUltiple Signal Classification (MUSIC) technique. A more precise TOA is thus determined from the first peak detected on the enhanced channel profile. This methodology provides an estimation accuracy improvement.

Subspace based methods require a full-rank signal covariance matrix, which exists if the LOS and the multipath reflections are uncorrelated. However, in many cases, the rank of this matrix reduces to unity due to signal coherency (Bouchereau et al 2001). Therefore, different techniques such as diversity reception have been employed in practice to combat signal coherency. Common diversity techniques include antenna diversity, time diversity, frequency diversity and polarization diversity. Diversity techniques take advantage of the random nature of the radio propagation channel by combining uncorrelated signal

versions. However, most of the diversity techniques have been reported in the literature to be ineffective for the purpose of signal decorrelation (e.g. Li & Pahlavan 2004). For example, in time diversity the path gain coefficients remain unchanged together with path delays and in spatial and polarization diversities, radio channels from the transmitter to different diversity branches of the receiver are most likely not the same. Bouchereau et al (2001) have applied frequency diversity to de-correlate multipath signals. However, most of the commercial GPS receivers are single frequency receivers. Furthermore, the presence of atmospheric errors decreases the effectiveness of using this diversity (Ziedan 2011).

A fast fading wireless channel, where the receiver or the surrounding objects are in motion, such that the coherence time of the channel is smaller than the symbol period of the received signal (Rappaport 2002), intrinsically provides another opportunity to combat the problem of signal coherency. This means that the received signal consists of a linear combination of independent frequency shifted copies of the transmitted signal (Sadowsky & KafedZiski 1998). These independent copies of the signal produced by the wireless channel provide an inherent mechanism (Sayeed & Aazhang 1999) that can be exploited for the purpose of signal decorrelation via appropriate signal processing. The goal of this chapter is to use a framework to fully take advantage of this opportunity in urban vehicular navigation. In this way, a trade-off can be made between the coherent integration time of the receiver and the number of available signal copies depending on the speed of the vehicle. Herein, the channel is assumed to follow the Rician fading model with a few strong multipath components and numerous weak reflections

representative of most typical urban environments (Steingass & Lehner 2004). This implies that the LOS is assumed to be present but may be weaker than some of the signal reflections.

In this chapter, the Doppler spectrum broadening of the fast fading channel resulting from the motion of the receiver is utilized to decorrelate signal reflections and increase the rank of the signal covariance matrix in a subspace based multipath delay estimation technique. In the proposed algorithm, delay-domain correlator outputs at different Doppler frequencies will be combined in the computation of the signal covariance matrix. Simulations and real data processing results will be then presented to compare the performance of the proposed method with other high performance algorithms.

6.2 Signal and Channel Model

This section provides the time-frequency based channel and signal models that underlie the development presented herein. The specular multipath channel considered here is assumed to be Wide Sense Stationary (WSS). Recall from Chapter 2 that the baseband signal at the transmitter side $s(t)$ can be represented by

$$s(t) = \sum_{q} \sqrt{E_b} b_q p\left(t - qT_p\right) \tag{6.1}$$

where T_p is the code period duration, E_b is the bit energy and b_q 's are the navigation data bits. $p(t)$ is the spreading waveform with the chip interval of T_c and the autocorrelation function of $g(\tau)$. The signal bandwidth is $B \approx \frac{1}{T_c}$ and the spreading factor of the system

is $N_c = \frac{T_p}{T_c} \approx T_p B \gg 1$. The complex baseband signal $x(t)$ at the output of the channel is related to the transmitted complex baseband signal $s(t)$ by

$$x(t) = \int h(t,\tau) s(t-\tau) d\tau + n(t) \tag{6.2}$$

where $h(t,\tau)$ is the time-varying impulse response of the channel and $n(t)$ is zero-mean, additive white circular Gaussian noise. The specular multipath channel with *time variant* coefficients can be modeled as

$$h(t,\tau) = \sum_{m=0}^{M-1} \alpha_{m,t} \delta(\tau - \tau_m) \tag{6.3}$$

where $\delta(.)$ denotes the Dirac delta function, M is the number of multipath components, $\alpha_{m,t}$ and τ_m are the complex attenuation factor and the propagation delay of the m^{th} path, respectively.

An equivalent representation of the channel can be described in terms of the spreading function $\psi(\theta,\tau)$, defined as

$$\psi(\theta,\tau) = \int h(t,\tau) e^{-j2\pi\theta t} dt. \tag{6.4}$$

Under the assumption that the observation time (integration time) is smaller than the coherence time of the channel, (6.4) will result in

$$\psi(\theta,\tau) = \sum_{m=0}^{M-1} \alpha_{m,\theta} \delta(\tau - \tau_m) \tag{6.5}$$

where $\alpha_{m,\theta} = \int \alpha_{m,\mathrm{t}} e^{-j2\pi t\theta}$. The spreading function quantifies the time-frequency spreading produced by the channel, θ corresponds to the Doppler shifts introduced by the channel temporal variations and τ corresponds to the multipath delays. The time-varying channel impulse response $\psi(\theta,\tau)$ is often modeled as a stochastic process and the wide-sense stationary uncorrelated scatters (WSSUS) model is widely used (Bello 1963). In this model, the temporal variations in $\psi(\theta,\tau)$ are represented by a stationary Gaussian process and the channel response at different lags are assumed independent (Proakis 1995). The second order statistics characterizing the channel are given by

$$E\{\psi(\theta_1,\tau_1)\psi^*(\theta_2,\tau_2)\} = E\left\{\left|\psi(\theta_1,\tau_1)\right|^2\right\}\delta(\theta_1-\theta_2)\,\delta(\tau_1-\tau_2). \tag{6.6}$$

The function $\varphi(\theta,\tau) = E\left\{\left|\psi(\theta,\tau)\right|^2\right\}$ is called the scattering function (Sadowsky & KafedZiski 1998) and represents the distribution of channel power as a function of multipath and Doppler shifts. The support of this function over τ denoted by T_m is the delay spread of the channel and its support over θ, denoted by B_d, is the channel's Doppler spread. The Doppler spread of the channel is linearly proportional to the speed of the receiver and can be expressed as $B_d = \frac{v}{\lambda}$ (Rappaport 2002) where *v* is the speed of the receiver and λ is the wavelength of the signal.

6.3 Doppler-Delay Representation of Multipath Signal

Considering the definition in (6.6), the received signal at the receiver consists of a linear combination of time shifted and frequency shifted copies of the transmitted signal. The Doppler frequency shifted copies of the transmitted signal produced by the fading channel (caused by user or scaterer's motion) provide an inherent mechanism that can be exploited to improve the delay estimation accuracy via appropriate signal processing schemes. A representation of the received signal that provides a framework for exploiting this opportunity can be described as (Sayeed et al 1998)

$$x(t) \approx \sum_{k=-K}^{K} \sum_{m=0}^{M} \psi\left(\frac{k}{T}, \tau_m\right) p(t-\tau_m) e^{j(2\pi kt/T)} + n(t) \qquad (6.7)$$
$$0 \le t < T,$$

where $K = \lceil B_d T \rceil$ and T is the coherent integration period. Considering the assumption of the statistical independence of the channel coefficients, $\psi(\theta, \tau)$, the expression in (6.7) effectively decomposes the channel into $2K+1$ independent flat fading channels by appropriately sampling the multipath-Doppler plane. The number of these available channel copies is proportional to $B_d T$. For fixed channel parameters, this number is proportional to the time-bandwidth product of the signaling waveform. The approximation in (6.7) can be made arbitrarily close by increasing the number of terms in the summation. However, virtually all the signal energy is captured by $2K+1$ Doppler components. Using (6.7), the incoming signal after correlation with a replica of the modulated PRN code and sampling at the rate of $F_s = 1/T_s$ can be expressed as

$$
\begin{aligned}
y[n,i] &= \sum_{m=0}^{N_T-1} x[m]\,p[m-n]\,e^{j2\pi i\frac{m}{N_T}} + w[n,i] \\
&= \sum_{m'=0}^{M-1}\sum_{k'=-K}^{K} \psi[k',m']\left(\sum_{m=0}^{N_T-1} p[m-m']\,p[m-n]\,e^{j2\pi(i-k')\frac{m}{N_T}}\right) \\
&\quad + w[n,i] \\
&\approx \sum_{m'=0}^{M-1} \psi[i,m']\,g[n-m'] + w[n,i] \\
&\qquad\qquad 0 \le n \le N_T - 1,\ -K \le i \le K
\end{aligned}
\tag{6.8}
$$

where n and i are the delay and frequency indexes respectively, $N_T = \left\lceil \frac{T}{T_s} \right\rceil$ and w is the noise term at the output of the correlator with a variance of $\sigma_w^2 = \frac{2N_0}{T_s}$. A matrix representation for the relation in (6.8) can be expressed as

$$\mathbf{Y} = \mathbf{G}\boldsymbol{\Psi} + \mathbf{W}, \tag{6.9}$$

where $\mathbf{Y}$ is a $N \times (2K+1)$ matrix in which

$$\mathbf{Y}_{n,i} = y[n,i], \tag{6.10}$$

and $N = \left\lceil \frac{T_p}{T_s} \right\rceil$. $\mathbf{G}$ is a $N \times M$ matrix wherein

$$\mathbf{G}_{n,m} = g\left((n-m)T_s\right), \tag{6.11}$$

$\boldsymbol{\Psi}$ is the $M \times (2K+1)$ matrix described by

$$\boldsymbol{\Psi}_{m,i} = \psi\left(\tau_m, \frac{i-K-1}{T}\right), \tag{6.12}$$

and finally $\mathbf{W}$ is the $N\times(2K+1)$ matrix of the noise samples at the output of the correlator with a covariance matrix of $\mathbf{Q}=\sigma_w^2\mathbf{G}'$ where $\mathbf{G}'$ is a $L\times L$ matrix so that $\mathbf{G}'_{n,m}=g\left((n-m)T_s\right)$.

6.4 Subspace-Based Multipath Delay Estimation

In the previous section, it was shown that the output of the correlator in a fast fading channel can be represented as a matrix of independent samples for different values of the delay and Doppler shift. This matrix was shown to be linearly proportional to the matrix of scattering function of the channel. In this section, this time-frequency representation of the channel is employed to estimate the multipath times of arrival using the MUSIC technique.

In (6.9), every row of the scattering function matrix corresponds to one of the true multipath delays (τ_ms). Given that the true multipath delays are not known to the receiver beforehand, (6.9) is rewritten for the receiver side considering an equi-spaced search region with a duration of $\Delta>\max\{\tau_1,...,\tau_M\}$ including $L=\left\lceil\frac{\Delta}{T_s}\right\rceil$ samples so that

$$\mathbf{Y}\approx\tilde{\mathbf{G}}\tilde{\mathbf{\Psi}}+\mathbf{W}. \tag{6.13}$$

In (6.13), assuming that the sampling period is small enough, the $L\times(2K+1)$ matrix $\tilde{\mathbf{\Psi}}$ is formed by adding some all-zero rows to $\mathbf{\Psi}$ at the position of delays that do not correspond to the true multipath delay. Then, the k-th column of $\tilde{\mathbf{\Psi}}$, namely $\tilde{\mathbf{\Psi}}_k$, that

contains the channel impulse response at the frequency shift of $\frac{k-K-1}{T}$, by considering (6.5), can be expressed as

$$\tilde{\mathbf{\Psi}}_k = \left[a_{1,k} \;\; a_{2,k} \;\; \ldots \; a_{\mathrm{L},k} \right]^T, \tag{6.14}$$

in which

$$a_{i,k} = \begin{cases} \alpha_{\mathrm{m},k} & \text{if } iT_s \simeq \tau_m \in \{\tau_1, \ldots, \tau_M\} \\ 0 & \text{otherwise} \end{cases}. \tag{6.15}$$

Also $\tilde{\mathbf{G}}$ in (6.13) is a $N \times L$ matrix so that $\tilde{\mathbf{G}}_{n,m} = g\left(\left(n-m\right)T_s\right)$.

Taking these into account, the rows of $\tilde{\mathbf{\Psi}}$ can be grouped into two sets. The first set includes the rows that correspond to the true multipath delays (τ_m's) and the second set includes the rest of the rows consisting of zero elements. Consequently, $\tilde{\mathbf{\Psi}}$ can be separated into two subsections as $\tilde{\mathbf{\Psi}}^{(1)}$ (with M rows) and $\tilde{\mathbf{\Psi}}^{(2)}$ (with $L-M$), corresponding to the first and second sets, respectively.

The MUSIC algorithm uses a coarse estimate of the Fourier transform of the $\tilde{\mathbf{\Psi}}_k$'s to find an estimate for the multipath delays (Li & Pahlavan 2004). Assuming $\mathbf{H}$ to be a $L \times \left(2K+1\right)$ matrix whose k^{th} column is the Fourier transform of $\tilde{\mathbf{\Psi}}_k$, a coarse estimate of this matrix (which can be obtained by a simple spectrum division (Klukas 1997)) is expressed as

$$\hat{\mathbf{H}} \approx \mathbf{F}\tilde{\mathbf{\Psi}} + \mathbf{W}', \tag{6.16}$$

where $\mathbf{F}$ is the $L \times L$ Discrete Fourier Transform (DFT) matrix so that $\mathbf{F}_{k,l} = e^{\frac{-jkl}{L}}$ and $\mathbf{W}'$ is the $L \times (2K+1)$ noise matrix with a covariance matrix $\mathbf{Q}' = \sigma_w^2 \mathbf{I}_L$, where $\mathbf{I}_k$ indicates a $k \times k$ identity matrix. Considering the two subsections of $\tilde{\mathbf{\Psi}}$, since the elements of $\tilde{\mathbf{\Psi}}^{(2)}$ are zero, (6.16) can be written as

$$\hat{\mathbf{H}} \approx \mathbf{F}_1 \tilde{\mathbf{\Psi}}^{(1)} + \mathbf{F}_2 \tilde{\mathbf{\Psi}}^{(2)} + \mathbf{W}' = \mathbf{F}_1 \tilde{\mathbf{\Psi}}^{(1)} + \mathbf{W}', \tag{6.17}$$

where $\mathbf{F}_1$ is a subsection of $\mathbf{F}$ including those columns of $\mathbf{F}$ that correspond to the rows of $\tilde{\mathbf{\Psi}}^{(1)}$.The other subsection of $\mathbf{F}$ that includes the columns of $\mathbf{F}$ corresponding to the rows of $\tilde{\mathbf{\Psi}}^{(2)}$ is referred to as $\mathbf{F}_2$. Moreover, since the columns of a DFT matrix are orthonormal, it can be shown that

$$\begin{aligned} \mathbf{F}_1^{\mathrm{H}} \mathbf{F}_2 &= \mathbf{0}_{M \times (L-M)} \\ \mathbf{F}_2^{\mathrm{H}} \mathbf{F}_1 &= \mathbf{0}_{(L-M) \times M} \end{aligned} \tag{6.18}$$

where $\mathbf{0}_{a \times b}$ stand for $a \times b$ all zero matrix, and the superscript H denotes the Hermitian matrix transpose. Considering (6.18), the estimated autocorrelation matrix of the measured data can be expressed as

$$\hat{\mathbf{R}} = \hat{\mathbf{H}} \hat{\mathbf{H}}^H = \mathbf{F}_1 \mathbf{A} \mathbf{F}_1^H + \sigma_w^2 \mathbf{I} \tag{6.19}$$

where A is a $M \times M$ matrix defined as

$$\mathbf{A} = \tilde{\mathbf{\Psi}}^{(1)} \left(\tilde{\mathbf{\Psi}}^{(1)} \right)^H = \sum_{k=-K}^{k=-K} \tilde{\mathbf{\Psi}}_k^{(1)} \left(\tilde{\mathbf{\Psi}}_k^{(1)} \right)^H, \tag{6.20}$$

Eq. (6.18) demonstrates the contribution of the channel frequency response at different Doppler frequency shifts in constructing the channel autocorrelation function and increasing its rank.

In rest of this section the Music algorithm is explained for two different cases: where **A** is non-singular and ten singular.

6.4.1 6.4.1 A is Non-Singular

MUSIC super-resolution techniques are based on the eigen-decomposition of the autocorrelation matrix in (6.19). In the case where **A** is non-singular ($2K+1 \geq M$), since $\mathbf{F}_1$ has a full column rank, the rank of $\mathbf{F}_1\mathbf{A}\mathbf{F}_1^H$ is *M*. Therefore, in this case, the $L-M$ smallest eigenvalues of $\hat{\mathbf{R}}$ are equal to σ_w^2 and their corresponding eigenvectors (EVs) are called noise EVs, whereas EVs corresponding to the *M* largest eigenvalues are called signal EVs. Thus, the L-dimensional subspace that contains the signal vectors $\hat{\mathbf{H}}$ can be split into two orthogonal subspaces, known as the signal subspace $\mathbf{U}_S$ and the noise subspace $\mathbf{U}_N$, by the signal EVs and noise EVs, respectively. Taking this into account, the autocorrelation matrix in (6.19) can be written as

$$\hat{\mathbf{R}} = \mathbf{U}\mathbf{\Lambda}\mathbf{U}^H = \begin{bmatrix}\mathbf{U}_S & \mathbf{U}_N\end{bmatrix}\begin{bmatrix}\mathbf{\Lambda}_S + \sigma_w^2\mathbf{I}_M & 0 \\ 0 & \sigma_w^2\mathbf{I}_{L-M}\end{bmatrix}\begin{bmatrix}\mathbf{U}_S \\ \mathbf{U}_N\end{bmatrix}, \tag{6.21}$$

where $\mathbf{\Lambda}_S$ is a diagonal matrix containing the signal eigenvalues on its diagonal. The signal and noise subspace matrixes have the following properties:

$$\mathbf{U}_S\mathbf{U}_S^H + \mathbf{U}_N\mathbf{U}_N^H = \mathbf{I}_L$$
$$\mathbf{U}_N^H\mathbf{U}_S = \mathbf{U}_S^H\mathbf{U}_N = 0 \tag{6.22}$$

and (6.19) can therefore be rewritten as

$$\hat{\mathbf{R}} = \mathbf{U}_S\boldsymbol{\Lambda}_S\mathbf{U}_S^H + \sigma_w^2\mathbf{U}\mathbf{U}^H = \mathbf{U}_S\boldsymbol{\Lambda}_S\mathbf{U}_S^H + \sigma_w^2\mathbf{I}_L. \tag{6.23}$$

Comparing (6.23) with (6.19) results in

$$\mathbf{U}_S\boldsymbol{\Lambda}_S\mathbf{U}_S^H = \mathbf{F}_1\mathbf{A}\mathbf{F}_1^H. \tag{6.24}$$

Hence, since $\mathbf{A}$ was assumed non-singular, the columns of $\mathbf{F}_1$ span the signal subspace and are orthogonal to the noise subspace. Therefore, the projection matrix of the noise subspace, $\mathbf{P}_{\mathbf{U}_N} = \mathbf{U}_{\mathbf{U}_N}\mathbf{U}_{\mathbf{U}_N}^H$, is orthogonal to $\mathbf{F}_1$ which is expressed as

$$\mathbf{P}_{\mathbf{U}_N}\mathbf{F}_1 = 0\,. \tag{6.25}$$

The equality in (6.25) implies that those columns of $\mathbf{F}$ that correspond to the true multipath delays are orthogonal to the noise subspace. Thus, the multipath delays, $\tau_1,...,\tau_M$, can be determined by finding the delay values at which the following MUSIC Super-resolution Delay Profile (SDP) achieves its maximum values, namely

$$SDP(\tau_i) = \frac{1}{\left\|\mathbf{P}_{\mathbf{U}_N}\mathbf{F}_{\tau_i}\right\|^2} = \frac{1}{\mathbf{F}_{\tau_i}^H\mathbf{P}_{\mathbf{U}_N}\mathbf{F}_{\tau_i}} = \frac{1}{\left\|\mathbf{U}_N^H\mathbf{F}_{\tau_i}\right\|^2} \tag{6.26}$$

where $\mathbf{F}_{\tau_i}$ denotes the i-th column of $\mathbf{F}$ that corresponds to $\tau_i = iT_s$. It should be noted here that (6.25), which is the basis of multipath delay estimation by the function in (6.26), holds only when the matrix $\mathbf{A}$ is non-singular. This is valid when the number of linearly independent copies of the signal that contribute to the computation of the autocorrelation

matrix, which is the number coarse estimates of CFR on the columns of $\hat{\mathbf{H}}$, is larger than the number of multipath components. This is how independent estimates of CFR at different Doppler frequencies aim to increase the rank of **A**. It is important to consider at this point the problem that arises if **A** is singular.

It should be noted at this point that when applying the various diversity techniques, (6.26) is used exactly in the same way. The only difference is in the formation of the autocorrelation matrix in (6.19). For example, in time diversity the columns of $\hat{\mathbf{H}}$ are the coarse estimates of CFR at consecutive time snapshots with a duration of T and for spatial diversity they are the coarse estimate of CFR at the different receiver antennas. Spatial-temporal diversity is the same as time diversity when the receiver is in motion (Broumandan et al 2011). Taking this into account, in the next section, the experimental results for the Doppler combining technique will be compared with the ones for the spatial-temporal diversity technique.

A block diagram of a receiver employing Doppler combining in super-resolution multipath delay estimation is shown in Figure 6-1. The delay-Doppler grid of the received signal is first formed at the output of the correlator filter. Next, a rough estimate of the channel frequency response (CFR) is computed for the signal at each Doppler branch (each column of **Y** in (6.13)) by spectrum division (Klukas 1997). The resultant coarse CFRs are combined using (6.19) to form the channel autocorrelation matrix for each distinct peak (the estimated rough CFRs are located on the columns of $\hat{\mathbf{H}}$). Next, a singular decomposition (SVD) is applied to the estimated autocorrelation matrix to

separate signal and noise subspaces and form the $\mathbf{P}_{\mathbf{U}_N}$ matrix. Finally the super-resolution algorithm is used to transform the channel autocorrelation matrix to the super-resolution delay profile, as defined in (6.26). The estimate of the LOS time of arrival (TOA) is then found by detecting the first peak of the delay profile obtained by applying MUSIC to each local maximum of the correlation grid. The final estimate of the TOA will be selected as the minimum of the estimated TOAs for all distinct peaks.

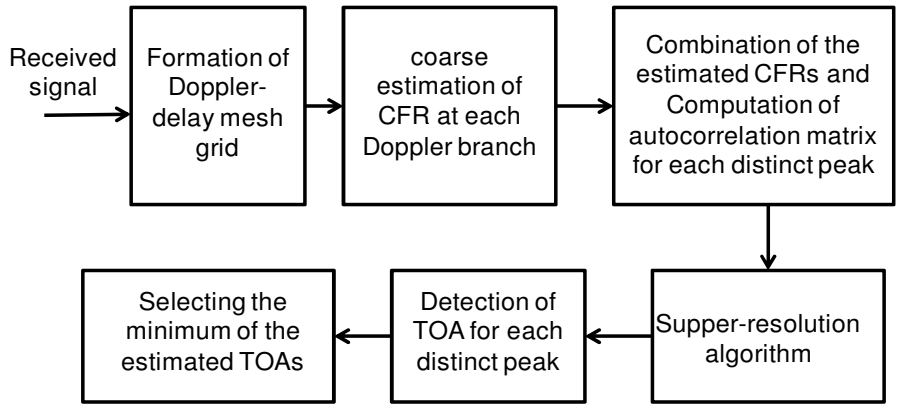

Figure 6-1: Block diagram of proposed method

In Figure 6-2, the output of the SDP function is evaluated and plotted for a simulated 8-path channel profile for different values of the rank of the signal autocorrelation matrix. As can be observed, the height of the maxima of the function decreases with a decreasing rank of the autocorrelation matrix. This effect can be so severe that at low SNR values, the peaks due to noise may be even larger than the peaks due to multipath signals, leading to incorrect delay estimation.

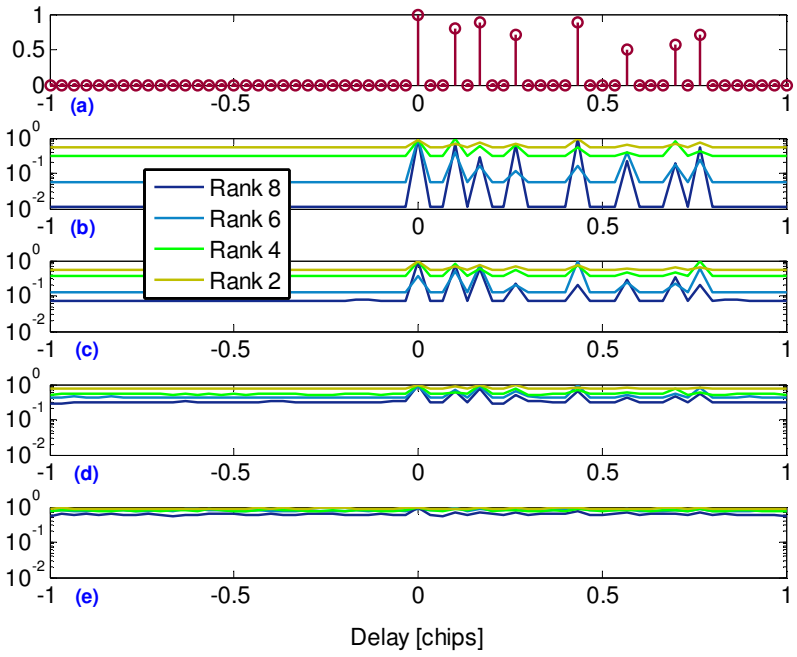

Figure 6-2: (a) CIR of an 8-path channel profile, (b-d) Normalized outputs of the SDP function at SNR values of 20, 10, 5 and 0 dB, respectively

6.4.2 6.4.2 When A is Singular

Consider the case where the matrix $\mathbf{A}$ in (6.19) is singular with the column rank of $M' = 2K+1 < M$. In this case, $\mathbf{U}_S$ and $\mathbf{U}_N$ have column rank of M' and $L-M'$, respectively. Since (6.24) still holds, multiplying both sides of this equation by $\mathbf{P}_{\mathbf{U}_N}$ results in

$$\mathbf{P}_{\mathbf{U}_N}\mathbf{F}_1\mathbf{A}\mathbf{F}_1^H = 0. \tag{6.27}$$

By multiplying both sides of (6.27) by $\mathbf{F}_1$ from the right side and using (6.18), one obtains

$$\mathbf{P}_{\mathbf{U}_N}\mathbf{F}_1\mathbf{A} = 0. \tag{6.28}$$

Moreover, **A** can be expressed in its singular decomposition form as

$$\mathbf{A} = \mathbf{U}_A\mathbf{\Lambda}_A\mathbf{U}_A^H, \tag{6.29}$$

where the $M \times M'$ matrix $\mathbf{U}_A$ is the vector of the eigenvectors of A and $\mathbf{\Lambda}_A$ is a $M' \times M'$ diagonal matrix with the singular values of A on its diagonal. Substituting (6.29) into (6.28) results in

$$\mathbf{P}_{\mathbf{U}_N}\mathbf{F}_1\mathbf{U}_A = 0 \tag{6.30}$$

Since the matrix $\mathbf{U}_A$ has the full column rank of M', (6.30) implies that $\mathbf{P}_{\mathbf{U}_N}$ is orthogonal to M' independent linear combinations of the columns of $\mathbf{F}_1$. In other words, the column rank of $\mathbf{F}_1\mathbf{U}_A$ is M', which is the same as the column rank of the signal space. This fact results in the conclusion that the projection of the matrix $\mathbf{F}_1\mathbf{U}_A$ is equal to the projection of the signal space (the columns of $\mathbf{F}_1\mathbf{U}_A$ span the signal space or $span\{\mathbf{F}_1\mathbf{U}_A\} = span\{\mathbf{U}_S\}$), which can be expressed as

$$\mathbf{F}_1\mathbf{U}_A\mathbf{U}_A^H\mathbf{F}_1^H = \mathbf{U}_s\mathbf{U}_s^H. \tag{6-31}$$

On the other hand, by substituting $\mathbf{U}_N\mathbf{U}_N^H = \mathbf{I} - \mathbf{U}_S\mathbf{U}_S^H$ from (6.22) to the denominator of (6.26), the SDP function can be rewritten as

$$\begin{aligned} SDP(\tau_i) = \frac{1}{\mathbf{F}_{\tau_i}^H\mathbf{P}_{\mathbf{U}_N}\mathbf{F}_{\tau_i}} &= \frac{1}{\mathbf{F}_{\tau_i}^H\left(\mathbf{I} - \mathbf{U}_S\mathbf{U}_S^H\right)\mathbf{F}_{\tau_i}} \\ &= \frac{1}{1 - \mathbf{F}_{\tau_i}^H(\tau)\mathbf{U}_S\mathbf{U}_S^H\mathbf{F}_{\tau_i}} \end{aligned} \tag{6.31}$$

Substituting (6.30) into (6.31) results in

$$SDP(\tau_i) = \frac{1}{1 - \mathbf{F}_{\tau_i}^H \mathbf{F}_1 \mathbf{U}_A \mathbf{U}_A^H \mathbf{F}_1^H \mathbf{F}_{\tau_i}}. \tag{6.32}$$

Evaluating the normalized SDP function at different values of the delay while considering that the columns of **F** are orthonormal results in

$$SDP(\tau_i) = \begin{cases} \dfrac{1}{1 - \mathbf{F}_{\tau_m}^H \mathbf{F}_1 \mathbf{U}_A \mathbf{U}_A^H \mathbf{F}_1^H \mathbf{F}_{\tau_m}} = \dfrac{1}{1 - \mathbf{U}_A^{(m)} \left(\mathbf{U}_A^{(m)}\right)^H} > 1 & if \ \tau_i = \tau_m \in \{\tau_1, ..., \tau_M\} \\ \dfrac{1}{1 - \mathbf{F}_{\tau_i}^H \mathbf{F}_1 \mathbf{U}_A \mathbf{U}_A^H \mathbf{F}_1^H \mathbf{F}_{\tau_i}} = 1 & if \ \tau_i \notin \{\tau_1, ..., \tau_M\} \end{cases} \tag{6.33}$$

where $\mathbf{U}_A^{(m)}$ is the m-th row of $\mathbf{U}_A$. Therefore, the denominator of the SDP function is minimized but non-zero at the delays corresponding to the true multipath delay when A is not full rank and consequently the SDP function is maximized at these points. In other words, in the case where A is rank deficient, the poles of SDP function are no more located on the unit circle. As the rank of A becomes closer to the number of multipath components, the denominator of the SDP function approaches zero.

It should be noted that the above result was derived based on the assumption that the columns of **F** were orthogonal to each other. If instead of the DFT matrix, we had chosen **F** to be the matrix of shifted versions of the ideal autocorrelation function of the PRN code, as it is the case in many references (e.g. Bouchereau et al 2001), (6.33) would not apply. In Figure 6-3 these two cases are compared for an 8-path simulated channel. It is observed that since the number of diversity branches (N_B = 3) is smaller than the number

of multipath components (M=7), for the case where the columns of F are the shifted version of the PN correlation function and are not orthogonal (SDP_C), the resulting supper-resolution delay profile does not follow the true simulated channel.

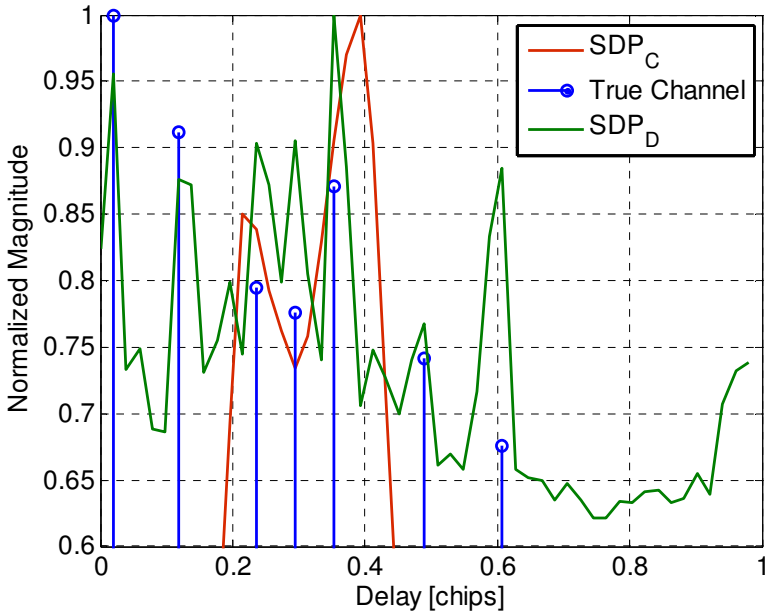

Figure 6-3: Comparison between two cases where the columns of F are orthogonal (SDP_D) and non-orthogonal (SDP_C)

6.5 Experimental Results

In the previous sections, the possibility of taking advantage of frequency shifted copies of the signal in a fast fading channel for the purpose of signal decorrelation in a MUSIC-based delay estimation technique was discussed. In this section, the performance of the proposed estimation technique is assessed by processing the data described in Chapter 3 where estimated reference data was used to define the centre of the search space by using a software receiver. The output file of the software receiver contains a set of adjustable

Doppler-delay correlation grids for each time interval equal to the coherent integration time. These correlation grids are centered on the true LOS delay which is provided by the aiding process.

The output correlation grids produced by the software receiver were used for the computation of coarse CFR estimates by applying simple spectrum divisions at each Doppler branch (delay-domain correlation functions corresponding to each Doppler bin) and for each time interval. The outer products of each estimated CFR vector with itself were then computed and averaged depending on each combination approach to form the autocorrelation matrix. In the Doppler combining approach, the self-outer-products of the estimated CFRs on N_B adjacent Doppler branches around each distinct peak were averaged to form the autocorrelation matrix whereas in the spatial-temporal diversity approach, the outer product of the estimated CFRs at the main peak over each N_{NC} consecutive time snapshots (each equal to the coherent integration time) were averaged to form this matrix. Therefore, the computation of the autocorrelation matrix based on these two techniques can be written as

$$\mathbf{R}_D^k = \sum_{i=1}^{N_B} \mathbf{H}_i^k \left(\mathbf{H}_i^k\right)^H \tag{6.34}$$

$$\mathbf{R}_{ST} = \sum_{n=1}^{N_{NC}} \mathbf{H}_n \left(\mathbf{H}_n\right)^H \tag{6.35}$$

where $\mathbf{R}_D^k$ is the autocorrelation matrix computed by the Doppler combing technique for the *k*-th distinct peak, $\mathbf{R}_{ST}$ is the autocorrelation matrix computed by the spatial-temporal

diversity technique and $\mathbf{H}_i^k$'s and $\mathbf{H}_n$'s are the vectors of estimated CFRs. The ranks of the signal sub-space of $\mathbf{R}_D^k$ and $\mathbf{R}_{ST}$ are smaller than or equal to N_B and N_{ST}, respectively, and the equality holds only if $\mathbf{H}_i^k$'s (or $\mathbf{H}_n$'s) are statistically independent (independence of only the magnitudes or only the phases of the element of $\mathbf{H}$'s suffices).

The MUSIC algorithm was finally applied to the estimated autocorrelation matrices to form the super-resolution delay profiles (SDP) from which the estimates of the LOS times of arrival were obtained. Among all of the peaks in the output SDP that pass a threshold equal to the average magnitude of the SDP, the one that corresponds to the minimum delay is selected as the LOS signal. The difference between the estimated TOAs by the three algorithms discussed above and the one obtained from the SPAN data (the centre of the correlation function), measured in units of length (metres), determines the estimated pseudorange error. The values of estimated pseudoranges for all of the visible satellites were finally used to compute the position solution.

It is important to notice that, in practice, during the time interval that it takes to compute every estimate of the autocorrelation matrix from (6.34) or (6.35) and result in a single estimate of the LOS delay, the true value of the delay slightly varies. Therefore, the final estimate is indeed an average of the true delay values within this time period.

Figure 6-4 shows an example of the Doppler-delay correlation function obtained by processing the received signal of PRN 15. In this figure, since the coherent integration time (120 ms) was longer than the coherence time of the channel, three distinct peaks appeared at the correlation surface. These peaks are highlighted in subplot (c). The delay-

domain autocorrelation functions corresponding to each peak are shown in subplot (b). Each of these peaks corresponds to a cluster of multipath signals. The speed of the vehicle at the time corresponding to this figure was approximately 9 m/s. For every independent peak, $N_B = 3$ delay-domain correlation functions around the main peak were selected for use in the computation of the CFRs. In Figure 6-5, the super-resolution delay profiles that correspond to each of the three Doppler branches of peak 1 in Figure 6-4 and the SDP resulting from their combination using (6.19) are depicted. As can be seen, the curve representing the combination of Doppler branches includes a clear peak at the center of the delay range, corresponding to the true LOS time of arrival.

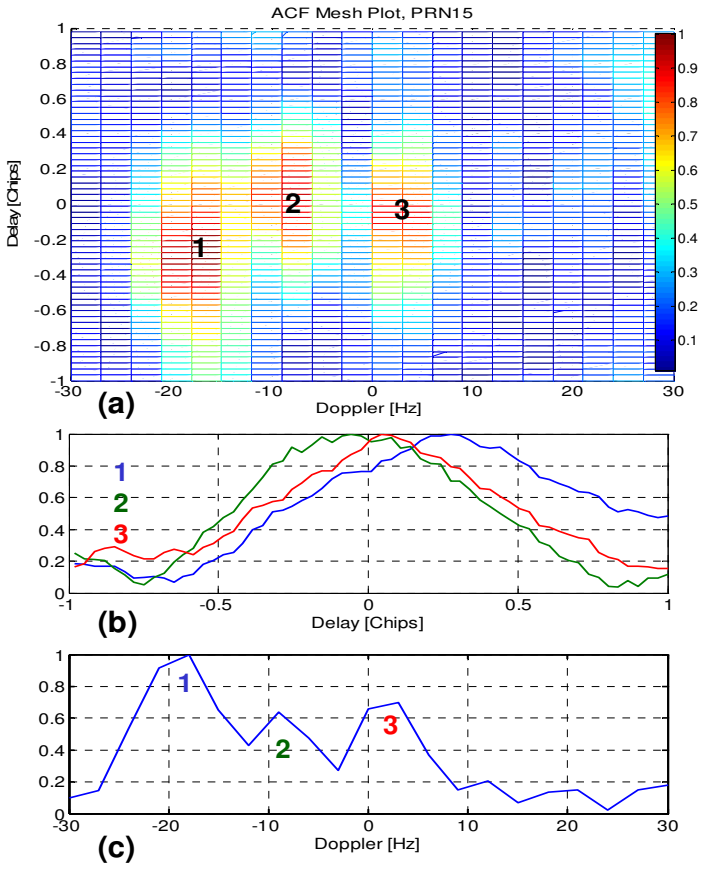

Figure 6-4: (a) Example of a Doppler-delay correlation curve with three distinct peaks shown in (c), the delay-domain autocorrelation functions corresponding to each independent peak are shown in (b)

Referring to Section 6.2, the maximum number of effective Doppler branches is $2K+1=2\lceil B_d T \rceil+1$. For an average speed of 5 m/s, the Doppler spread is $B_d = \frac{\overline{v}}{\lambda} \approx 25\,Hz$, where $\overline{v}$ is the average speed and λ is the wavelength of signal which is almost equal to 0.2 m for L1. Considering this approximated value as the Doppler spread of the channel, Table 6-1 summarizes the effective number of Doppler

branches and the approximated frequency step size for some different values of coherent integration time.

Table 6-1: Effective numbers of Doppler branches for some different values of *T*

Coherent integration time (ms)	Effective value of N_B	Doppler Step Size (Hz)
120	7	8
80	5	12
60	3	16
40	3	25
20	1	-

Herein, the range and the resolution of the code delay in the correlation grid were set to ± 1 chips (300 m) and 0.03 chips (10 m) respectively, and the range and the resolution of Doppler frequency were set to ± 28 Hz and 4 Hz, respectively. Therefore, the size of the correlation grid was 61 by 15. For the first analysis, the coherent integration time of the software receiver was set to $T = 60$ ms. According to Table 6-1, for this value of coherent integration time, the maximum number of effective Doppler branches is $N_B = 3$. In order to have comparable results for the Doppler diversity and spatial-temporal diversity techniques, the value of N_{NC} should be equal to N_B.

Since a slight overestimation of the rank of the signal subspace in the evaluation of (6.26) does not have a significant effect on the output of the function in practice, N_B and N_{NC} have been considered as the rank of the signal subspace of $\mathbf{R}_D^k$ and $\mathbf{R}_{ST}$ in the computation of (6.26).

Figure 6-6 shows the estimated pseudorange errors for all visible PRNs, computed by the (1) Doppler combining based SDP algorithm (SDP_D), (2) SDP based on spatial-temporal diversity (SDP_{ST}) and (3) the double delta correlator technique.

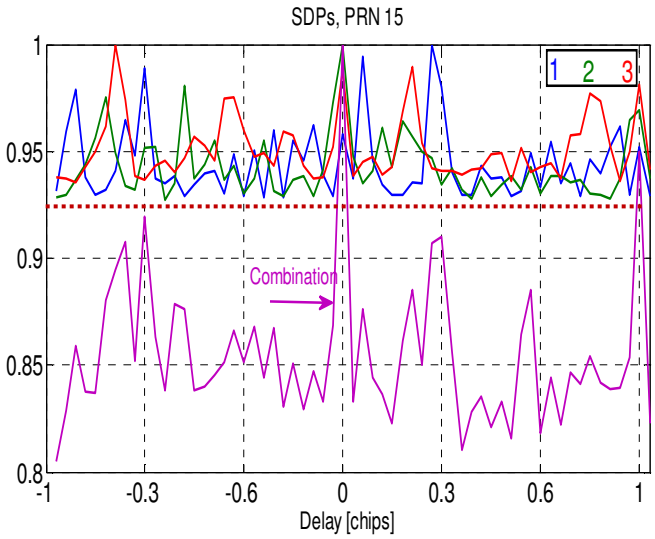

Figure 6-5: SDPs corresponding to each of the three Doppler branches on peak 1 in Figure 6-4 and the resulting SDP from their combination

The correlator spacing parameters for the double delta correlator algorithm was set to 0.1 and 0.2 of a chip (Irsigler & Eissfeller 2003). The coherent integration time for all of the techniques was 60 ms but for the double delta algorithm, the signals on every three successive time snapshots were again coherently averaged for the sake of comparability to the other two combining techniques.

The vehicle entered the high building zone marked by the yellow rectangle in Figure 4-6 at 2000 s. Large errors occurred in the estimated pseudoranges for most PRNs as seen in Figure 6-6. Specifically, the transmitted LOS signals from satellites with lower elevation

angles, such as PRN 7, were blocked in some parts of the trajectory. The performance comparisons of the three techniques in terms of pseudorange errors in Figure 6-6 imply that although exploiting the spatial-temporal diversity could slightly improve the performance of the subspace based method, this improvement, especially in terms of error bias, is not considerable. For example in Figure 6-6, large biases can be observed in the values of estimation errors produced by this technique during the time interval 2600-3200 s for PRN 15. The reason is that, in a fast fading situation, the wireless channel observed from the receiver rapidly changes as the antenna moves in the dense multipath environment. For some PRNs such as PRN 15 and 24, even the conventional double delta technique outperforms the temporal diversity based SDP. On the other hand, taking advantage of only three Doppler branches and combining them in the computation of the signal autocorrelation matrix could result in a noticeable decrease of the estimated biases. Although the resulted improvement is not dramatic for some PRNs, such as 17, a considerable improvement can be observed for PRN 11 and 7. For PRN 28, the estimation errors produced by all the three techniques are very small for the entire test. The reason is that this satellite was located at the zenith during the test time as shown in Figure 4-6, and this results in a strong LOS signal and insignificant multipath components.

In Figure 6-7, the RMS values of the computed pseudorange errors for all available PRNs during the yellow area of the test are compared. Figure 6-8 shows the corresponding least squares position solution errors using the three methods and in Figure 6-9, their RMS values are compared.

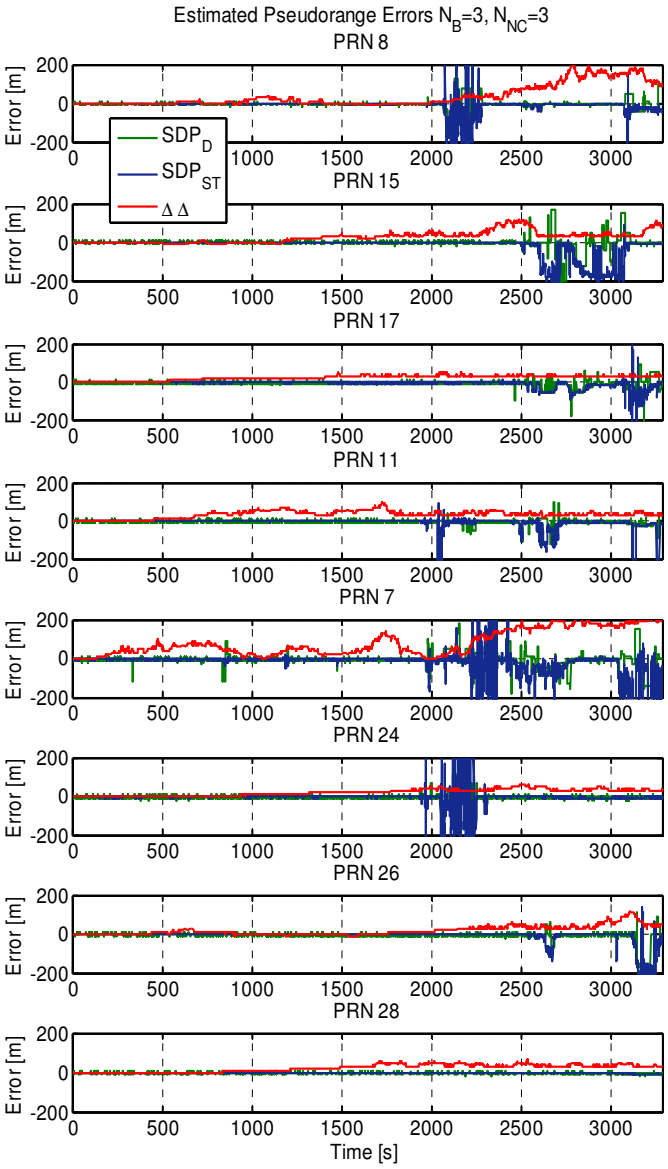

Figure 6-6: Values of estimated pseudorange errors obtained with the three methods

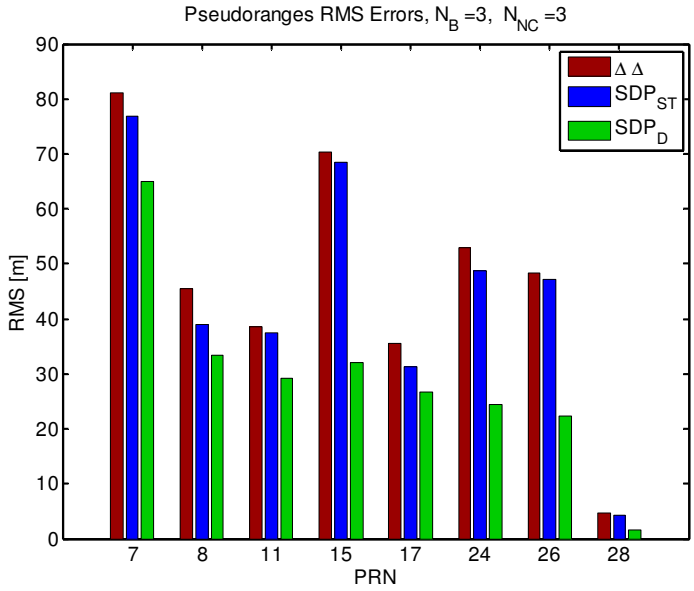

Figure 6-7: Estimated pseudorange error RMS values for the three methods

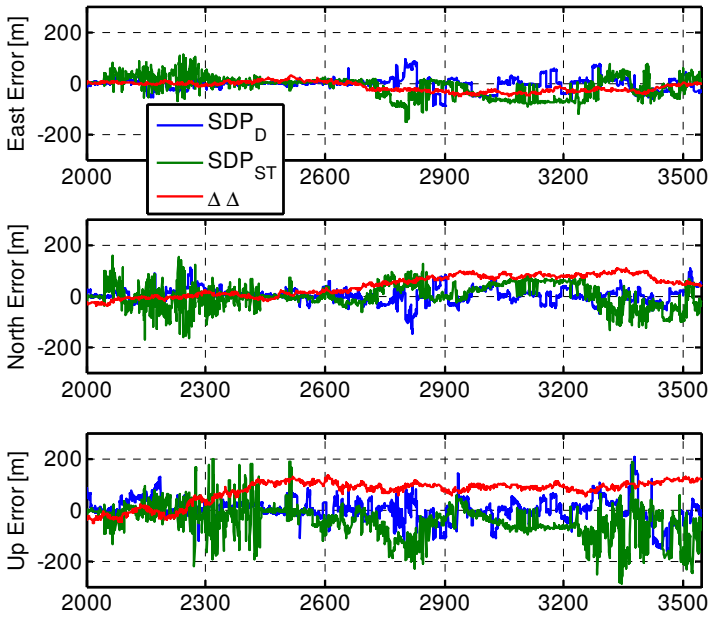

Figure 6-8: Position solution errors computed by the three algorithms

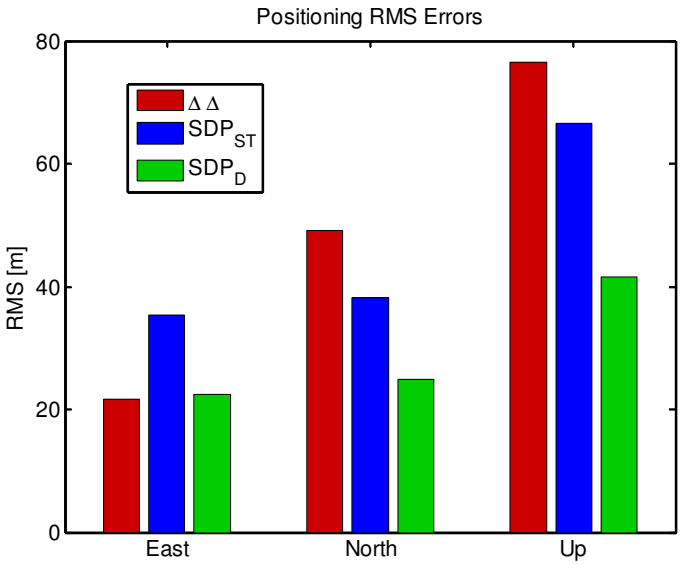

Figure 6-9: Comparison of the position error RMS values computed by the three methods

As it was expected from the diagrams of the estimated pseudorange errors, the bias values of the position errors computed by the Doppler combining based method improve as compared to the two other methods. As it can be observed in Figure 6-6, the position errors that correspond to the double delta technique are highly biased in the time duration of 2500-3500 s. The maximum RMS errors produced by Doppler combining based method for East and North components are around 20 m (within different PRNs).

In Figure 6-10 and Figure 6-11, the pseudorange estimation errors and their RMS values computed by the Doppler combining method for three different values of the receiver's coherent integration time are compared.

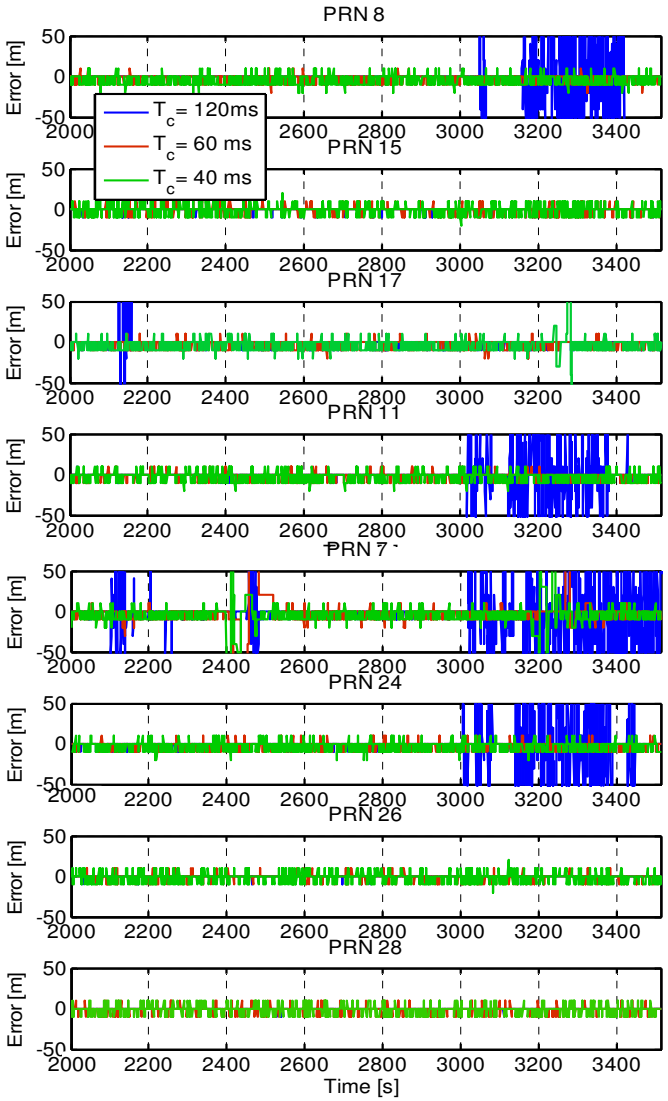

Figure 6-10: Comparing pseudorange estimation errors for three different values of receiver's coherent integration time

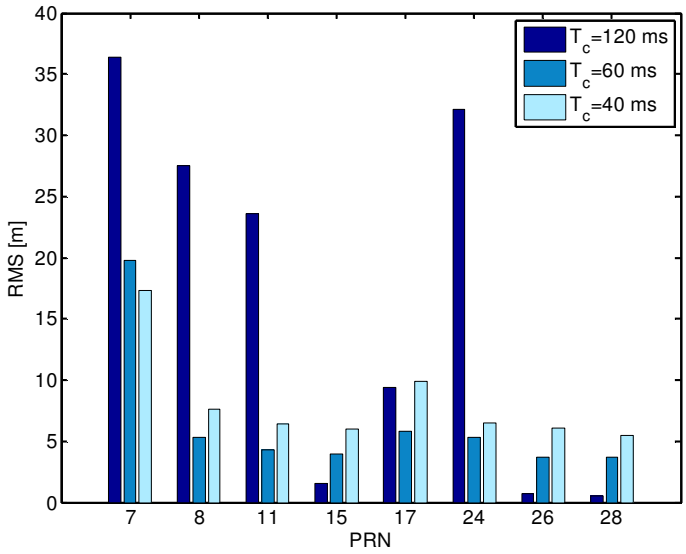

Figure 6-11: RMS values of the pseudorange estimation errors in Figure 11

The most important point that can be inferred from Figure 6-11 is that the comparison of the receiver's performance is not the same for all of the satellites. The reason is that the relative velocity between the receiver and each of the satellites and consequently the coherence time of the channel for each satellite is a function of the direction and elevation angle for that satellite. For the satellites with higher elevation angles, such as satellites with PRN numbers of 28 and 26, the coherent integration time of the channel has a greater value. Therefore they can benefit from longer coherent integration durations at the receiver side. On the other hand for the satellites with the lower elevation angles and lower channel coherence time, long integrations have an adverse effect. For the signals of these satellites, the performance of the receiver can be improved by decreasing the coherent integration and increasing the number of Doppler branches instead. Therefore, depending on the relative velocity between the receiver and a satellite, optimum values for the integration time and the number of diversity branches can be

found. For the case of Figure 6-11, if a fixed integration time is to be considered for all of the satellites, $T_c = 60ms$ seems to be the best choice among the three tested values of the integration time.

It is important to mention here that for those portions of data that corresponded to the sub-urban environment, where the effect of multipath was insignificant, the performance of the three techniques in the sense of pseudorange and positioning errors was similar (as it can be observed from the first 500 seconds in Figure 6-6 and Figure 6-8) and the maximum error produced by all of the three techniques was less than 20 m. The complexity of a subspace-based method such as MUSIC (regardless of whether it is based on Doppler combining or spatial-temporal diversity) is considerably larger than a conventional correlation-shape-based method such as the double-delta-correlator, which requires only five correlators. Therefore, the optimum choice of a signal processing technique is dependent on the application and environment. Specifically, the type of the propagation channel and the expected maximum speed of the mobile device are the main parameters that should be considered.

6.6 Summary and Conclusions

The idea of exploiting the spectral broadening of the Doppler spectrum in fast fading channels for high resolution estimation of multipath delays was explored and an in-depth theoretical analysis of the problem was presented. A real data test was used to assess the performance of the proposed approach and to compare it to the case where spatial-temporal diversity is applied and to the conventional correlation based double delta correlator method. The data analysis results revealed that the spatial-temporal diversity

based subspace method did not provide a considerable advantage over the classical correlation based method for most of the tested signals. On the other hand, the Doppler combining based method could considerably decrease the amounts of bias in the estimated pseudorange values and decrease the total position error. These results indicate that proper sampling of the signal correlation function in the Doppler and code phase domains and combining the delay-domain outputs at different Doppler bins can be effective in combatting the signal coherency and rank deficiency of the autocorrelation matrix. In other words, this helps to some extent to compensate for the loss due to the limitation of the effective coherent integration time in a fast fading channel.

Chapter Seven: Conclusions and Recommendations

This thesis has proposed a number of different multipath mitigation techniques and has analyzed their performance under realistic scenarios. This chapter summarizes the results and provides the conclusions. Recommendations for possible future work in this context are then presented to further extend and develop the proposed methods.

7.1 Conclusions

It was shown in Chapter 2 that un-resolvable signal reflections encountered in severe multipath environments not only distort the shape of the correlation function of the received GNSS signals, but also they may result in shifting its peak. It was shown that under these severe conditions the conventional correlation-shape-based delay discriminators produce biased estimates. This necessitates the application of some post correlation signal processing remedies for multipath high resolution. Performance and computation complexity are the two important indicators that are considered in studying and evaluating these techniques.

In this thesis, four different advanced multipath mitigation techniques were analyzed and tested. The first class of techniques studied was the maximum-likelihood-based estimators for their superior estimation performance.

In chapter 3, a novel ML-based delay estimation technique was proposed that targeted some of the primary limitations of contemporary ML-based algorithms. The proposed algorithm, namely MSML, uses one important key point to increase performance. That key point is that increasing the number of parameters to be estimated decreases the

estimation accuracy of an ML estimator. For this reason the algorithm estimates the multipath components one by one in a sequential manner. The novel algorithm adds a detection procedure before estimating each path to avoid applying the estimation procedure when there is no more significant multipath component and to make sure all the present components are estimated. This strategy results in an improved estimation performance compared to MEDLL. Moreover, since the structure of the refinement stage in MSML is not iterative, it is less complex than MEDLL. MSML considers the effect of all of the previously estimated components when trying to estimate a new component. This is why its performance is considerably superior to SML that assumes that only one component is present every time it tries to find a new path. The simulation results shows that the proposed MSML algorithm outperforms the other techniques in the sense of LOS delay estimation RMSE, in particular for lower values of signal-to-noise ratios under the three urban, suburban and rural simulation scenarios.

Although the MSML technique is less complex than MEDLL, it is still complex since it designed based on maximum likelihood estimation principles to find the parameters of each path. For this reason, in Chapter 4 it was suggested to multiplex MSML with a less complex tracking approach, namely the sequential LMMSE technique. The idea is that the two algorithms switch turns based on rate of the variation of the channel. Furthermore, the estimation performance of the system is compared for three different cases where MSML-only, LMMSE-only, and MSML-LMMSE techniques are applied. Those results show that the performance of MSML-LMMSE in terms of LOS time of arrival estimation RMSE is very close to MSML-only technique at values of C/N_0 larger

than 32 dB-Hz. Moreover, in terms of channel MSE, MSMSL-LMMSE always outperforms MSML-only. A set of real data processing results was presented to compare the performance of MSML-LMMSE with some classical delay DLLs in terms of ranging and positioning errors. Those results also verified the superiority of MSML-LMMSE to the classical delay estimation approaches in terms of estimation RMSE. Moreover, in Chapter 4, the distribution of the number of paths for the visible satellites was compared to the theoretical distributions for the number of paths in urban environments. The results show a reasonable fit between the histograms of the number of paths extracted from the real data and the Poisson distribution. However, the mean parameters measured from these histograms are usually smaller than those predicted in theory. It was concluded that the very weak multipath components are not detectable by the discussed estimation/detection algorithm.

In Chapter 5, a set of channel equalization algorithms, stochastic gradient (SG) techniques, were modified to be applicable to GNSS multipath mitigation. It was shown that the computational complexity of these sets of approaches is smaller than the previously discussed ML-based algorithms. However in terms of estimation performance, some of them are very close to the ML-based techniques. The simulation results in this chapter show that the convergence of SG algorithms depends on the choice of the initial value and the step-size. The simulation results for an urban channel scenario showed that the RLS and APA approaches outperform the rest of the SG algorithms in terms of LOS delay estimation RMSE and minimum MSE cost function. However, these two approaches are the most complex ones. It was shown that the LMS algorithm, which is

the simplest approach, is not able to track channel variations and produces biased estimates when these variations are fast. The NLMS algorithm, however, is a trade-off between estimation performance and computation complexity.

When a receiver is in fast motion, the received signal de-correlates fast in time. This phenomenon limits the duration of the effective coherent integration time that the receiver can use. However, when a signal shrinks in one of the frequency or time domains it spreads in the other domain. This simple rule is the basic idea behind the work of Chapter 6. In this chapter, the Doppler frequency spreading of signals when the receiver is in fast motion is used to compensate the performance loss due to reduced receiver's coherent integration time. In other words, the shifted copies of the received signal in the Doppler-domain were used in the computation of the correlation matrix to enhance the rank of this matrix and improve the estimation accuracy of the sub-space-based MUSIC algorithm. Although, a sub-space-based algorithm is normally too complex to be implemented in a hand-held GNSS receiver, it can be used as a high resolution algorithm for the purpose of channel characterization. The data processing results presented in this chapter showed that Doppler-combining could make a considerable difference in the delay estimation performance of MUSIC as compared to the diversity technique (such as temporal or spatial diversity techniques).

Finally, as a general comparison between all of the algorithms discussed in this thesis, it was observed that the ML-based algorithms present the best estimation performance and they are the most complex ones. The subspace algorithms are as complex as the ML-based algortithms but their estimation performance is not as good as the ML-based

techniques. On the other hand, the stochastic gradient algorithms impose a considerably smaller computational load to the receiver than the ML-based techniques. However, it was shown that at moderate to high values of C/N_0, the performance of the RLS and APA algorithm was as good as the ML-based techniques. For these reasons, the RLS and APA algorithms can be considered as the best trade-off between the LOS delay estimation accuracy and system's complexity. In Table 7.1, the position estimation RMSE of four groups of multipath mitigation techniques for the data explained in chapter four is compared.

Table 7-1: Range of position estimation RMSE for the techniques within different groups of multipath mitigation methods

Method	RMSE, East [m]	RMSE, North [m]	RMSE, Up [m]
Classic DLLs	22-44	34-76	41-125
SG Algorithms	13-51	27-66	45-98
MSML-LMMSE	10.1	18.3	41.1
Subspace	21-36	25-39	44-67

It is important to recall that the software receiver that was applied here for processing the data used assistance information such as the data bits and the reference trajectory to limit the search space to two chips around the maximum of the received correlation function. This limited search space was used for all of the algorithms including the ones used as the bench mark to be compared to the proposed algorithms. However, limiting the search space might affect different algorithms in different ways and impact the overall comparisons.

7.2 Recommendations

Considering the presented work and the experimental results in this thesis, we suggest the following recommendations for future work:

1. In this thesis, simulations and real data tests were limited to GPS L1 signal. Although the principles based on which the proposed algorithms were developed and the general methodologies are the same for other GNSS signals, different modifications and considerations may be required for each case. Modifying the proposed methods for other GNSS signals, as well as simulating and performing real data tests for these signals, are recommended as further developments and confirmation of the research presented herein.
2. In Chapter 3 it was mentioned that the threshold of detection for the MSML approach is set based on a certain value of the probability of false alarm. It was suggested that as more multipath components are detected and estimated, the probability of false alarm is decreased based on the CDF of Poisson distribution to decrease the probability of detection according to the measured statistics of the channel. It was shown in this chapter that the mean of this Poisson distribution depends on the type of the environment, e.g. Urban, suburban or rural. One interesting recommendation for future work can be preparing a set of look-up-tables that provide the values of the detection threshold as a function of the number of the multipath component that is going to be tested through GLRT for

different environments. When the receiver has access to these look-up tables, the computational complexity of the receiver is greatly reduced.

3. In Chapter 4, the proposed MSML approach was used to provide a statistical characterization for the number of multipath components for a data collected in an urban area. In a similar way, the MSML algorithm can be used to characterize some other statistics of the channel such as the distribution of the relative delays and/or amplitudes of the signal reflection for different environments.
4. In Chapter 4, the Wiener filter was used to track the estimated channel by the MSML approach with low complexity when the channel variations are slow. Other low complexity tracking techniques can be used instead of the Wiener filter. One very suitable option for a low complexity tracking technique is the LMS algorithm introduced in Chapter 5. It was mentioned in Chapter 5 that the only problem with LMS is that it cannot track the fast variations of the channel, which is the same issue with LMMSE. However, the complexity of LMS is even lower than LLMSE. Therefore, this technique can be reset and initiated by the MSML algorithm whenever a sudden change happens in the channel. The same methodology that was used in Chapter 4 can be used in this system to switch between the two modes of operation of the receiver.
5. In Chapter 3, the covariance matrix of the noise was estimated and updated sequentially as part of the proposed algorithm. This approximation introduces some performance loss to the system. The effect of this loss on the performance of LOS delay estimation can be studied.

6. In was mentioned in Chapter 4 that the length of the sliding window used in the computation of the averaged MSE that determines when the transition between the two modes of operation takes place, affects the ratio of time durations that the system spends in the two modes. This in turn affects the trade-off of between the accuracy/reliability of the system and its computational complexity. In the simulation and data processing results in Chapter 4 the value of this parameter was fixed. The effect of this parameter can be studied by using simulations and real data processing wherein the value of this parameter is changed within a reasonable range to figure out whether an optimum value can be found.
7. In Chapter 6, the effect of Doppler-combining algorithm on the estimation performance of the MUSIC algorithm was studied. However, Doppler combing can aid any other subspace method in the same way. The effect of this strategy on other subspace method such as signal parameters via rotational invariant technique (ESPRIT) (Groh & Sand 2011) can be studied.
8. The received signal on GPS L1 and L2 pass through the same wireless channel since they arrive from the same transmitter and are received by the same receiver. These two signals can be used as two branches of frequency diversity to enhance the de-correlation of multipath components in sub-space algorithms.

References

Akaike, H. (1974), "A new look at the statistical model identification," *IEEE Transaction on Automatic Control*, vol. 19, no. 6, December, pp. *Navigation* 716-723

Benveniste, A., M. Goursat, and G. Ruget (1980), "Robust identification of a non-minimum phase system," *IEEE Transactions on Automatic Control*, vol. AC-25, no. 3, June, pp. 385–399

Betz, J. W. and K. R. Kolodziejski (2000) "Extended theory of early-late code tracking for a band-limited GPS receiver," *Journal of the Institute of Navigation*, vol 47, no 3, Fall, pp. 211–226

Bhuiyan, M. Z. H., E. S. Lohan, and M. Renfors (2008), "Code tracking algorithms for mitigating multipath effects in fading channels for satellite-based positioning," *EURASIP Journal on Advances in Signal Processing*, vol. 2008, Article ID 863629, September, 17 pages

Bhuiyan M.Z.H., E.S. Lohan, and M. Renfors (2009), "A Reduced Search Space Maximum Likelihood delay estimator for mitigating multipath effects in satellite-based positioning", IAIN World Congress, Stockholm, Sweden, October

Bhuiyan, M. Z. H. and E.S. Lohan (2010) "Advanced Multipath Mitigation Techniques for Stallite-Based Positioning Applications," *International Journal of Navigation and Observation*, vol 2010, Article ID 412393, October, 15 pages

Bhuiyan M.Z.H., E.S. Lohan, and M. Renfors (2010), "A Slope-Based Multipath Estimation Technique for Mitigating Short-Delay Multipath in GNSS Receivers," *IEEE ISCAS 2010*, Paris, France, May

Bouchereau, F., D. Brady and C. Lanzl (2001) "Multipath Delay Estimation Using a Super Resolution PN-Correlation Method," *IEEE Transactions on Signal Processing*, vol 49, no 5, May, pp. 938-949

Braasch, M. S. and Dierendonck (1999) A. J. V. "GPS Receiver Architectures and Measerements," *Proceedings of the IEEE*, vol. 87, no. 1, January, pp. 48 - 64

Chen, X., F. Dovis and M. Pini (2010) "An Innovative Multipath Mitigation Method Using Coupled Amplitude Delay Lock Loops in GNSS Receivers", *Position Location and Navigation Symposium (PLANS 2010)*, 4-6 May, Indian Wells CA, USA, pp. 1118 - 1126

Chen, X. and D. Fabio (2011), "Enhanced CADLL Structure for Multiple Mitigation in Urban Scenarios," *International Technical Meeting of the Institute of Navigation*, 24-26 January, San Diego CA, pp. 678 - 686

Closas, P., C. Fernandez-Prade and J. A. Fernandez-Rubio (2006) "Bayesian DLL for Multipath Mitigation in Navigation Systems Using Particle Filters," In *Proceeding of IEEE ICASSP 06*, 14-19 May, Toulouse, France, pp. 129-132

Closas, P., C. Fernandez-Prade, J. A. Fernandez-Rubio (2009) "A Bayesian Approach to Multipath Mitigation in GNSS Receivers," *IEEE Journal of Selected Topics in Signal Processing* ,vol 3, no 4, August, pp. 695-706

Dierendonck, A. J. V., P. Fenton, and T. Ford (1992) "Theory and performance of narrow correlator spacing in a GPS receiver," *Journal of the Institute of Navigation*, vol 39, no 3, June, pp. 265–283

Ding, Z. and Y. Li (2000) *Blind equalization and identification*, Marcel Dekker, Inc., New York, Basel

Dragunas, K. and K. Borre (2011) "Multipath Mitigation Based on Deconvolution," *Journal of Global Positioning Systems*, vol 10, no 1, October, pp. 79-88.

Fenton, P. and J. Jones (2005) "The theory and performance of NovAtel Inc.'s vision correlator," in *Proc. ION GNSS*, 13-16 September, Palm Springs CA, pp. 2178 - 2186

Fock, G., J. Baltersee, P. Schulz-Rittich, and H. Meyr (2001), "Channel Tracking for Rake Receivers in Closely Spaced Multipath Environments," *IEEE Journal on Selected Areas in Communications*, vol 19, no 12, December, pp. 2420–2431

Fontan F. P., M. Vaquez-Castro, C. E. Cabado, J. P. Garcia and E. Kubista (2001) "Statistical modeling of the LMS channel," *IEEE TRANSACTIONS ON VEHICULAR TECHNOLOGY*, vol. 50, no. 6, November, pp. 1549-1567

Garin, L. and J. M. Rousseau (1997) "Enhanced strobe correlator multipath rejection for code & carrier," in *Proceedings of the 10th International Technical Meeting of the Satellite Division of the Institute of Navigation (ION GPS '97)*, 16-19 September, Kansas City MO, USA, pp. 559–568.

Graybill, F. A. (1969), "Introduction to matrices with application in statistics," Wadsworth, Belmont, California

Groh I. and S. Sand " Decoupled delay and doppler acquisition in DS-CDMA systems at low signal to noise ratios," In *Proceedings of the International Conference on Localization and GNSS (ICL-GNSS) 2011*, Tampere, Finland, June

Guo Y. and B. C. Levy (2006),"Robust MSE Equalizer Design for MIMO Communication Systems in the Presence of Model Uncertainties," *IEEE TRANSACTIONS ON SIGNAL PROCESSING*, vol. 54, no. 5, pp. 1840-1852, May

Haykin, S. (2001) *Adaptive Filter Theory*, Prentice Hall, 4th-edition.

Hayes, Monson H. (1996). "9.4: Recursive Least Squares". Statistical Digital Signal Processing and Modeling. Wiley. p. 541. ISBN 0-471-59431-8

Hurskainen, H., E. S. Lohan, X. Hu, J. Raasakka, and J. Nurmi (2008) "Multiple gate delay tracking structures for GNSS signals and their evaluation with Simulink, SystemC, and VHDL," *International Journal of Navigation and Observation*, vol 2008 , Article ID 785695, December, 17 pages

Hurskainen, H. (2009), "Research Tools and Architectural Considerations for Future GNSS Receivers", Ph.D. Thesis, Tampere University of Technology, December

Irsigler, M. and B. Eissfeller (2003) "Comparison of multipath mitigation techniques with consideration of future signal structures," in *Proceedings of the 16th International Technical Meeting of the Satellite Division of the Institute of Navigation*, 9-12 September, Portland OR, USA pp. 2584–2592

Jahn A., H. Bischl, and G. Heis (1996), "Channel characterization for spread spectrum satellite communications," in *Proceedings of IEEE 4th International Symposium on Spread Spectrum Techniques and Applications (ISSSTA'96)*, Mainz, Germany, September, pp. 1221–1226

Jardak N., A. Vervisch-Picois, N. Samana (2011), "Multipath Insensitive Delay Lock Loop in GNSS Receivers, " *IEEE TRANSACTIONS ON AEROSPACE AND ELECTRONIC SYSTEMS,* vol. 47, no. 4, October, pp. 2590-2609

Jones, J., P. Fenton, and B. Smith (2004) *Theory and performance of the pulse aperture correlator,* Technical Report, Novatel, Alberta, Canada, 13 pages

Jeon, N. R., H. B. Lee, C. G. Park, S. Y. Cho and S. C. Kim (2010) "Super Resolution TOA Estimation with Computational Load Reduction," *IEEE Transactions on Vehicular Technology*, vol. 59, no. 8, October, pp. 4139-4144

Kaplan, E. (2006), *Understanding GPS: Principles and Applications*, Artech House, Norwood, Mass, USA, 2nd Ed.

Kay, S. M. (1993), *Fundamentals of Statistical Signal Processing: Estimation Theory*, vol 1, PTR Prentice Hall, New Jersey

Kay, S. M. (1998), *Fundamentals of Statistical Signal Processing: Detection Theory*, vol 2, PTR Prentice Hall, New Jersey

Kanekal, S. M. and Braasch, M. S. (1998), "Multipath Mitigation with Gated Signal technology," in *Proc. Of the 54th Ann. Meeting of the Inst. of Navigation,* Denver, CO, pp. 535–542, June 1–3

Kim C., (2004) "Statistical modeling of W-CDMA signals for use over frequency-selective multipath channels," *IEEE TRANSACTIONS ON COMMUNICATIONS,* vol. 2, no. 1, January, pp. 1803-1808

Klukas, R. (1997) "A Superresolution Based Cellular Positioning System Using GPS Time Synchronization," Ph.D. dissertation, Department of Geomatics engineering, University of Calgary, Canada (Available at http://plan.geomatics.ucalgary.ca)

Kostic Z., G. Pavlovic (1999), "Resolving subchip-spaced multipath components in CDMA communication systems", *IEEE TRANSACTIONS ON VEHICULAR TECHNOLOGY*, vol. 48, no. 6, 1999, pp.79-88

Li, X. and K. Pahlavan (2004) "Super-Resolution TOA Estimation with Diversity for Indoor Geolocation," *IEEE Transactions on Wireless Communications*, vol 3, no 1, January, pp. 224 – 234

Lin T., C. O'Driscoll and G. Lachapelle (2011), "Development of a Context-Aware Vector-Based High-Sensitivity GNSS Software Receiver," International Technical Meetings (ITM) 2011, San Diego, CA. , 24-26 January

Lohan, E. S., R. Hamila, A. Lakhzouri, and M. Renfors (2005) "Highly Efficient Techniques for Mitigating the Effects of Multipath Propagation in DS-CDMA delay Estimation," in *Proceedings of IEEE Transactions in Wireless Communications*, vol 4, no 1, January, pp. 149 – 162

Lohan E. S., A. Lakhzouri, and M. Renfors (2006), "Feedforward delay estimators in adverse multipath propagation for Galileo and modernized GPS signals," *EURASIP Journal of Advances in Signal Processing*, doi:10.1155/ASP/2006/50971, January

Lu T. Z. and S.-H. Shiou (2002), Inverses of two block matrices, Computers Math. Appl. 43, 119–129

Manandhar, D. and R. Shibasaki (2004) "Possibility Analysis of Polarization Diversity Scheme for Multipath Mitigation in GPS Receivers," *The 2004 International Symposium on GNSS/GPS Sydney 2004*, 6-8 December, Sydney, Australia

McGraw, G. A. and M. S. Braasch (1999) "GNSS multipath mitigation using gated and high resolution correlator concepts," in *Proceedings of the The National Technical Meeting of the Satellite Division of the Institute of Navigation*, 25-27 January, San Diego CA, USA, pp. 333-342

Mayyas K. , and Aboulnasr T. (2002) " Leaky LMS Algorithm: MSE Analysis for Gaussian Data," *IEEE Transaction on Signal Processing*, vol. 45, no. 4, pp. 927-934, August.

Nee, R. D. J. V. (1992) "The Multipath Estimating Delay Lock Loop," in *Proceedings of the IEEE 2nd International Symposium on Spread Spectrum Techniques and Applications*, November 29- December 2, Yokohama, Japan, pp. 39–42

Nee, R. D. J. V., C. Siereveld, P. Fenton, and B. Townsend (1994), "Multipath Estimating Delay Lock Loop: Approaching Theoretical Accuracy limits," in *Proceedings of the IEEE PLANS, Position Location and Navigation Symposium*, 11-15 April, Las Vegas NV, USA, pp. 246–251

Nee R. D. J. V. (1997), "Method of estimating a line of sight signal propagation time using a reduced multipath correlation function," U.S. Patent no. 5 615 232, Mar. 25,

Nee R. D. J. V. (2001) "Spread-spectrum code and carrier synchronization errors caused by multipath and interference" *IEEE TRANSACTIONS ON AEROSPACE AND ELECTRONIC SYSTEMS* vol. 29, no. 4, January pp. 1359 - 1365

Noble, B., J. W. Daniel (1977), "Applied Linear Algebra, Prentice-Hall, Englewood Cliffs, N.J.

Petovello, M. G., C. O'Driscoll, G. Lachapelle, D. Borio and H. Murtaza (2008) "Architecture and Benefits of an Advanced GNSS Software Receiver," Journal of Global Positioning Systems, vol 7, no 2, pp. 156-168

Proakis, J. G. (2000) *Digital communication*, McGraw Hill, 4th-edition.

Puntanen S. and G.P.H. Styan (2005), "Schur complements in statistics and probability", Chapter 6 in "The Schur Complement and Its Applications" (F. Zhang ed.), Springer, pp. 163–226, ISBN:978-0-387-24271-1

Rappaport, T. S. (2002) *Wireless Communications: Principles and Practice*, Prentice Hall PTR, 2nd Ed, Chapter 4, pp. 139-196

Ray J. K., M. E. Cannon, P. Fenton (2001), "GPS Code and Carrier Multipath Mitigation Using a Multi-antenna System," *IEEE TRANSACTIONS ON AEROSPACE AND ELECTRONIC SYSTEMS,* vol. 37, no. 1, January, pp. 183 – 195

Rissanen J. (1978), "Modeling by shortest data description," *Automatica*, vol. 14, no. 5, September, pp. 465-471

Sahmoudi, M. and M. G. Amin (2008) "Fast Iterative Maximum Likelihood Algorithm for Multipath Mitigation in the Next Generation of GNSS Receivers," *IEEE Transactions on Wireless Communication,* vol 7, no 11, November, pp. 4362-4374

Sahmoudi, M. and M. G. Amin (2009) “Robust Tracking of Weak GPS Signals in Multipath and Jamming Environments,” *Signal Processing*, Elsevier, vol 89, no 7, July, pp. 1320-1333

Sayed, A. H. (2008) *Adaptive Filters*, John Wiley & Sons, Inc., Hoboken, New Jersey.

Sayeed, A. M., and B. Aazhang (1999) “Joint Multipath-Doppler Diversity in Mobile Wireless Communications,” *IEEE Transactions on Communications*, vol. 47, no.1, January, pp. 123-132

Seco-Granados G. (2000), “Antenna Arrays for Multipath and Interference Mitigation in GNSS Receivers,” Ph.D. dissertation, Dept. of Signal Theory and Communications, Universitat Polit`ecnica de Catalunya (UPC), Barcelona, Spain, July

Shuanggen Jin (2012), *Global Navigation Satellite Systems: Signal, Theory and Applications*, Chapter 17, InTech Ed., ISBN 978-953-307-843-4

Skournetou D., A.H. Sayed, and E.S. Lohan (2011), “Cramer Rao Bounds for Multipath Channel Estimation in GNSS Receivers”, *Hindawi International Journal of Navigation and Observation, IJNO*, vol. 2011, Article ID 356975, 15 pages

Slavakis K., and S. Theodoridis (2008) "Sliding Window Generalized Kernel Affine Projection Algorithm using Projection Mappings", *EURASIP Journal on Advances in Signal Processing*, vol. 2008, Article ID 830381, doi:10.1155/2008/830381

Steingass, A. and A. Lehner (2004), “Measuring the navigation multipath channel–A statistical analysis”. *ION GNSS 2004*, 21- 24 September, Long Beach, CA

Townsend, B. R. and P. Fenton (1994), "A Practical approach to the reduction of pseudorange multipath errors in a L1 GPS receiver," in *Proceedings of the 7th International Technical Meeting of the Satellite Division of the Institute of Navigation (ION-GPS '94)*, 20-23 September, Salt Lake City Utah, USA, pp. 143–148

Townsend, B., D. J. R. van Nee, P. Fenton, and K. Van Dierendonck (1995) "Performance evaluation of the multipath estimating delay lock loop," *Navigation Journal of the Institute of Navigation*, vol 42, no 3, Fall, pp. 503-514

Turin, G. L., F. D. Clapp, T. L. Johnston, S. B. Fine, and D. Lavry (1972) "A statistical model of urban multipath propagation," *IEEE Transactions on Vehicular Technology,* vol 21, no 1, February, pp. 1-9

Tsui, J. B. (2000), "Fundamentals of Global Positioning System Receivers: A Software Approach", John Willey & Sons, Inc.

Van Trees, H. L. (2002) "Optimum Detection, Estimation, and Modulation Theory" Part IV. John Wiley & Sons, Inc, 1st edition.

Wallach E. , and B. Widrow (1984) "The Least Mean Fourth (LMF) Adaptive Algorithm and Its Family," *IEEE Transactions on Information Theory*, vol. IT-30, no.2, pp. 275-283, March.

Ward, P.W. (1995) "GPS receiver interference monitoring, mitigation and analysis," *Journal of ION*, vol 41, no 4, September, pp. 63-78

Weill, L. R. (2002), "Multipath Mitigation Using Modernized GPS Signals: How Good Can it Get?," In *Proceedings of the 15th International Technical Meeting of the Satellite*

Division of The Institute of Navigation (ION GPS 2002), 24-27 September, Portland OR , pp. 493 - 505

Weill, L. R. (2003) "Multipath mitigation-how good can it get with new signals?," *GPS World*, vol 16, no 6, June, pp. 106–113.

Widrow B., J. R. Glover, J. M. McCool, J. Kaunitz, C. S. Williams, R. H. Hearn, H. R.

Yamada, H., M. Ohmiya, Y. Ogawa, and K. Itoh (1991) "Super-resolution techniques for time-domain measurements with a network analyzer," *IEEE Transaction on Antennas Propagation*, vol. 39, no 2, February, pp. 177–183

Zeidler and R. C. Goodlin (1975) "Adaptive Noise Cancelling: Principals and Applications," *PROCEEDINGS OF THE IEEE*, vol. 63, no. 12, pp. 1692-1716, December.

Ziedan, N.I. (2006) *GNSS Receivers for Weak Signals*, Artech House, Norwood

APPENDIX A: THE ESTIMATION ACCURACY AND THE NUMBER OF PARAMETERS TO BE ESTIMATED

In this appendix we prove that when the number of parameters to be estimated is and therefore the fisher information matrix (FIM) is expanded, the variance of estimation of the original parameters decreases.

Assume that $\mathbf{I}(\bar{\mathbf{a}}_1)$ is the FIM of the original parameters. Then we extend $\bar{\mathbf{a}}_1$ to $\bar{\mathbf{a}}_2$ by adding more parameters to be estimated. For simplicity and without loss of generality we assume that these new parameters have been inserted to end of $\bar{\mathbf{a}}_1$. Considering the fact that the FIM is a symmetric matrix, $\mathbf{I}(\bar{\mathbf{a}}_2)$ can be represented as

$$\mathbf{I}(\bar{\mathbf{a}}_2)=\begin{bmatrix}\mathbf{I}(\bar{\mathbf{a}}_1) & \mathbf{B}\\ \mathbf{B}^T & \mathbf{I}(\bar{\mathbf{a}}_3)\end{bmatrix}, \tag{A.1}$$

where $\bar{\mathbf{a}}_3$ is the vector including only the newly added parameters. Therefore, the estimation covariance matrix for $\bar{\mathbf{a}}_2$, $\mathbf{C}_{\bar{\mathbf{a}}_2}$, can be represented as (Lu & Shiou 2002, Puntanen & Styan 2005).

$$\mathbf{C}_{\mathbf{a}_2}=\begin{bmatrix}\mathbf{I}(\bar{\mathbf{a}}_1) & \mathbf{B}\\ \mathbf{B}^{\mathrm{H}} & \mathbf{I}(\bar{\mathbf{a}}_3)\end{bmatrix}^{-1}=$$
$$\begin{bmatrix}\left(\mathbf{I}(\bar{\mathbf{a}}_1)-\mathbf{B}\mathbf{I}^{-1}(\bar{\mathbf{a}}_3)\mathbf{B}^{\mathrm{H}}\right)^{-1} & -\mathbf{I}^{-1}(\bar{\mathbf{a}}_1)\mathbf{B}\left(\mathbf{I}(\bar{\mathbf{a}}_3)-\mathbf{B}^{\mathrm{H}}\mathbf{I}^{-1}(\bar{\mathbf{a}}_1)\mathbf{B}\right)^{-1}\\ -\mathbf{I}^{-1}(\bar{\mathbf{a}}_3)\mathbf{B}^{\mathrm{H}}\left(\mathbf{I}(\bar{\mathbf{a}}_1)-\mathbf{B}\mathbf{I}^{-1}(\bar{\mathbf{a}}_3)\mathbf{B}^{\mathrm{H}}\right)^{-1} & \left(\mathbf{I}(\bar{\mathbf{a}}_3)-\mathbf{B}^{\mathrm{H}}\mathbf{I}^{-1}(\bar{\mathbf{a}}_1)\mathbf{B}\right)^{-1}\end{bmatrix}. \tag{A.2}$$

Thus, the part of the covariance matrix that is related to the primary set of the parameters is $\left(\mathbf{I}(\bar{\mathbf{a}}_1)-\mathbf{B}\mathbf{A}^{-1}\mathbf{B}^{\mathrm{H}}\right)^{-1}$. We refer to this matrix as $\mathbf{C}'_{\bar{\mathbf{a}}_1}$. Furthermore, this matrix can be rewritten as

$$\begin{aligned}\mathbf{C}'_{\mathbf{a}_1} &= \left(\mathbf{I}(\bar{\mathbf{a}}_1)-\mathbf{B}\mathbf{I}^{-1}(\bar{\mathbf{a}}_3)\mathbf{B}^{\mathrm{H}}\right)^{-1} \\ &= \mathbf{I}^{-1}(\bar{\mathbf{a}}_1)+\mathbf{I}^{-1}(\bar{\mathbf{a}}_1)\mathbf{B}\left(\mathbf{B}^{\mathrm{H}}\mathbf{I}^{-1}(\bar{\mathbf{a}}_1)\mathbf{B}+\mathbf{I}(\bar{\mathbf{a}}_3)\right)^{-1}\mathbf{B}^{\mathrm{H}}\mathbf{I}^{-1}(\bar{\mathbf{a}}_1) \\ &= \mathbf{C}_{\bar{\mathbf{a}}_1}+\mathbf{C}_{\bar{\mathbf{a}}_1}\mathbf{B}\left(\mathbf{B}^{\mathrm{H}}\mathbf{C}_{\bar{\mathbf{a}}_1}\mathbf{B}+\mathbf{I}(\bar{\mathbf{a}}_3)\right)^{-1}\mathbf{B}^{\mathrm{H}}\mathbf{C}_{\bar{\mathbf{a}}_1}\end{aligned} \qquad \text{(A.3)}$$

In the second term of (A-3), $\mathbf{B}^{H}\mathbf{C}_{\bar{\mathbf{a}}_1}\mathbf{B}+\mathbf{I}(\bar{\mathbf{a}}_3)$ is a positive definite (PD) matrix (because both of the FIM matrix and the covariance matrix which is the inverse of FIM matrix are PD) and so is its inverse. Therefore, the quadratic form term $\mathbf{C}_{\bar{\mathbf{a}}_1}\mathbf{B}\left(\mathbf{B}^{\mathrm{H}}\mathbf{C}_{\bar{\mathbf{a}}_1}\mathbf{B}+\mathbf{I}(\bar{\mathbf{a}}_3)\right)^{-1}\mathbf{B}^{\mathrm{H}}\mathbf{C}_{\bar{\mathbf{a}}_1}$ has real positive elements on its main diagonal. Hence, the diagonal elements of $\mathbf{C}'_{\mathbf{a}_1}$ which are the variances of estimation of the original set of the parameters are greater than corresponding diagonal elements of $\mathbf{C}_{\bar{\mathbf{a}}_1}$ and therefore, the variance of estimation of the primary parameters have been increased after inserting the new set of the parameters to be estimated.

APPENDIX B: GLRT WHEN PREVIOUSLY ESTIMATED PARAMETERS ARE ASSUMED KNOWN

In Chapter 3, the problem of detecting the (m+1)-th multipath component through GLRT when the parameters of the first m signal components are considered as nuisance parameters was discussed. In this appendix a simplified version of the GLRT presented in Chapter 3 is developed which is based on the assumption that at time of performing the GLRT for the (m+1)-th path, all of the m previously detected paths have been correctly estimated and their parameters can be considered as deterministic.

A new path (path m+1) is assumed present if the following test ratio passes the threshold: (H_1)

$$L\left(\mathbf{y}^{(m)}\right)=\frac{p\left(\mathbf{y}^{(m)};\,\hat{\mathbf{s}},H_1\right)}{p\left(\mathbf{y}^{(m)};\,H_0\right)}>\gamma \tag{B.1}$$

where

$$\mathbf{y}^{(m)}=\ \mathbf{y}-\sum_{i=1}^{m}\hat{a}_i g\left(t-\hat{\tau}_i\right), \tag{B.2}$$

and

$$\begin{aligned}\hat{\mathbf{s}}&=\hat{a}_{m+1}\mathbf{g}\left(\tau-\hat{\tau}_{m+1}\right)\\&=\frac{\mathbf{g}^{\mathrm{H}}\left(\tau-\hat{\tau}_{m+1}\right)\mathbf{Q}^{-1}\mathbf{y}^{(m)}\mathbf{g}\left(\tau-\hat{\tau}_{m+1}\right)}{\mathbf{g}^{\mathrm{H}}\left(\tau-\hat{\tau}_{m+1}\right)\mathbf{Q}^{-1}\mathbf{g}\left(\tau-\hat{\tau}_{m+1}\right)}\end{aligned} \tag{B.3}$$

which is the estimation for next potential signal component wherein $\hat{a}_{m+1}$ is obtained from (3.18) . (B.1) can be expanded as

$$L\left(\mathbf{y}^{(m)}\right)=\frac{\exp\left(-\frac{1}{2}\left(\mathbf{y}^{(m)}-\hat{\mathbf{s}}\right)^{\mathrm{H}}\mathbf{Q}^{-1}\left(\mathbf{y}^{(m)}-\hat{\mathbf{s}}\right)\right)}{\exp\left(-\frac{1}{2}\left(\mathbf{y}^{(m)}\right)^{\mathrm{H}}\mathbf{Q}^{-1}\left(\mathbf{y}^{(m)}\right)\right)}>\gamma. \tag{B.4}$$

Taking the logarithm of both sides of (B.4) and retaining only the data dependent terms, it simplifies to

$$T\left(\mathbf{y}^{(m)}\right)=\left(\mathbf{y}^{(m)}\right)^{\mathrm{H}}\mathbf{Q}^{-1}\hat{\mathbf{s}}-\frac{1}{2}\hat{\mathbf{s}}^{\mathrm{H}}\mathbf{Q}^{-1}\hat{\mathbf{s}}>\gamma'. \tag{B.5}$$

After substituting $\hat{\mathbf{s}}$ from (B.3) into (B.5) and simplifying the scalar constant coefficients, (B.5) can be represented as

$$\begin{aligned}&T\left(\mathbf{y}^{(m)}\right)=\\&\mathbf{g}^{\mathrm{H}}\left(\tau-\hat{\tau}_{m+1}\right)\mathbf{Q}^{-1}\mathbf{y}^{(m)}\left(\mathbf{y}^{(m)}\right)^{\mathrm{H}}\mathbf{Q}^{-1}\mathbf{g}\left(\tau-\hat{\tau}_{m+1}\right)>\gamma''\end{aligned} \tag{B.6}$$

Applying the variable change of $z=\left(\mathbf{y}^{(m)}\right)^{\mathrm{H}}\mathbf{Q}^{-1}\mathbf{g}\left(\tau-\hat{\tau}_{m+1}\right)$, the sufficient statistics can be expressed as $T\left(z\right)=z^{\mathrm{H}}z$. z is a complex Gaussian scalar random variable and its statistics under the two hypotheses can be expressed as

$$z\sim\begin{cases}\mathrm{N}\left(0,\sigma_{m+1}^{2}\right) & \text{under } \mathrm{H}_0\\ \mathrm{N}\left(\lambda_{m+1},\sigma_{m+1}^{2}\right) & \text{under } \mathrm{H}_1\end{cases} \tag{B.7}$$

where $\lambda_{m+1} = a_{m+1}\left(\mathbf{g}^{\mathrm{H}}(\tau-\tau_{m+1})\mathbf{Q}^{-1}\mathbf{g}(\tau-\tau_{m+1})\right)$ and σ_{m+1}^2 can be obtained as

$$\begin{aligned}\sigma_{m+1}^2 &= E\left\{zz^H\right\} \\ &= \mathbf{g}^{\mathrm{H}}(\tau-\tau_{m+1})\mathbf{Q}^{-1}E\left\{\mathbf{y}^{(m)}\left(\mathbf{y}^{(m)}\right)^{\mathrm{H}}\right\}\mathbf{Q}^{-1}\mathbf{g}(\tau-\tau_{m+1}) \\ &= \mathbf{g}^{\mathrm{H}}(\tau-\tau_{m+1})\mathbf{Q}^{-1}\mathbf{g}(\tau-\tau_{m+1})\end{aligned} \tag{B.8}$$

Therefore, $T(z)$ follows a Chi-squared distribution with two degrees of freedom and can be expressed as

$$\frac{T(z)}{\sigma_{m+1}^2} \sim\sim \begin{cases}\chi_2^2 & \text{under } \mathrm{H}_0 \\ \chi_2'^2(\lambda_{m+1}) & \text{under } \mathrm{H}_1\end{cases} \tag{B.9}$$

Given (B.9), the probability of false-alarm can be expressed as

$$\begin{aligned}P_{FA} &= \Pr\left\{\frac{T(z)}{\sigma_{m+1}^2} > \frac{\gamma''}{\sigma_{m+1}^2}\right\} \\ &= Q_{\chi_2^2}\left(\frac{\gamma''}{\sigma_{m+1}^2}\right) = \exp\left(-\frac{\gamma''}{2\sigma_{m+1}^2}\right).\end{aligned} \tag{B.10}$$

Thus, for a certain amount of probability of false-alarm, the threshold of detection can be determined as

$$\gamma'' = -2\mathbf{g}^{\mathrm{H}}(\tau-\tau_{m+1})\mathbf{Q}^{-1}\mathbf{g}(\tau-\tau_{m+1})\ln(P_{FA}). \tag{B.11}$$

Therefore, the presence of the (m+1)-th multipath component is accepted if $T(z)$ passes the threshold in (B-11).

APPENDIX C: LOCAL OPTIMALITY OF LMS

Given the two different error types introduced in (5.43) and (5.44), the local optimization problem is defined as

$$\min_{\mathbf{C}_k} tr\left\{\left(\mathbf{C}_k-\mathbf{C}_{k-1}\right)^{\mathrm{H}}\left(\mathbf{C}_k-\mathbf{C}_{k-1}\right)\right\} \text{ subject to } \mathbf{r}_k=\left(1-\mu\left\|\mathbf{y}_k\right\|^2\right)\mathbf{e}_k . \tag{C.1}$$

The idea behind $\mathbf{r}_k=\left(1-\mu\left\|\mathbf{y}_k\right\|^2\right)\mathbf{e}_k$ is to have $\left\|\mathbf{r}_k\right\|<\left\|\mathbf{e}_k\right\|$, assuming that μ is small enough to satisfy $1-\mu\left\|\mathbf{y}_k\right\|^2<1$. To proceed with the illustration, let $\delta\mathbf{C}=\mathbf{C}_k-\mathbf{C}_{k-1}$, then

$$\begin{aligned}\mathbf{y}_k\delta\mathbf{C}&=\mathbf{y}_k\mathbf{C}_k-\mathbf{y}_k\mathbf{C}_{k-1}\\&=\left[\mathbf{y}_k\mathbf{C}_k-\mathbf{d}_k\right]+\left[\mathbf{d}_k-\mathbf{y}_k\mathbf{C}_{k-1}\right]\\&=-\mathbf{r}_k+\mathbf{e}_k=\mu\left\|\mathbf{y}_k\right\|^2\mathbf{e}_k\end{aligned} . \tag{C.2}$$

Considering (C.2), 0 can be represented as

$$\min_{\mathbf{C}_k} tr\left\{\delta\mathbf{C}^{\mathrm{H}}\delta\mathbf{C}\right\} \text{ subject to } \mathbf{y}_k\delta\mathbf{C}=\mu\left\|\mathbf{y}_k\right\|^2\mathbf{e}_k . \tag{C.3}$$

It is easy to find that one solution to $\mathbf{y}_k\delta\mathbf{C}=\mu\left\|\mathbf{y}_k\right\|^2\mathbf{e}_k$ is

$$\delta\mathbf{C}_o=\mu\mathbf{y}_k^{\mathrm{H}}\mathbf{e}_k , \tag{C.4}$$

so when both sides of (C.4) are multiplied by $\mathbf{y}_k$, the result is $\mathbf{y}_k\delta\mathbf{C}_o=\mu\left\|\mathbf{y}_k\right\|^2\mathbf{e}_k$. However, there are infinitely many other solutions to (C.3) that can be represented as $\delta\mathbf{C}_o+\mathbf{D}$. Replacing this general solution into the condition in 0 results in: $\mathbf{y}_k\left(\delta\mathbf{C}_o+\mathbf{D}\right)=\mu\left\|\mathbf{y}_k\right\|^2\mathbf{e}_k$, which after substituting 0 leads to: $\mathbf{y}_k\mathbf{D}=0$. This means that

all solutions to $\mathbf{y}_k \delta\mathbf{C} = \mu \|\mathbf{y}_k\|^2 \mathbf{e}_k$ can be obtained by adding a matrix to $\delta\mathbf{C}_o$ which is orthogonal to $\mathbf{y}_k$. Substituting this general solution in $tr\{\delta\mathbf{C}^{\mathrm{H}}\delta\mathbf{C}\}$ results in:

$$\begin{aligned} tr\left\{(\delta\mathbf{C}_o + \mathbf{D})^{\mathrm{H}}(\delta\mathbf{C}_o + \mathbf{D})\right\} &= tr\{\delta\mathbf{C}_o^{\mathrm{H}}\delta\mathbf{C}_o\} + tr\{\mathbf{D}^{\mathrm{H}}\delta\mathbf{C}_o\} + tr\{\delta\mathbf{C}_o^{\mathrm{H}}\mathbf{D}\} + tr\{\mathbf{D}^{\mathrm{H}}\mathbf{D}\} \\ &= tr\{\delta\mathbf{C}_o^{\mathrm{H}}\delta\mathbf{C}_o\} + 0 + 0 + tr\{\mathbf{D}^{\mathrm{H}}\mathbf{D}\} \\ &> tr\{\delta\mathbf{C}_o^{\mathrm{H}}\delta\mathbf{C}_o\}. \end{aligned} \tag{C.5}$$

Therefore, $\delta\mathbf{C}_o$ is the optimum solution to 0 and leads to: $\mathbf{C}_k = \mathbf{C}_{k-1} + \mu\mathbf{y}_k^{\mathrm{H}}[\mathbf{d}_k - \mathbf{y}_k\mathbf{C}_{k-1}]$, which is the LMS recursion as introduced in (5.42).